Coherence and Spin
in GaAs Quantum Dots

A thesis presented

by

Dominik Max Zumbühl

to

The Department of Physics

in partial fulfillment of the requirements

for the degree of

Doctor of Philosophy

in the subject of

Physics

Harvard University

Cambridge, Massachusetts

September 2004

Thesis Advisor:

Author:

Professor Charles M. Marcus

Dominik Max Zumbühl

Coherence and Spin in GaAs Quantum Dots

Abstract

This thesis describes a number of experiments performed in quantum dots as well as 2D systems fabricated in GaAs/AlGaAs 2D electron gases. The focus of the studies is set on spin, coherence and interaction effects of electrons in mesoscopic structures. Experiments investigating the rich physics of spin-orbit coupling in confined structures in presence of magnetic fields both perpendicular and parallel to the 2D plane, orbital effects of in-plane fields on average, variance and correlations of conductance as well as few electron physics focusing on the two electron system are presented.

In situ control of spin-orbit coupling in coherent transport using a clean GaAs/AlGaAs 2DEG is realized, leading to a gate-tunable crossover from weak localization to antilocalization. The necessary theory of 2D magnetotransport in the presence of spin-orbit coupling beyond the diffusive approximation is developed and used to analyze experimental data. Spin-orbit coupling in ballistic GaAs quantum dots is investigated. Antilocalization that is prominent in large dots is suppressed in small dots, as anticipated theoretically. Effects of parallel fields on average and variance of conductance reflect novel spin-rotation symmetries, consistent with random matrix theory once orbital coupling of the parallel field is included.

High sensitivity of mesoscopic conductance fluctuations to magnetic flux in large quantum dots is used to investigate changes in the two-dimensional electron dispersion caused by an in-plane magnetic field. In particular, changes in effective mass and the breaking of momentum reversal symmetry in the electron dispersion are extracted quantitatively from correlations of conductance fluctuations. New theory is presented, and good agreement

between theory and experiment is found.

Few-electron quantum dots are investigated in the regime of strong tunneling to the leads. Inelastic cotunneling is used to measure the two-electron singlet-triplet splitting above and below a magnetic field driven singlet-triplet transition. Evidence for a non-equilibrium two-electron singlet-triplet Kondo effect is presented. Cotunneling allows orbital correlations and parameters characterizing entanglement of the two-electron singlet ground state to be extracted from dc transport.

Contents

List of Figures

List of Tables

Acknowledgments

First and foremost my thanks go to Charlie Marcus, who has always been a great source of inspiration, encouragement and a very resourceful experimentalist. His deep insight into the physics and his never ending stream of new ideas have made it possible for me to complete the research presented in this thesis. From west coast to east coast and throughout the years, Charlie has never hesitated to support and encourage me, help me avoid bureaucratic hurdles and was always introducing me to his (scientific) friends, including a large number of great theorists who in some cases have ended up collaborating and contributing greatly to the work presented here.

Also, I would like to thank all my collaborators in the Marcus lab. In particular, it was always great fun to work with Jeff Miller, who is not only an exquisite physicist but also a real wizard with computers and numerics! Thank you so much for your great sense of humor and your incredible patience with some of the harder spin-orbit fits and occasional really long phone calls! It was also a great pleasure to work with Edward Laird, always the proper English man, who soon became an expert in device fabrication. Sara Cronenwett, Joshua Folk, Andy Huibers and Michael Switkes were the senior students who taught me everything about dilution and ^{3}He refrigerators, lock-ins and sample fabrication and the physics of quantum dots. In particular, Josh was always ready to teach me experimental techniques and tricks and answer any of my questions on quantum dot physics. Special thanks also go to Alberto Morpurgo for many interesting physics discussions but also for a crash course in Italian cursing. I would also like to thank all the other Marcus group members, past and present, including Michael Biercuk, Nathaniel Craig, Leo DiCarlo, Slaven Garaj, Michael Janus, Alex Johnson, Heather Lynch, Nadya Mason, Jason Petta, Ronald Potok, Esteban Real, Floris Zwanenburg and everybody else.

Soon after arriving here at Harvard we were greeted warmly by the groups of Prof. Westervelt and Prof. Tinkham. It was always great to have you as neighbors and to sometimes spend a break with you. I would like to thank all of you, in particular Kathy Aidala, Ania Bleszynski, Marc Bockrath, Dolores Bozovic, Ian Chan, Steve Cronin, Parisa Fallahi, John Free, Katie Humphry, Tom Hunt, Blake Johnson, Benjamin Lee, Hak-Ho Lee, Brian Leroy,

Jeanie Lau, Nina Markovic, William Neils, Mark Topinka, Sergio Valenzuela, Andy Vidan and Muhammed Yildirim.

Over the years, Charlie has introduced me to and encouraged me to actively collaborate with various theorists. Yuli Lyanda-Geller was an essential collaborator on our 2D antilocalization experiments. In numerous meetings and countless hours spent discussing on the phone, via e-mail and during his visits here, Yuli has given Jeff and me a much deeper understanding and appreciation of the underlying physics and developed an amazing new theory describing the quasi ballistic regime... we would have been truly lost without Yuli's help. Thank you so much for your insistence and patience. Then we found antilocalization in quantum dots, and to our surprise, almost magically at about the same time, a preprint describing a new random matrix theory including the effects of spin-orbit coupling and in-plane magnetic fields came out, written by Igor Aleiner and Volodya Fal'ko. Soon after that, Jahn-Hein Cremers, Piet Brouwer and Volodya were working out the details and ensemble crossovers of this theory, allowing direct fits to our data. Thanks to a close collaboration with Prof. Halperin, Igor, Jan-Hein, Piet and Volodya, including a memorable meeting with Charlie and Igor in a bar on the lago di como in Varenna, Italy, it became possible to shed some light on the physics behind our data and do the quantitative fits shown in this thesis. Thank you all for your great insight and efforts!!

Volodya, together with Tomas Jungwirth, also had predicted significant orbital effects of an in-plane field, something we were also hunting for in our experiments, with the additional encouragement of Boris Altshuler, who had just worked out the 2D version together with Julia Meyer. At some point I realized that probably there was a low-temperature assumption in the theory, and I asked Volodya about the high-temperature version of the theory, applicable to our data. Amazingly, only a few days later, I received a 10-page fax with the theory worked out in great detail, ready to fit to the data, including high- and low-temperature regimes. We were all quite stunned! And with the new formulas, everything fell into place and this soon led us to coauthor another paper with Volodya and Tomas on orbital effects of an in-plane field (Chapter 5). Thank you very much for all your efforts!

My many thanks also go to Vitaly Golovach and Daniel Loss, who suggested to us to use the our few electron data to extract the interaction parameter ϕ and concurrence c. They were

guiding me how exactly to go about this and were tireless to answer my many questions by e-mail and phone and during exciting meetings here at Harvard and elsewhere! Without their support and guidance, this work would have been impossible, and I would like to express my deep appreciation.

There are various theorists with whom I have enjoyed and am enjoying a continuing dialogue and interactions at various meetings, and whom I would also like to thank very much. In particular I would like to mention Dima Abanin, Boris Al'tshuler, Andrei Bernevig, Hendrik Bruus, Guido Burkard, Markus Büttiker, Domenico Giuliano, Leonid Glazman, Walter Hofstetter, Leonid Levitov, Boris Spivak, Mike Stopa, Ned Wingreen and Fei Zhou. Thank you so much for all your time and patience.

As experimentalists working on GaAs quantum dots we depend to a large extent on our material growers, and I would like to use this opportunity to thank Prof. Art Gossard and his group at UC Santa Barbara, in particular Micah Hanson and Ken Campman, for supplying us with the GaAs 2D electron gases without which we cannot do our experiments. Many thanks also to Cem Duruöz and Prof. J. S. Harris at Stanford for giving us GaAs/AlGaAs heterostructures. Thanks also to Lukasz Zielinski, Sam Patel and Andy Huibers for device fabrication. Thanks for all your time and effort!

There were several visitors and collaborators who spent several months with the Marcus-group, always a very refreshing and inspiring experience. It was a great pleasure to work with David Goldhaber-Gordon, who too soon left Harvard for Stanford. Leo Kouwenhoven also spent a sabatical year here at Harvard, and it was amazing to have one of the founders and continuing pioneers of mesoscopic physics around to discuss and hang out with. Andy Kent was visiting Harvard for a year and had to suffer my endless typing on the computer upstairs in the visitor office. Thanks for your patience and companionship. Susan Watson from Middlebury college also visited Harvard several times, and was always a great to have around. Amir Yacoby was at Harvard on sabatical leave all year and was an important influence and inspiration with his deep physical insight on many (of my) experiments as well as great fun to have around! He also invited some of his students to Harvard, and it was a lot of fun meet and to host Hadar Steinberg, Jens Martin as well as Ophir Auslaender, who each stayed in my apartment for a few months. Thanks so much for your friendship

and many fascinating discussions!

All the cleanroom and facilities staff both here at Harvard as well as at Stanford deserve a big thanks for their commitment and relentless efforts to keep the facilities up and running, particularly Paul Jerabek, Tom Carver and John Schott at Stanford as well as Yuan Lu, Steve Shepard and John Tsakirgis here at Harvard. Many thanks also go to the group administrators, including Roberta Edwards, James Houlahan and particularly Jim Reynolds.

I would also like to extend my thanks to the Stanford crew and friends for their continuing friendship, in particular Adela Ben-Yakar, Andrei Bernevig, Ania Bujak, Soad Gileili, Domenico Giuliano, Dagmara Janowicz, Christian Kohler, Piefrancesco Landolfi, Alessandra Lanzara, Rodney Leng, Laila Mattos, Yamile Mejia, Alberto Morpurgo, Linda Oloffson, Mark Peterman, Laura Piccolo, Dana Porrat, Maria Paola Scaparra, Piero Scaruffi, Luis Sentis, Beata Szkop and Daniel Turler.

My friends here in Cambridge were always around for support and companionship, many thanks go to all of you, including Tzeni Aga, Adel Ahanin, Anne-Marie Aubert, Alceste Bonanos, Yue Nina Chen, Emmanouela Filippidi, Sandra Francisco, Andrea Gorbatai, Mohammad Hafezi, Cindy Hancox, Maria Kandyla, Eleni Katifori, Maryam Mirzakhani, Maryam Modjaz, Sara Passone, Farzan Persinejad, Bianca Santoro, Dee Sidalis, Ania Szybowski.

I would like to thank Jameson Marvin, Kevin Leong and all the guys from the Harvard Glee Club for a fantastic singing experience over the past three years, which includes performances of Mozarts Requiem and Beethovens Missa Solemnis as well as the traditional football concerts here in Sanders and at Yale, Princeton and a special excursion to Columbia University as well as some great spring tours to Florida and Northern California!

I would also like the Professors on my committee for their support and time to hear oral exams and thesis defense talks, as well as patience with the introduction of this thesis.

Very special thanks go to Parisa Fallahi, first for being a great travel companion in Japan, all across Europe as well as Iran, second for never getting tired of discussions of physics and

experiments, but most of all for being so encouraging, positive and supportive of me all the time with her generous love.

Last but not least, I would like to thank my family for their never ending support and love.

1.1 Introduction

The theory of quantum mechanics is among the most significant developments in science of the 20th century, with widely celebrated successes such as a deep understanding of the stability of matter, discrete emission and absorption spectra of atoms as well as the periodic table of elements. Quantum mechanics describes physics on a very small length scale comparable to the size of atoms and molecules, which are typically measured in units of Angstroms. With the recent advent of techniques that allow researchers to fabricate structures on a sub-micron length scale, quantum effects such as discrete energy levels due to size quantization, shell filling and various spin effects of electrons confined in so-called quantum dots have been observed. The fundamental quantum mechanics for these types of artificial atoms is the same as for natural atoms. However, there are several important differences that make these systems an excellent laboratory to investigate various aspects of quantum mechanics and give us access to exciting new regimes that are impossible to achieve in natural atoms. These systems are therefore very suitable for fundamental scientific study, but also offer great technological promise, as witnessed by the emerging fields of coherent electronics, spintronics and quantum computation. Besides the obvious quantum of electric charge which is readily accessible with electrical transport measurements, electrons also carry spin, a property which is interesting for many reasons, not the least of which is that it has no classical analog. Spin effects such as level pairing [186], bidirectional spin filtering [60], spin splitting in Zeeman fields [89, 168], millisecond long spin life times [66, 51], shell filling [193] and spin blockade [160, 167] have been reported in semiconductor quantum dots in recent years.

While the manipulation and study of single atoms has become possible in condensed matter experiments [47, 38, 140], the systems investigated in this thesis are mesoscopic objects, with length scales between the macroscopic every-day world and the microscopic world of elementary particles and atoms. Mesoscopic length scales span a range from tens of nanometers up to a few microns in size, typically encompassing hundreds to ten thousands of atoms of the semiconductor material that the dots studied here are fabricated in. A very important parameter characterizing mesoscopic systems is the coherence time τ_φ or equivalently, the coherence length L_φ, the length an electron can travel without loss of quantum mechanical
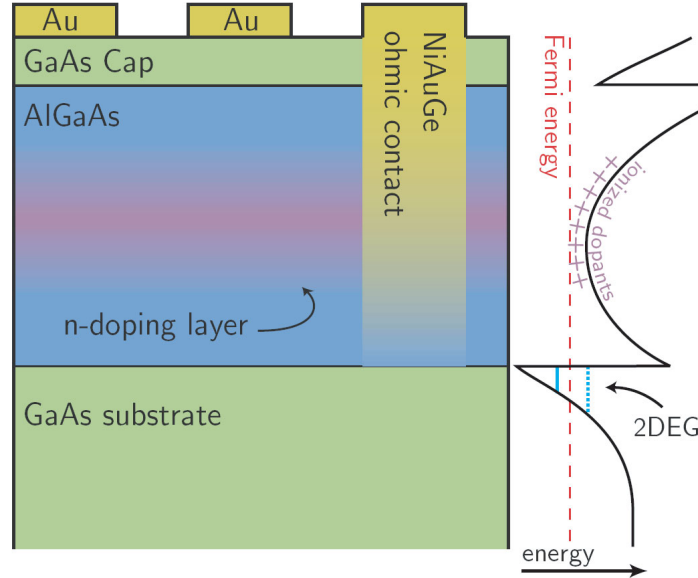
Figure 1.1: (left) Schematic diagram of a GaAs/AlGaAs heterostructure with Au Schottky gates deposited on the surface and annealed NiAuGe ohmic contact. The purple region represents modulation doping of the AlGaAs with an n-type dopant, typically Si. (right) Conduction band energy diagram showing the well at the GaAs/AlGaAs interface which confines the 2DEG and its quantum energy levels. At low temperatures, only the lowest energy level is populated. (Courtesy of M. Switkes, Ph. D. Thesis, Stanford University (1999))

phase coherence. This length sets the scale for observation of coherent quantum mechanical effects such as in interference experiments. In mesoscopic devices, the coherence length L_φ is larger than the size of the device investigated. This usually requires experiments to be performed at cryogenic temperatures and materials able to sustain sufficiently long coherence lengths.

1.2   GaAs 2D Electron Gases

The experiments reported in this thesis are based on a 2D electron gas (2DEG) formed at the interface of GaAs and AlGaAs layers. The choice of this material has several advantages which will be briefly summarized here, including mean free paths and coherence lengths exceeding tens of microns at base temperature of a dilution refrigerator. These heterostructure materials have enjoyed tremendous progress since the early 1980's and are the best realization of a two dimensional metal available today, with extremely high electron mobilities corresponding to mean free paths by far larger than typical device sizes, sometimes even
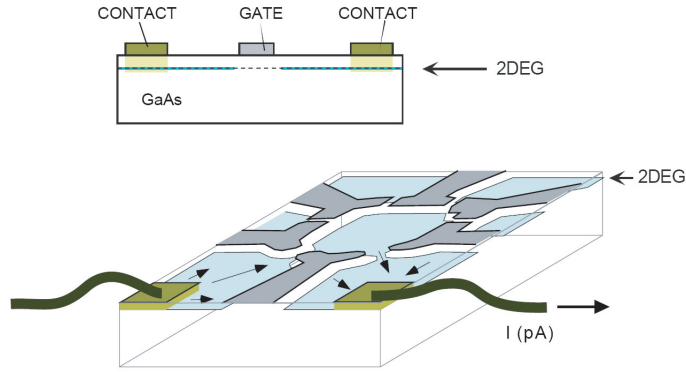
Figure 1.2: Side and perspective view of gated quantum dot structure (Courtesy of A. Huibers, Ph. D. Thesis, Stanford University (1999))

exceeding hundred microns. The electrons are typically confined along one direction in the lowest quantum mechanical state in a triangular potential at the GaAs/AlGaAs interface, see Figure 1.1, and move like free particles with a renormalized effective mass $m^* = 0.067 m_e$ (m_e is the free electron mass) in the plane of the remaining two dimensions, which is buried typically around 100nm below the surface. The combination of GaAs and AlGaAs materials which have practically identical lattice constants minimizing strain, super clean growth conditions in molecular beam epitaxy chambers resulting in nearly defect free interfaces and the modulation doping technique that removes the ionized Si-donor atoms away from the interface minimizing scattering allows the fabrication of extremely high mobility electron gases. Transistors built on these GaAs 2DEG's are today's lowest noise and highest frequency transistors and are extensively used in mobile telecommunication. If cooled to low temperatures and placed in high magnetic fields, integer [198] and fractional quantum Hall effects [188, 195, 189, 127] appear.

What makes semiconductor heterostructure materials attractive for mesoscopic experiments is a relatively large Fermi wavelength typically around 50 nm (compared to Angstroms in most metals) due to low carrier densities in the 2DEGs, long coherence times enabling the observation of coherent quantum mechanical effects as well as the easy gateability of this material, resulting in tunable devices. With today's micro fabrication techniques, in particular electron beam lithography, features comparable to the Fermi wavelength can readily be made. Fabrication of metallic gates on the surface of the heterostructure and application of voltages on these gates can be used to control the carrier density in the 2DEG and upon

3

application of a sufficiently negative voltage (typically around -0.3 V) the 2DEG underneath the gate can be depleted completely, creating a shadow of the gate in the 2DEG which electrons are forbidden to travel through, the size of which can be controlled by the applied voltage. This also enables one to confine the electrons in the remaining two dimensions in a tunable way, see Figure 1.2, allowing for the creation of quantum dots, in which the electrons are confined in all three directions [106, 118, 120]. The confinement at the heterointerface is usually substantially stronger than the lateral confinement due to the surface gates, with characteristic widths of the wave function of around $10\,\mathrm{nm}$ in the $\hat{z}$-direction perpendicular to the interface, whereas laterally the electrons are confined on a length scale of $30\,\mathrm{nm}$ or larger. Consequently, the electrons usually occupy only the lowest quantum mechanical state in the $\hat{z}$-direction, making these quantum dots two dimensional. While quantum dots fabricated in semiconductor materials are highly tunable by applying voltages that can control the confinement potential of the dot as well as the number of electrons on the dot, electrons in natural atoms are always bound by the spherically symmetric Coulomb potential generated by the nuclear charge.

1.3   The Closed Dot Regime

Whereas attaching leads to an atom is relatively difficult, it is easy to connect quantum dots to reservoirs allowing electrons to tunnel onto and out of the artificial atoms and hence probe the regime of measurable coupling. Direct measurement of electrical transport through a quantum dot is a very common method to investigate these systems, for a review see [118], although there are other ways to study quantum dots, including capacitance spectroscopy [13, 12]. All experiments reported in this thesis are based on electrical transport measurements. The coupling to the reservoirs can be achieved either with tunnel barriers— resulting in so called closed dot experiments because this type of coupling is relatively weak, effectively closing off the dot from the reservoirs—or with quasi 1D leads that carry one or more modes of quantum conductance, resulting in so called open dot experiments. Both the closed and open dot regimes are of great interest; I will focus first on closed dot experiments and discuss the open dot regime later.

In closed dot experiments, current through the dot can only flow if a state in the quantum

dot is available in the window of energy between the source and drain chemical potentials, which can be controlled with a bias voltage V_{SD} applied across the leads. Because of the sub-micron device sizes, which results in a small capacitance C of the dot to the rest of the system, adding an electron with charge e, in addition to the quantum confinement energy, costs a classical Coulomb charging energy $E_C = e^2/2C$ that can be much larger than the temperature T of the electrons, resulting in Coulomb Blockade of electrons [69, 173, 84, 146, 16, 190, 13]. The coupling strength of the dot to the leads can in many cases be tuned during the experiment with gate voltages. In the limit of weak coupling giving only lowest order sequential tunneling [16], which is the most commonly investigated case, electrons tunnel through the dot one by one. By supplying a finite energy via a source-drain voltage V_{SD}, not only ground states but also excited states can be observed [104, 62]. When coupling to the leads is increased, higher order cotunneling processes can become significant and in the limit of strong tunneling [42, 200], coherent superposition of all cotunneling processes involving spin flips can result in the Kondo effect [74, 39], a correlated many body effect which entangles electrons in the leads with the dot [73, 155].

1.4 Few Electron Quantum Dots

Though historically not the first quantum dots to be created, systems containing only a few electrons have become available over the last several years, both in structures where the tunneling onto and out of the dot is in the vertical direction [193, 118, 119] as well as in dots which couple to adjacent reservoirs laterally [176, 204, 36, 50, 168], see Figure 1.3. The number of electrons on the dot can be controlled one by one by changing a plunger gate voltage that effectively controls the size of the lateral confinement, allowing these devices to be completely emptied of electrons and enabling observation of one, two, three and larger number of electron systems all in the same device. While the confinement potential in quantum dots is tunable and often breaks circular symmetry [36, 168], fabrication of dots with circularly symmetric and close to harmonic potentials has also been achieved [193, 121] by etching a circular pillar into a 2DEG with a metallic gate covering part of the walls of the cylinder that is used to control the number of electrons on the dot. In these structures, electrons are confined in a circular 2D disc of variable radius where angular momentum is
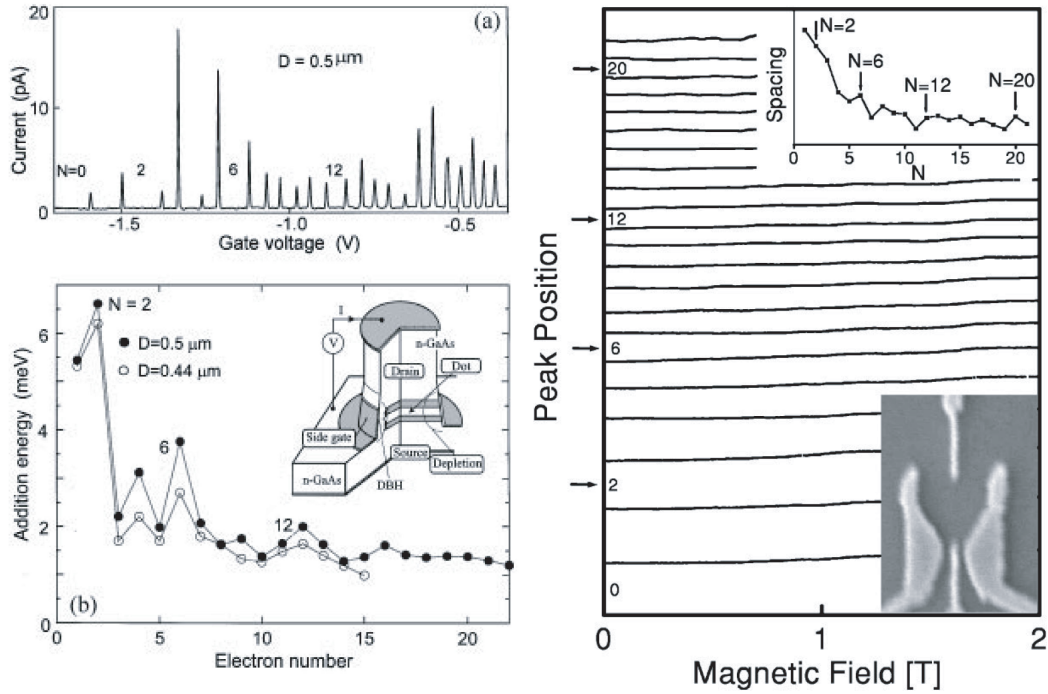
Figure 1.3: (left) Vertical few electron quantum dot displaying shell filling. (Courtesy of M. Ciorga, Reference [36]) (right) Lateral few electron dot where the confinement potential breaks rotation symmetry. (Courtesy of S. Tarucha, Reference [193])

a good quantum number, giving rise to a 2D shell structure in the addition energies which are filled according to Hund's rule [193, 121], in analogy with the 3D shell structure of atoms. Due to the 2D nature of these systems, the magic numbers of elements that have particularly large addition energies ("noble elements") are different from their 3D atomic counterparts.

The fact that these artificial atoms are substantially larger than their natural counterparts not only makes their fabrication possible, but also opens up magnetic field regimes that are not accessible in atoms. Due to the relatively large cross sectional area of these dots, application of magnetic fields $B_\perp$ perpendicular to the 2DEG on the order of a few Teslas, easily produced in laboratories with superconducting solenoid magnets, allows for observation of orbital effects of the applied magnetic field causing transitions in the level structure of the dot, for example a singlet to triplet ground state transition in quantum dot "helium" [191, 13, 182, 121, 194, 126]. In real atoms, this singlet-triplet transition is predicted to occur in a huge magnetic field on the order of 10^5 T, which is impossible to generate in a laboratory.

1.5 Larger Dots containing Many Electrons

By simply increasing the lithographic area enclosed by the gates when fabricating lateral dots, it is easy to make devices that contain essentially arbitrarily large numbers of electrons [141, 33], typically reaching up to hundreds or thousands in number but not usually exceeding ten thousands, as the loss of coherence coming with very large device sizes prohibits observation of the quantum mechanical effects of interest. These dots, though large compared to few electron dots discussed earlier, are still sufficiently small to be in the ballistic regime where electrons scatter only off the walls of the dot and impurity scattering is essentially absent. As most shapes of confinement potentials are classically chaotic with only a few highly symmetric exceptions such as the circle, these large quantum dots allow us to investigate the quantum mechanics of classically chaotic systems in the semiclassical limit of large quantum numbers.

The theory of quantum mechanics as developed by the pioneers of the early 20th century gives a prescription how to quantize systems with classically stable periodic orbits, such as the hydrogen atom, but fails to quantize classically chaotic systems. Though this was already pointed out by Einstein in 1917 [48], progress has been made only in 1970: chaotic systems can be quantized semiclassically via the Gutzwiller trace formula [83] which gives the energy eigenvalues in terms of unstable periodic orbits embedded in a sea of non-periodic, chaotic orbits. These unstable periodic orbits turned out to be important not only for the eigenvalues but also for the eigenfunctions of the system [93], which can have high probability amplitude along certain periodic orbits ("scarred states"). The tunability of the confinement potential with gate voltages as well as the quantum phase effects of orbital magnetic fields—readily observable even in small, mT-scale magnetic fields in such large devices—make large quantum dots suitable systems for investigating open questions of the correspondence principle and quantum chaos.

1.6 The Open Dot Regime

Often these larger devices are studied in the open dot regime where the quantum point contacts coupling the dot to the reservoirs are tuned to support one or a few fully trans-
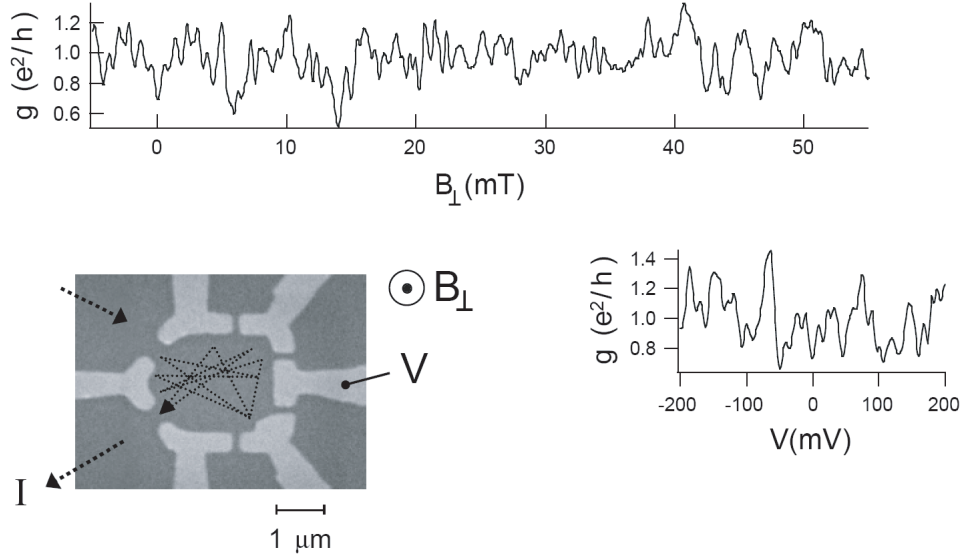
Figure 1.4: Conductance fluctuations through a quantum dot (left) as a function of perpendicular magnetic field (top) and gate voltage (right) . (Courtesy of A. Huibers, Ph. D. Thesis, Stanford University (1999))

mitting quantum modes of conductance each [141, 33, 97], since Coulomb Blockade may become harder to observe because the charging energy decreases with increasing dot area and can become smaller than the available temperature of the electrons. The level broadening $\Gamma = (N_L + N_R)\Delta/(2\pi)$ of a dot of area A due to escape out through the point contacts with N_L and N_R modes in the left and right leads is significant in this regime, becoming larger than the spin degenerate average level spacing $\Delta = 2\pi\hbar^2/(m^*A)$ even for only one mode in each point contact. Typical escape times $\tau_{esc} = \hbar/\Gamma$ are significantly larger than the crossing time $\tau_{cross} = \sqrt{A}/v_F$ an electron takes to traverse the device with the Fermi velocity v_F, corresponding to multiple bounces of electron trajectories in a semiclassical picture.

1.7 Mesoscopic Conductance Fluctuations

Transport through the dot occurs via a number of levels proportional to $\max(3.5kT, \Gamma)$ which can fluctuate randomly as a function of controllable parameters such as device shape, magnetic field and Fermi energy, resulting in a fluctuating conductance through the dot. These mesoscopic fluctuations of conductance can also be understood in terms of interference of multiple transport paths through the device, see Figure 1.4, in analogy to universal

conductance fluctuations in disordered mesoscopic samples [61, 125, 196, 6, 130]. Due to the large number of electrons in these devices, a description in terms of individual states is not usually convenient and one instead uses a statistical description of the system in terms of, for example, average, variance, correlations or distributions of conductance. This requires gathering of statistically independent samples, which in some earlier experiments had to be done in a cumbersome way, for example by thermal cycling the sample, but is easily accomplished in semiconductor quantum dot samples by simply changing gate voltages.

1.8   Weak Localization

Besides mesoscopic conductance fluctuation, weak localization [1, 7, 129] is another hallmark feature of mesoscopic systems, first discovered in disordered metallic samples [43, 19], and widely used to measure phase coherence in various systems [35]. Weak localization is a quantum mechanical interference effect of trajectories scattering back to their point of origin, see Figure 1.5. In the absence of a magnetic field breaking time reversal symmetry and assuming coherence is not lost, the quantum phase of a semiclassical electron accumulated along a closed trajectory returning to its origin is exactly the same as the phase of the time reversed trajectory, creating constructive interference and an increased probability for the electron to remain at the origin, hence increasing the backscattering amplitude and decreasing conductance. To obtain the conductance, all possible trajectories need to be summed up. If time reversal symmetry is broken with a small orbital magnetic field, the phases of the two trajectories can differ due to a Aharonov-Bohm phase [2] and the constructive interference can be suppressed, resulting in a characteristic dip at zero field in the magneto conductance. If coherence is lost on a length scale L_φ, then effectively all trajectories of length L greater than L_φ are cut off from the sum and reduction of conductance at zero field is less pronounced than in the fully coherent situation. The 0D equivalent of weak localization was observed in closed quantum dots [59] as well as open quantum dots [98, 96], and was used to study the coherence time τ_φ, finding that τ_φ is independent of the dot size.
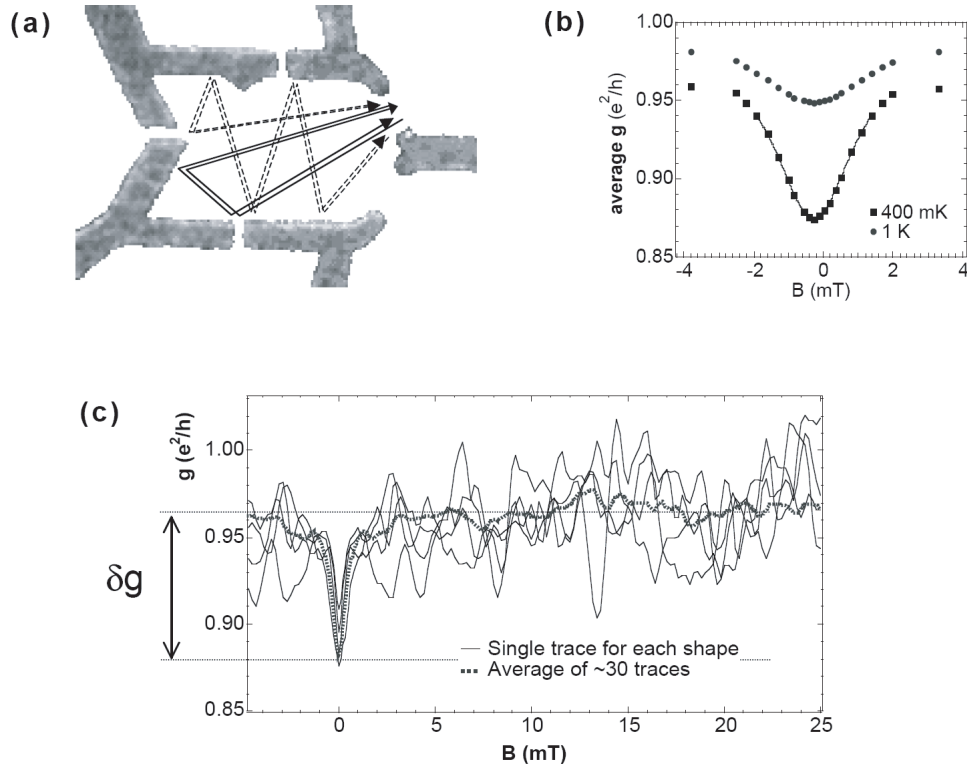
Figure 1.5: (a) A pair of paths contributing to weak localization in a $4\,\mu\mathrm{m}^2$ quantum dot. (b) Average conductance as a function of magnetic field obtained from sampling different dot shapes using a gate at $T = 400\,\mathrm{mK}$ and $T = 1\,\mathrm{K}$. (c) Average conductance and individual conductance traces as a function of magnetic field. (Courtesy of A. Huibers, Ph.D. Thesis, Stanford University (1999))

1.9   Universal Distributions of Level Spacings

Obviously, the spectral properties of these dots are very important and determine transport through the dot. Quite remarkably, the distribution of eigenenergies displays universality, depending only on whether the dot is classically chaotic or integrable and depending on additional symmetries of the system, such as time reversal symmetry and spin rotation symmetry, but is independent of other details of the system, such as the particular device shape, which of course is what determines the detailed dynamics [20]. The quantum level spacing probability distribution of an ergodic, classically chaotic system turns out to be given by Wigner-Dyson statistics, whereas a classically regular system has a Poissonian distribution of quantum level spacings. Interestingly, the imaginary parts of the zeros of the Riemann Zeta function follow exactly the same Wigner-Dyson statistics as the quantum

levels of a classically chaotic system when time reversal symmetry is broken, giving a seemingly deep but curious connection between the distribution of prime numbers and quantum chaos [21]. Maybe more importantly, the eigenvalue distributions of complex Hermitian matrices also obey the same Wigner-Dyson statistics, allowing a description of chaotic, ergodic quantum dots in terms of theories of random matrices, which were first developed by Wigner, Dyson, Metha and others starting in the 1950s to describe the complex many-body physics of compound nuclei.

1.10 Random Matrix Theory

Random matrix theories ignore the particular details determining the microscopic Hamiltonian and retain only the fundamental symmetries of the system which are used to constrain the random matrices H based upon which calculations are done, assuming the system is ergodic. For a thorough review see [17, 5]. A characterization of systems can be done using a symmetry parameter β that counts the degrees of freedom of the elements of H. β can take the values $\beta = 1$ for systems with time reversal symmetry resulting in the real, symmetric matrices H of the Gaussian orthogonal ensemble (GOE), $\beta = 2$ for systems with broken time reversal symmetry giving the matrices of the Gaussian unitary ensemble (GUE) and $\beta = 4$ for systems with time reversal symmetry intact but broken spin rotation symmetry, giving the matrices of the Gaussian symplectic ensemble (GSE), whose matrix elements are the four dimensional quaternions which can be parameterized in terms of pauli spin matrices. The matrix elements in all of these ensembles are taken to have an independent Gaussian distribution. Coherent transport through quantum dots is very successfully described by random matrix theories, see Figure 1.6.

1.11 Scattering Matrix Formalism

As the dots are connected to the leads via a variable number of open channels, a description in terms of an isolated Hamiltonian is no longer appropriate. Rather, a formalism based on the scattering matrix S of the dot is often used, where S describes the reflection and transmission probabilities of the dot coupling to the various channels. The conductance through
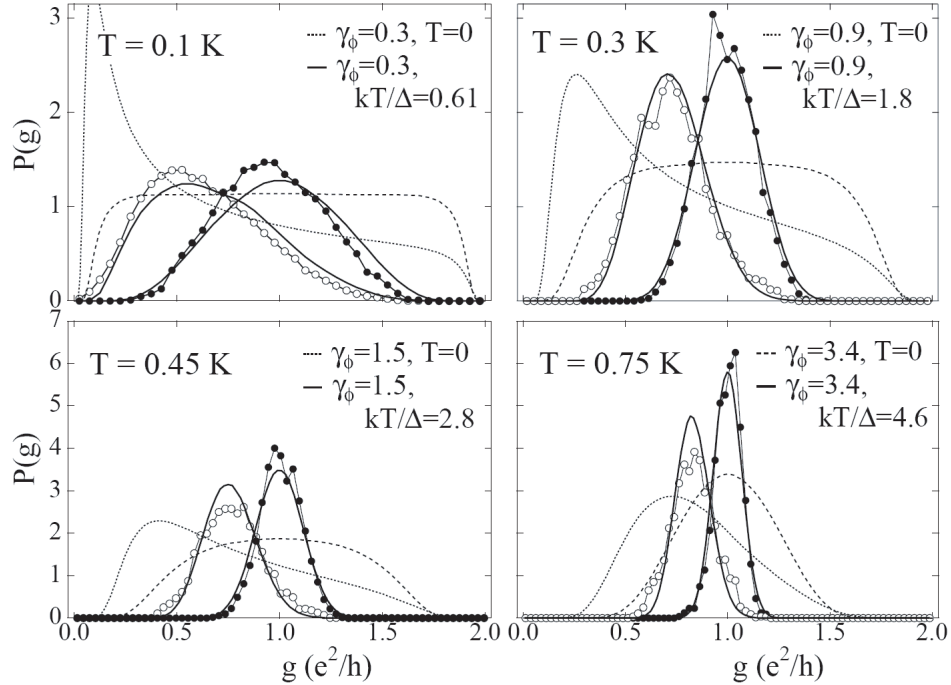
Figure 1.6: Measured conductance distributions for $B = 0$ (open circles) and $40\,\mathrm{mT}$ (closed circles) for a $0.5\,\mu\mathrm{m}^2$ dot at four temperatures. Curves show theoretical $\beta = 1$ (dotted) and $\beta = 2$ (dashed) distributions for $T = 0$ and for measurement temperatures (solid). (Courtesy of A. Huibers, Reference [97])

the dot can then be written with the widely used Landauer formula as $g = (2e^2/h)\,Tr\,tt^{\dagger}$, where the transmission matrix t relates an incoming wave from one lead to an outgoing wave in the other lead. The scattering matrix can be related to the isolated Hamiltonian via a simple matrix equation involving coupling constants $W_{\mu,a}$ that characterize the coupling of the scattering states $|a\rangle$ at the Fermi energy in the leads with the eigenstates $|\mu\rangle$ of the dot [25]. There are various approaches to calculate statistical properties of conductance through the dot, including Monte-Carlo simulations and diagrammatic Green's function methods to average over the Hamiltonian. Instead of considering random Hamiltonians, a random matrix theory can be constructed based on random unitary scattering matrices, which can in principle be done for any number of open channels in the leads, though often calculations become substantially easier in the limit of a large number of modes in the point contacts $N \to \infty$. It is common to include the effects of decoherence into random matrix theories via a third voltage probe [29, 25] that decoheres electrons but draws no current, characterized with a non-integer number of decoherence modes $\gamma_{\varphi} = h/(\tau_{\varphi}\Delta)$. Effects of finite temperature can also be included via thermal smearing the zero temperature expressions.

1.12 Spin-Orbit Coupling

1.12.1 Introduction and Basics

Another interesting property of GaAs 2D electron gases is spin-orbit coupling. Spin-orbit coupling is a relativistic effect that can be derived from first principles starting with the covariant Dirac equation of a spin 1/2 particle and shows up as one of the lowest order relativistic corrections to the non-relativistic pauli theory, leading to the fine-structure splitting in atomic spectra [99]. In atoms, it is due to the nuclear electric field and becomes strong for large nuclear charges. On a more intuitive level, it can be understood as a coupling of the electron spin to a magnetic field arising from a Lorentz-transformed electric field. As is known from the theory of special relativity, an electron moving with velocity $\overrightarrow{v}$ through an electric field $\overrightarrow{E}$ also feels a magnetic field $\overrightarrow{B_{so}} = -(\overrightarrow{v}/c \wedge \overrightarrow{E})/\sqrt{1 - v^2/c^2}$ in its rest frame [103] which is orthogonal to both the direction of motion as well as the electric field, where c is the speed of light. This spin-orbit magnetic field couples to the electron spin via $\overrightarrow{\sigma} \cdot \overrightarrow{B_{so}}$ and leads to a Larmor spin precession. To calculate the coupling constant correctly, the Thomas precession, a further relativistic effect leading to an opposite precession of half the size, needs to be taken into account as well. However, direct expansion of the Dirac equation in the non-relativistic limit to first order in c^{-2} directly yields the correct coupling strength

$$H_{so} = -\overrightarrow{\sigma} \cdot (\overrightarrow{E} \wedge \overrightarrow{p}) e\hbar/(4m^2c^2). \tag{1.1}$$

Note that spin-orbit coupling, though involving effective spin-orbit magnetic fields, does not break time reversal symmetry and therefore the Kramers degeneracy holds.

1.12.2 Rashba Term

The conduction band electrons involved in transport in GaAs 2DEG's are moving with the Fermi velocity of typically a few $100,000\,\mathrm{m/s}$ in electric fields that can be present either due to the heterointerface resulting in the Rashba term [31] or due to absence of inversion symmetry in the Zinc-blende structure of GaAs, leading to the Dresselhaus term [44]. The Rashba term originates from the electric field perpendicular to the 2DEG that confines the the electrons at the heterointerface and is therefore a pure 2D term which is absent in bulk

GaAs. The Rashba spin-orbit magnetic fields therefore always lie in the plane of the 2DEG. It has the form

$$H_R = \alpha_2(\sigma_x k_y - \sigma_y k_x), \tag{1.2}$$

i.e. linear in momentum or wave vector $k_{x,y}$, with a coupling constant α_2. The Rashba term causes the spin to precess around the $\hat{x}$-axis if an electron is moving along the $\hat{y}$-direction and vice versa, with the axis of rotation perpendicular to the velocity and in the plane of the 2DEG for motion in an arbitrary direction in the 2DEG. The Rashba term by itself is isotropic, i.e. the precession frequency is independent of the direction of motion of the electron, but the axis of rotation depends on the direction of motion. Though seemingly intuitive, it is wrong to think that the Rashba term is proportional to the average electric field confining the electrons. Rather, a full bandstructure calculation needs to be performed to capture the Rashba effect quantitatively. In nearly symmetric quantum wells, the Rashba term has been shown to be tunable with externally applied gate voltages that control the asymmetry of the well [115, 156]. However, in heterostructures which have a triangular confinement potential, the Rashba coefficient α_2 is roughly independent of gate voltage [91], but H_R depends on carrier density via the wave vector $|\vec{k_F}| = \sqrt{2\pi n}$.

1.12.3 Dresselhaus Terms

The Dresselhaus terms appear in semiconductor crystals lacking inversion symmetry giving polar bonds which cause electric fields between the atoms leading to spin-orbit coupling. The crystal structure of GaAs is face centered cubic with a 2 atomic basis, with one Ga and one As atom each in the unit cell, yielding the zinc blende structure of two simple cubic lattices offset by a quarter of the body diagonal. Inversion symmetry about the point midway between two nearest neighbor atoms is broken because one of the atoms is Ga and the other one is As with a polar bond between them, unlike in Si, which has the same crystal structure but all filled with Si atoms conserving inversion symmetry. The bulk 3D spin-orbit Hamiltonian for conduction electrons near the bottom of the band can be derived in a band structure calculation treating the spin-orbit Hamiltonian $H_{so} = -\vec{\sigma} \cdot (\vec{\nabla} V \wedge \vec{p}) e\hbar/(4m^2 c^2)$ as a perturbation, giving [44]

$$H_D^{3D} = \gamma[\sigma_x k_x(k_y^2 - k_z^2)] + cyclic, \tag{1.3}$$

where γ is a material parameter characterizing the polarity of the Ga-As bond. Note that $H_D^{3D} = 0$ if the motion is purely along one of the axes $\hat{x}, \hat{y}, \hat{z}$ and the dependence on k is cubic in 3D. However, in a 2DEG grown along the [001] direction, the wave vector in the $\hat{z}$-direction is quantized. Using $\langle k_z \rangle = 0$ but keeping terms $\langle k_z^2 \rangle \neq 0$, the 2D form follows, with a term linear in k given by

$$H_D^{(1)} = \alpha_1(-\sigma_x k_x + \sigma_y k_y), \tag{1.4}$$

where $\alpha_1 = \gamma \langle k_z^2 \rangle$ depends on the width of the wave function in the $\hat{z}$-direction, and a term cubic in k reading

$$H_D^{(3)} = \gamma(\sigma_x k_x k_y^2 - \sigma_y k_y k_x^2). \tag{1.5}$$

Because the width of the wave function is typically only weakly dependent on the carrier density, the linear Dresselhaus coefficient α_1 is also roughly independent of density, similar to the Rashba coefficient, but all three spin-orbit terms can be tuned by changing the fermi velocity, for example with a gate changing the carrier density in the 2DEG. Due to the relatively stronger k-dependence of the cubic Dresselhaus term compared with the linear terms, the cubic term is relatively weak at low densities and can become somewhat stronger in magnitude than the linear terms at densities, though all three terms turn out to be of the same order of magnitude in typical GaAs heterostructure materials.

1.12.4 Weak Antilocalization

The signature of spin-orbit coupling in quantum transport is weak antilocalization, a maximum of conductance at zero magnetic field [94, 8]. It is the analog of weak localization in the regime where the spin of the electron traveling along a closed trajectory interfering with its time-reversed path is rotated substantially compared to the initial spin state. Because the rotation group of a spin 1/2 particle is SU(2), which has the characteristic property that a full 2π rotation around any axis gives *minus* the unrotated spinor, the constructive interference which gives rise to the conductance minimum of weak localization of the spin-less particle becomes *destructive* interference if the relative rotation of the electron spin having completed a closed trajectory and its time-reversed echo is 2π. Note that because spin-orbit coupling conserves time reversal symmetry, the spin rotation $R \in SU(2)$ undergone by the

electron completing a closed trajectory forward in time is exactly the inverse of the rotation of the electron spin traveling along the time reversed trajectory. Starting with an initial spin $|s\rangle$, the two final spin states corresponding to the two directions in which a closed trajectory can be traversed are $|s'\rangle = R|s\rangle$ and $|s''\rangle = R^{-1}|s\rangle = R^{\dagger}|s\rangle$, due to the property $R^{\dagger}R = \mathbf{1}$ of all $R \in SU(2)$. The relevant interference term therefore contains the projection $\langle s'|s''\rangle = \langle s|R^2|s\rangle$. In the limit of strong spin-orbit coupling, the rotated spins $|s'\rangle$ are as likely to point in a specific direction as in any other direction after completion of a closed trajectory, giving an isotropic distribution of spinors on the pauli sphere over which $\langle s|R^2|s\rangle$ needs to be averaged when summing up all possible trajectories. It is straightforward to perform this isotropic spin average, for example using an Euler angle parametrization of R [58], giving exactly $\langle s|R^2|s\rangle = -1/2$ [18], which is negative and half the amplitude of the spin-less case. This results in a conductance maximum at zero field and in the opposite sign of magneto conductance compared to weak localization. In the regime of intermediate strength spin-orbit coupling where trajectories resulting in significant spin rotations need to be rather long but are still shorter than the coherence length, a combination of weak localization at large magnetic fields where long trajectories are cut off and weak antilocalization at small magnetic fields also allowing longer trajectories is possible.

1.12.5 Elliot and Dyakonov-Perel Mechanisms

Weak antilocalization was first discovered in disordered metallic samples, for example in the elegant experiments of Bergmann [19]. In metals, the spin-orbit coupling mechanism is quite different from the semiconductor picture described above. Rotations occur during elastic scattering event with the heavy nucleus of the host atoms and the spins are invariant during ballistic motion. This situation is commonly referred to as the Elliot mechanism [49]. In semiconductors, on the other hand, the elastic scattering is due to remote donors and leaves the spin invariant, with the spin action taking place during ballistic propagation. This is referred to as the Dyakonov-Perel mechanism [46], though with this name it is usually additionally assumed that the electron motion is diffusive with only small spin rotations between elastic scattering events causing a spin random walk. This last assumption is not necessarily fulfilled in some of the higher mobility and high density 2DEG's investigated in this thesis, which has required us to search for a new theory applicable beyond the diffusive

approximation to interpret the measurements. In metals the spin-orbit coupling strength depends strongly on the nuclear charge, resulting in weak spin-orbit scattering in the light metals such as magnesium and in strong spin-orbit scattering in metals such as gold [19]. It is mentioned that spin-orbit scattering, even though it creates an effective randomization of the electron spin, is a coherent effect, markedly different from magnetic scattering or other spin flip scattering causing loss of coherence that results in a suppression of weak-localization but can never lead to antilocalization. The experimental observation of antilocalization in a solid state system is an elegant demonstration via a quantum interference experiment that spin $1/2$ particles must be rotated by 4π to transfer the spin wave function onto itself. This important consequence of the quantum mechanics of spin $1/2$ particles was previously only observable in rather sophisticated neutron interference experiments.

1.13   Preview of Chapters and Outlook

1.13.1   Chapter 2: Antilocalization Experiments in 2D

This rest of this thesis is organized by publications. Chapter 2 discusses 2D experiments investigating spin-orbit coupling in Hall bars, where a top-gate tuned transition from weak localization at low carrier concentrations to antilocalization at high carrier concentrations was observed. Though antilocalization had been observed previously in high density GaAs 2DEG's [45] establishing the Dyakonov-Perel mechanism of spin-orbit coupling as well as in other 2DEG materials, notably InGaAs [113], the samples investigated here have comparatively high mobility. This makes the diffusive approximation employed in existing theories not applicable for most of the data taken, and a new theory had to be developed that allowed for significant spin rotations between elastic scattering events and taking into account in a coherent way the various spin-orbit terms. Based on this theory, the Rashba as well as the linear and cubic Dresselhaus coefficients could be determined from the experiment by fitting to the density dependence of the spin-orbit fields H^*_{eff} and H^*_{so} characterizing the spin-orbit strength at a given density, allowing the angular dependence of the spin-rotation frequencies to be calculated. It was found that the Rashba and both Dresselhaus terms are of comparable magnitude, though the cubic Dresselhaus term depends more strongly on carrier density, and the coefficients extracted are consistent with both band structure

calculations as well as previous experiments.

1.13.2 Chapters 3 and 4: Spin-Orbit Experiments in Quantum Dots

Chapter 3 and 4 present an experimental investigation of spin-orbit coupling in quantum dots. These investigations are motivated by experiments of Folk et al. [59] and theory describing these experiments by Halperin et al. [87] finding evidence of spin-orbit coupling in the variance of open quantum dots in in-plane fields. Antilocalization in large dots made in high carrier density material was found, while a suppression of spin-orbit effects in smaller devices made on the same high density material was observed. Also, a suppression of spin-orbit effects in large quantum dots made on a more conventional, lower density 2DEG was also seen. The measurements presented include both average conductance as well as variance of conductance, and the effects of temperature as well as magnetic fields $B_\perp$ perpendicular and $B_\parallel$ in the plane of the 2DEG were investigated. $B_\parallel$ suppresses antilocalization and weak-localization is recovered at moderate in-plane fields $B_\parallel < 1\,\mathrm{T}$. The spin-orbit coupling strength is seen to be independent of temperature. The phase coherence time τ_φ depends strongly on temperature, in agreement with previous experiments. In a dot with a center gate covering a small area inside the dot, spin-orbit coupling could be tuned from more pronounced antilocalization than the ungated device to weak localization. The effects of spin-orbit coupling on the variance of conductance are also significant and can be characterized in terms of novel spin rotation symmetries in the system. When spin-rotation symmetry is broken due to spin-orbit coupling, such as in a dot showing antilocalization, the variance in presence of a small, time-reversal symmetry breaking perpendicular field depends only weakly on the in-plane magnetic field, whereas in devices showing weak localization where spin-rotation symmetry is intact, the variance in an in-plane field is reduced by a larger factor, consistent with the earlier experiments [59]. The measurements reported here are all in quite good agreement with a new extension of random matrix theory by Aleiner and Fal'ko [4] and Cremers, Brouwer and Fal'ko [37] that includes the effects of spin-orbit coupling and parallel magnetic fields.

Spin-Orbit Hamiltonian and Spin-Orbit Length

This random matrix theory includes the spin-orbit terms linear in momentum and neglects the cubic Dresselhaus term. Effects of the cubic term are subject of ongoing investigations, but are currently thought to not qualitatively change the physics, although there may be significant quantitative effects due to a possibly weaker suppression of the cubic term compared to the linear terms in small dots. Keeping only the linear terms, the spin-orbit Hamiltonian can then be rewritten as [4]

$$H_{so} = \frac{1}{2m^*}[(p_1 - \frac{\hbar\sigma_2}{2\lambda_1})^2 + (p_2 + \frac{\hbar\sigma_1}{2\lambda_2})^2] \tag{1.6}$$

using a coordinate transformation into a system with axes along the crystallographic directions $\vec{e_1} = [110]$ and $\vec{e_2} = [1\bar{1}0]$, where the spin-orbit lengths $\lambda_{1,2} = \hbar^2/(2m^*(\alpha_2 \pm \alpha_1))$ are defined as the distance an electron has to travel ballistically along the 1,2 direction to acquire a rotation of its spin by one radian. Note that motion along the 1-direction results in precession of the spin around the 2-axis. An interesting but unusual regime is obtained when Dresselhaus and Rashba coefficients are equal, resulting in one of the λ's being infinite, corresponding to no spin-orbit effects along that direction due to a cancelation of Dresselhaus and Rashba terms. It is convenient to introduce the average spin-orbit length $\lambda_{so} = \sqrt{|\lambda_1\lambda_2|}$ and the spin-orbit anisotropy $\nu_{so} = \sqrt{|\lambda_1/\lambda_2|}$. The suppression of antilocalization due to confinement in dots of size $L << \lambda_{so}$ is due to translational invariance combined with the fact that infinitesimal rotations commute.

Suppression of Spin-Orbit Coupling in Small Dots

To understand this in some more detail, consider a closed trajectory of an electron in the shape of a rectangle with elastic scattering at the corners (A,B,C,D) due to the confinement potential of the dot, see Figure 1.7. Magnetic fields weak enough to not bend electron trajectories significantly are assumed. Due to time reversal symmetry, the spin-rotation R_{BA} acquired by going from A to B is the inverse of going from B to A, $R_{AB} = R_{BA}^{-1}$. If translational symmetry is present as well, R_{BA} is also the inverse of going from C to D, $R_{DC} = R_{BA}^{-1}$. An electron going once around the rectangle starting in a spin state $|s\rangle$ ends up in a state $|s'\rangle = R_{AD}R_{DC}R_{CB}R_{BA}|s\rangle = R_{CB}^{-1}R_{BA}^{-1}R_{CB}R_{BA}|s\rangle$. Note that the first
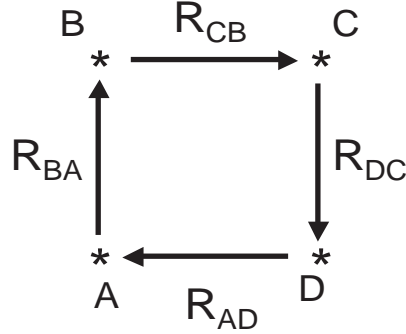
Figure 1.7: Illustration of a rectangular trajectory.

two rotations $R_{CB}R_{BA}$ are not undone in reverse order $R_{BA}^{-1}R_{CB}^{-1}$, in which case $|s\rangle = |s'\rangle$ would always result. Due to the non-Abelian nature of the SU(2) spin rotations, the order in which rotations are applied matters. This results in appreciable spin-rotations $|s'\rangle \neq |s\rangle$ and antilocalization in the case where the device size is comparable with the spin-orbit length giving substantial spin rotations upon traversing the dot. However, as is known from elementary mechanics [75], infinitesimal rotations commute to lowest order, and in the limit $L << \lambda_{so}$, the rotations a spin feels when traversing the dot are infinitesimal rotations giving $R_{CB}^{-1}R_{BA}^{-1} \sim R_{BA}^{-1}R_{CB}^{-1}$ resulting in $|s'\rangle = |s\rangle$ and a suppression of antilocalization. Interestingly, if $\alpha_1 = \alpha_2$, half of the rotation matrices are the identity matrix, say $R_{CB} = \mathbf{1}$, resulting also in $|s'\rangle = |s\rangle$. The particular geometry of a rectangular trajectory can easily be extended to all closed, returning paths. The discussion of the suppression of spin-orbit effects applies to the linear as well as cubic terms, as the rotations used above are generic. However, the linear terms are strongly suppressed scaling in size with a large power as $(L/\lambda_{so})^4$, whereas the cubic term might scale with a weaker power. Therefore, the cubic term might possibly become stronger than the linear terms in small dots.

Conclusions

The good agreement between theory and experiment represents quite a stringent test on quantum mechanics, the special theory of relativity from which spin-orbit coupling arises as well as the statistical description employed by random matrix theory. Further, a spin-filter based on a quantum dot in the regime of strong spin-orbit coupling can be proposed, working analogous to the quantum interference based bipolar quantum dot spin-filter recently shown

20

experimentally by Folk et al. [60], but replacing the strong Zeeman field that creates the spin splitting with the spin-orbit coupling in the dot where time reversal symmetry is broken with a small mT-scale perpendicular field. The challenge is to build a device small enough to have only one or a couple of levels in the window of transport of width $3.5kT$ while still maintaining significant spin-orbit coupling. This may potentially be achieved in GaAs by using a proposal by Brouwer et al. [26], where spatially inhomogeneous spin-orbit coupling can undo the suppression of spin-orbit coupling in small devices, essentially by breaking the translational symmetry mentioned in the above discussion. Alternatively, materials with stronger spin-orbit coupling could be of interest, such as InAs or hole systems, where the spin-orbit coupling is very strong, with a spin-orbit length of the order of $100\,\mathrm{nm}$. However, one of the properties that makes GaAs electrons so attractive is that by using devices of different sizes, spin-orbit coupling can be controlled very effectively, going from a regime of significant rotations in large devices to very weak spin-orbit effects in small devices. The suppression of the energy scales describing spin-orbit effects is quite strongly dependent on the dot size and for the linear spin-orbit terms scales as $(L/\lambda_{so})^4$ [4], allowing for very long spin life times of up to a ms in few electron dots, as recently reported [66, 52].

1.13.3   Chapters 3-5: Orbital Effects of an In-Plane Magnetic Field

Even though the GaAs 2DEG's used in the experiments reported are the best realization of a two-dimensional metal available, there are still effects representing a deviation from true 2D behavior due to the finite width of the wave function that can become important when modest in-plane fields $B_\parallel$ of about $1\,\mathrm{T}$ are applied, even in the absence of occupation of higher sub-bands and in the absence of spin-orbit coupling effects. This was first predicted by Fal'ko and Jungwirth [56] in 2D quantum dots and Meyer and Alt'shuler [148, 149] in bulk 2D. The naive view of transport in a planar, 2D metal suggesting that in-plane fields $B_\parallel$ couple only to the spin degree of freedom, allowing applied magnetic fields to be separated in spin and orbital parts, has to be replaced with a more rich picture of quantum transport in 2D systems, where in-plane fields can have significant orbital coupling, break time reversal symmetry and generate mesoscopic conductance fluctuations. In chapters 3 and 4, these effects are evident as a suppression of weak-localization corrections to conductance on a one-Tesla $B_\parallel$ field scale, due to breaking of time reversal symmetry by $B_\parallel$. Analogously,

on the same $B_\parallel$ scale, the variance at $B_\perp = 0$, which is also sensitive to time reversal symmetry, is reduced to the variance at $B_\perp \neq 0$ in an in-plane field $B_\parallel$. By assuming that the combined effects of spin-orbit coupling and orbital effects of the in plane field can be written as a product of the random-matrix theory and a correction factor due to the Fal'ko-Jungwirth theory [56], good agreement with theory is found. The orbital effects of $B_\parallel$ breaking time reversal symmetry are due to a trivial term due to surface/interface roughness effectively converting the applied $B_\parallel$ into a $B_\perp$ fluctuating in space and an additional term due to the inversion-asymmetry of a triangular heterostructure, which would be absent in a symmetric well. The later term has a strong B^6 term and can be estimated from self-consistent simulations, which gives reasonable agreement with the experiment.

In Chapter 5, orbital effects of $B_\parallel$ on the electron dispersion relation going beyond breaking of time reversal symmetry are investigated using mesoscopic conductance fluctuations and their correlations, finding effects of an anisotropic effective mass term. Symmetries of conductance in $B_\perp$ and $B_\parallel$ are investigated, and a $B_\parallel$ correlation field that depends strongly on $B_\parallel$ is observed, which is attributed to the anisotropic mass term and the term due to absence of inversion symmetry in a triangular heterostructure. The coefficients extracted from the full correlations of conductance fluctuations at a field $B_{\parallel 1}$ with conductance fluctuations at a field $B_{\parallel 2}$ are in good agreement with the previous weak-localization measurements. The measurements of conductance correlations requires a dot stable over the period of measurements up to several hours staying free from switching noise of charged impurities, which, when present, can artificially destroy the conductance correlations. A way to quantize switching noise is to correlate $g(B_\perp, B_1 \parallel)$ with $g(-B_\perp, -B_\parallel)$, which, in the absence of switchers, has to be maximally correlated due to Landauer-Büttiker symmetry $g(B_\perp, B_\parallel) = g(-B_\perp, -B_\parallel)$. The devices made on the low density material were fairly stable, giving correlations > 0.8, whereas in the high density devices, switching was far more frequent, making such a measurement unfeasible. In fact, one of the major practical limitations today in the field of GaAs quantum dots is switching noise due to charge rearrangement somewhere in the material rather close to the dot and it is not quite known yet how create quiet GaAs 2DEG materials.

1.13.4 Chapter 6: Cotunneling Spectroscopy in Few Electron Quantum Dots

Chapter 6 presents experiments done in few electron quantum dots in the regime of strong coupling to the leads allowing cotunneling processes. Inelastic cotunneling is used to measure the singlet-triplet splitting J of the two electron dot both below and above a singlet-triplet transition induced with a perpendicular magnetic field. J is an important parameter for realizing a proposed scheme of a spin-based qubit in GaAs quantum dots [133]. It controls the Heisenberg exchange interaction $J\overrightarrow{S_1} \cdot \overrightarrow{S_2}$ [28], which can be used to perform quantum gate operations such as a swap and square-root of swap that can be used to entangle two electrons if J can be controlled as a function of time. The $J \sim 0.2\,\mathrm{meV}$ measured here was significantly smaller than the single particle excited state energy of $\Delta_1 = 1.2\,\mathrm{meV}$, indicating strong electron-electron interactions, and could also be tuned with a plunger gate voltage V_g due to effects going beyond a simple shift of the dot potential [194, 117]. The field dependence $J(B)$ is in reasonable quantitative agreement with theoretical calculations. From the magnetic field dependence of the single-particle excited state splitting $\Delta_1(B)$, an anisotropic confinement was deduced, based on a 2D anisotropic harmonic oscillator model, which also gave consistent results for the second single-particle excited state $\Delta_2(B)$. The harmonic confinement energies found are $\hbar\omega_a = 1.2$ meV and $\hbar\omega_b = 3.3$ meV, giving a spatially elongated potential with main axes of lengths $\ell_a = \sqrt{\hbar/(m^*\omega_a)} = 31$ nm and $\ell_b = \sqrt{\hbar/(m^*\omega_a)} = 19\,\mathrm{nm}$.

Inelastic cotunneling through the single-particle Zeeman split ground state [116] was used to measure the Zeeman energies in the one electron system as a function of different directions of an in-plane magnetic field $B_\parallel$, finding no directional dependence of the Zeeman splitting. A zero-bias anomaly in the three electron system due to the Kondo effect was observed, and was seen to split in an in-plane magnetic field $B_\parallel$, confirming independence of the direction of $B_\parallel$ in the plane of the 2DEG. The slopes of the Kondo peak splitting Δ_K as a function of $B_\parallel$ are consistent with the isotropic g-factors $|g| \sim 0.44$ extracted from the $N = 1$ inelastic cotunneling splitting Δ_{Cot}, but the Kondo splitting $\Delta_K(B)$ does not extrapolate to $\Delta_K(0) = 0$, giving an additional small offset of $8 \pm 2\,\mu\mathrm{eV}$. The origin of this offset is not presently understood, though it is not excluded that it might be caused by spin-orbit coupling in the leads of the dot, keeping in mind that in the present measurements, time

reversal symmetry in the leads is broken due to a perpendicular component of the applied $B_\parallel$ due to sample misalignment. It has been shown theoretically that spin-orbit coupling in the leads can result in offsets of the Kondo-peak splitting when time reversal symmetry is broken [145]. If this explanation turns out to be applicable, it would alow for an *in-situ* measurement of the spin-orbit coupling strength in the leads of the dot, which might be interesting because spin-orbit coupling in combination with phonon emission is thought to be the dominant mechanism for spin-relaxation in few electron quantum dots [76]. Though it is the spin-orbit coupling in the dot itself which is really of interest, this could allow an *in-situ* measurement of the material spin-orbit parameters which are thought to be not be very different inside the quantum dot.

The inelastic cotunneling ridge shows a significant overshoot at $eV_{SD} \sim J$, particularly in a second device that showed qualitatively similar effects but had stronger coupling to the leads and a somewhat larger singlet-triplet spacing J. The peak conductance of this overshoot decreases linearly with increasing temperature when plotted against the logarithm of temperature, indicative of a Kondo-like correlation. This constitutes the first observation of a non-equilibrium singlet-triplet Kondo effect in the paradigmatic two electron system, for which there is currently no theory available which calculates the non-equilibrium conductance.

Finally, quantum correlations of the two electron singlet ground state wave function that are related to a non-trivial entanglement recently introduced [180] called concurrence have been extracted consistently using three different methods. Whereas measurements of entanglement often require comparatively complicated measurements of the noise of the system, this was done by considering dc-transport and using theory [77, 78] to extract the amount of entanglement. The maximal concurrence of $c = 1$ describes a state where the two electrons are spatially separated into two different orbital states, whereas for the minimal concurrence of $c = 0$ both electrons occupy the same orbital wave function. The present experiment finds that the concurrence is significant, $c \sim 0.75 \pm 0.07$, and increases slightly in a perpendicular magnetic field, consistent with the concept that $B_\perp$ introduces additional confinement separating the two electrons more strongly into their own spatially separated orbitals. The field dependence is shown in Figure 1.8, where additionally the double occupance D and the interaction parameter ϕ are plotted. The double occupancy D is the probability two find
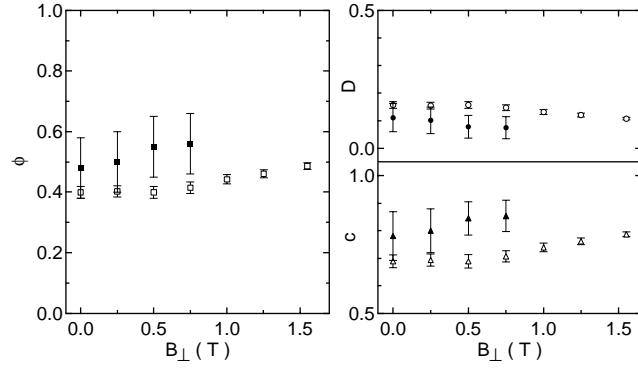
Figure 1.8: Interaction parameter ϕ, concurrence c and double occupance D as a function of magnetic field extracted using sequential tunneling (open symbols) and elastic cotunneling (filled symbols).

both electrons simultaneously in the same orbital. ϕ quantifies the amount of admixture of the excited orbital state.

Gate-Controlled Spin-Orbit Quantum Interference Effects in Lateral Transport

J. B. Miller*, D. M. Zumbühl, C. M. Marcus

Department of Physics, Harvard University, Cambridge, Massachusetts 02138
∗Division of Engineering and Applied Science
Harvard University, Cambridge, Massachusetts 02138

Y. B. Lyanda-Geller

Naval Research Laboratory, Washington, D.C. 20375

D. Goldhaber-Gordon

Department of Physics, Harvard University, Cambridge, Massachusetts 02138
Department of Physics, Stanford University
Stanford, California 94305

K. Campman, A. C. Gossard

Materials Department, University of California at Santa Barbara
Santa Barbara, California, 93106

In situ control of spin-orbit coupling in coherent transport using a clean GaAs/AlGaAs 2DEG is realized, leading to a gate-tunable crossover from weak localization to antilocalization. The necessary theory of 2D magnetotransport in the presence of spin-orbit coupling beyond the diffusive approximation is developed and used to analyze experimental data. With this theory the Rashba contribution and linear and cubic Dresselhaus contributions to spin-orbit coupling are separately estimated, allowing the angular dependence of spin-orbit precession to be extracted at various gate voltages.

2.1 Introduction

An important component along the path toward realizing quantum "spintronic" devices [202, 14] is a structure that allows manipulation of electron spin without destroying phase coherence. Spin-orbit (SO) coupling has been the focus of recent studies because of its potentially useful role in coherent spin rotators [40], spin interference devices [11], and spin-filters [114, 112]. The mechanisms by which SO coupling affects transport [94, 8, 19, 45] have recently been considered in the context of Aharonov-Bohm (AB) phase and Berry phase [11, 143, 137, 101, 136, 4, 205], underscoring the richness of the underlying physics. The results in this and other recent experiments [154] cannot be explained without considering these AB-like effects.

The conductivity of low-dimensional systems shows signatures of quantum interference that depend on magnetic field and SO coupling [94, 8, 1, 7, 79]. In particular, constructive (destructive) backscattering associated with pairs of time-reversed closed-loop electron trajectories in the absence (presence) of significant SO interaction leads to negative (positive) magnetoresistance effects known as weak localization (antilocalization). Antilocalization is the paradigmatic experimental signature of SO coupling in phase coherent electronic systems [19].

In this Letter, we demonstrate *in situ* control of SO coupling in a moderately high mobility GaAs/AlGaAs two-dimensional electron gas (2DEG), inducing a crossover from weak localization (WL) to antilocalization (AL) as a function of an applied top-gate voltage (see Figure 2.1). Theory beyond the diffusive approximation must be used to extract gate-voltage-dependent SO parameters from magnetotransport when the SO precession frequency becomes comparable to the inverse transport scattering time (τ^{-1}) as occurs here, and when the magnetic length becomes comparable to the mean free path. Such a theory, which also takes into account AB-like spin quantal phases and spin-relaxation [135], is developed here and used to estimate *separately* the various SO terms (Rashba, linear and cubic Dresselhaus, defined below) over a range of gate voltages, ranging from WL to AL.

2.2 Previous Theory and Experiments

Conventional WL theories assume SO times much longer than transport scattering times [94, 8, 101] and so cannot be applied to clean materials such as high-mobility 2DEGs. Previous theories that go beyond the diffusive approximation do not treat SO [70, 32], or treat it only as spin-relaxation [107, 203] without accounting for Berry phase effects which play a crucial role, as we show here.

Previous experiments in which SO rates are measured using WL/AL in a gated GaAs heterostructure have not reported *in situ* gate control [45, 88, 172]. Very recently, Koga *et al.* [115] demonstrated gate controlled SO coupling in InGaAs heterostructures using WL/AL, but did not report a full crossover from WL to AL in any single sample. We know of no previous study in which an *in situ* crossover from WL to AL is demonstrated. Modification of Rashba SO coupling using gated quantum wells has been observed using beating patterns in Shubnikov-de Haas oscillations in InGaAs [156, 178], InAs/AlSb [91] and HgTe [184]. Gate controlled SO coupling in GaAs 2D hole systems [164, 201, 134] has also been investigated using beating of Shubnikov-de Haas oscillations. The angular variation of SO coupling in GaAs quantum wells has been measured using Raman scattering [105], but to our knowledge has not been extracted from transport data.

2.3 Theory of Two-Dimensional Magnetotransport with Spin-Orbit Coupling beyond the Diffusive Approximation

The Hamiltonian for conduction band electrons in a [001] 2DEG is $\mathcal{H} = \frac{\hbar^2 k^2}{2m^*} + (\sigma \cdot \boldsymbol{\Omega})$, where m^* is the effective mass, $k = |\mathbf{k}|$ ($\mathbf{k} = (k_x, k_y)$) is the in-plane wave vector, $\sigma = (\sigma_x, \sigma_y)$ is the Pauli spin operator and $\boldsymbol{\Omega} = (\Omega_x, \Omega_y)$ is the total SO frequency. $\boldsymbol{\Omega} = \boldsymbol{\Omega}_{D1} + \boldsymbol{\Omega}_{D3} + \boldsymbol{\Omega}_R$ can be written as the vector sum of linear ($\boldsymbol{\Omega}_{D1}$) and cubic ($\boldsymbol{\Omega}_{D3}$) Dresselhaus terms and

the Rashba term ($\mathbf{\Omega}_R$),

$$\mathbf{\Omega}_{D1} \;=\; \alpha_1 \left(-\hat{\mathbf{x}} k_x + \hat{\mathbf{y}} k_y\right)/\hbar, \tag{2.1a}$$

$$\mathbf{\Omega}_R \;=\; \alpha_2 (\hat{\mathbf{x}} k_y - \hat{\mathbf{y}} k_x)/\hbar, \tag{2.1b}$$

$$\mathbf{\Omega}_{D3} \;=\; \gamma(\hat{\mathbf{x}} k_x k_y^2 - \hat{\mathbf{y}} k_x^2 k_y)/\hbar. \tag{2.1c}$$

where γ arises from the lack of inversion symmetry of the GaAs crystal, while $\alpha_1 = \gamma\langle k_z^2\rangle$ also depends on the thickness of the wave function in the quantization direction. The Rashba coefficient α_2 depends on the potential profile of the heterointerface. In fitting the data below, we assume the effect of gate voltage, V_g, on Ω ($\equiv |\mathbf{\Omega}|$) is through the carrier density, $n = k^2/2\pi$. Good agreement between theory and experiment (Figure 2.2) supports this assumption, as do previous studies of SO coupling in single-interface heterostructures [113]. Although α_2 can be treated as directly proportional to a *uniform* electric field [102], the magnitude of α_2 in a single-interface heterostructure originates mainly from the band-offset at the heterointerface, which is essentially independent of V_g [91, 166].

The symmetry of the linear (in k) SO terms, $\mathbf{\Omega}_{D1}$ and $\mathbf{\Omega}_R$, allows these terms to be represented as a spin-dependent vector potential $\mathbf{A}$ that affects the orbital motion and phase of electrons, $\sigma \cdot (\mathbf{\Omega}_{D1} + \mathbf{\Omega}_R) \propto \mathbf{k} \cdot \mathbf{A}$ [11, 143, 137, 101, 136, 4]. That is, the linear terms affect electronic interference as a spin-dependent AB-like effect. In contrast, the cubic term, Eq. (1c), upon removing terms with the symmetry of Eq. (1a), only causes spin relaxation in the diffusive regime (although it also can produce AB-like effects in the quasi-ballistic regime [11]).

To develop the theory of 2D magnetotransport with SO coupling beyond the diffusive approximation [135], we follow Refs. [70, 32, 107], which treat the quasi-ballistic case $\ell_B < \ell$ ($\ell_B = \sqrt{\hbar/2eB}$ is the magnetic length and ℓ is the transport mean free path) without spin-orbit coupling. The approach is to introduce an operator $P = G^R_{\epsilon+\omega}(\mathbf{r}_1, \mathbf{r}_2, \sigma_1) G^A_\epsilon(\mathbf{r}_1, \mathbf{r}_2, \sigma_2)\hbar/2\pi\nu\tau$ for the probability of an electron to propagate both forward and backward along a path segment from $\mathbf{r}_1$ to $\mathbf{r}_2$, where G^R (G^A) are single-electron retarded (advanced) Green functions, $\sigma_{1(2)}$ are the Pauli spin operators for particle

29

moving forward (backward), ν is the density of states per spin, and τ is the scattering time. The interference contribution from the nth traversal of a closed path is given by the trace of $(P)^n$. In the presence of SO coupling of the form in Eq. (2.1), formulas in [32] remain valid once a summation over spins is included in the trace.

Introducing the total spin of interfering partial waves, $\mathbf{S} = \sigma_1 + \sigma_2$, we write $Tr[(P)^n] = \frac{1}{2}Tr[(P_1)^n - (P_0)^n]$, where operators P_0 and P_1 describe singlet $(S = 0)$ and triplet $(S = 1)$ contributions. To calculate $Tr[(P_{0(1)})^n]$, we diagonalize $P_{0(1)}$. We find that when $\mathbf{\Omega}_{D1}$ and $\mathbf{\Omega}_R$ are taken into account, $P_{0(1)}$ has the same eigenfunctions as the Hamiltonian $\mathcal{H}$ for particles with charge $2e$, spin $\mathbf{S}$ and spin frequency $2\mathbf{\Omega}$: $\mathcal{H} = \frac{\hbar^2}{2m^*}(\mathbf{k} - 2e\mathbf{A}_{em} + 2e\mathbf{A}_S)^2$, where $\mathbf{A}_{em}$ is the vector potential associated with the applied perpendicular magnetic field, B, and $\mathbf{A}_S = \frac{m^*}{2e\hbar^3}(-\alpha_1 S_x - \alpha_2 S_y, \alpha_2 S_x + \alpha_1 S_y)$ is the SO vector potential. For $S = 0$, the eigenstates are Landau levels for a charge $2e$ particle in the magnetic field B, analogous to the spinless problem [107]. For $S = 1$, eigenstates of $\mathcal{H}$ and P_1 in general require a numerical solution, although analytic solutions exist when either α_1 or α_2 equals zero [135]. An analytic solution is found when both α_1 and α_2 may be nonzero, when $\ell_B < \lambda_{so}$, where $\lambda_{so} = (2\alpha_{1(2)}m^*/\hbar^2)^{-1}$ is the distance over which spin rotates appreciably (if $\ell > \lambda_{so}$) or dephases (if $\ell < \lambda_{so}$) due to spin AB-like effects. Performing a unitary transformation $\mathcal{H} \rightarrow \tilde{\mathcal{H}} = U^\dagger \mathcal{H} U$, with $U = \exp(-ie\mathbf{A}_S \cdot \mathbf{r})$, and expanding in coordinates, we find $\tilde{\mathcal{H}} = \frac{\hbar^2}{2m^*}(\mathbf{k} - 2e\mathbf{A}_{em} + S_z\mathbf{a})^2$, where $\mathbf{a} = H_{\text{eff}}\,\mathbf{r} \times \hat{\mathbf{z}}/(2\hbar^2)$, and $H_{\text{eff}} = 2(\alpha_2^2 - \alpha_1^2)m^{*2}/e\hbar^3$ is the effective SO field. P_1 can then be block-diagonalized for each m ($m = 0, \pm1$) using the Landau basis for particles with charge $2e$ in the magnetic field $B - mH_{\text{eff}}$. Thus, the effect of $\mathbf{\Omega}_{D1}$ and $\mathbf{\Omega}_R$ is to produce spin quantal phases of the AB type [11, 143, 137, 101, 136, 4]. Higher expansion terms to $\tilde{\mathcal{H}}$ describe spin flip processes and can be taken into account by introducing a spin relaxation time τ_{so} and its corresponding field scale $H_{so} = \hbar\tau/(2e\ell^2\tau_{so})$. The resulting quantum interference contribution takes the form [135]

$$\Delta\sigma(B) = -\frac{e^2}{4\pi^2\hbar}\left[\sum_{m=-1,0,1} C(x_{1m}, f_{1m}) - C(x_{00}, f_{00})\right] \tag{2.2}$$

where $x_{Sm} = (B - mH_{\text{eff}})/H_{tr}$ describes the AB dephasing in H_{eff}, $C(x, f_{Sm}) = x \sum_{N=0}^{\infty} \frac{P_N^3(f_{Sm})}{1-P_N(f_{Sm})}$, $P_N(f_{Sm}) = y \int_0^{\infty} \exp(-y f_{Sm} t - t^2/2) L_N(t^2) dt$, $L_N(z)$ are Laguerre polynomials, $y = (2/|x|)^{1/2}$, and $H_{tr} = \hbar/(2e\ell^2)$. The dephasing factors f_{Sm} are given by $f_{1\pm1} = (1 + (H_\varphi + H_{so})/H_{tr})$; $f_{00} = (1 + H_\varphi/H_{tr})$; $f_{10} = (1 + (H_\varphi + 2H_{so})/H_{tr})$, where $H_\varphi = \hbar/(4eL_\varphi^2)$ and L_φ is the phase breaking length.

Equation (2.2) does not include all B-dependent interference terms, notably excluding Cooper-channel contributions due to electron-electron interactions [7] and a reduction of WL due to electron diffraction effects [70]. Also, in an attempt to capture the effects of cubic terms on H_{eff} and H_{so}, we introduce an effective vector potential $\mathbf{A}_S^* = \mathbf{A}_S + \gamma \frac{m^*}{e\hbar^2}(k_y{}^2, -k_x{}^2) \sim \mathbf{A}_S + \gamma \frac{m^*}{2e\hbar^2}(k^2, -k^2)$ which leads to an effective SO field,

$$H_{\text{eff}}^* = 2(\alpha_2^2 - \alpha_1^2 + 2\pi n\alpha_1\gamma - \pi^2\gamma^2 n^2)m^{*2}/e\hbar^3. \tag{2.3}$$

Equation (2.2) is applicable when $B > H_{\text{eff}}^*$, which corresponds in the present experiment to B between 20-100 μT depending on V_g (see Figure 3.2). We have confirmed that fitting only to data where $B > H_{\text{eff}}^*$ gives, within error bars, the same results as fitting over the entire measured range of B.

Modification of the commutator $[\mathbf{k} + 2e\mathbf{A}_S^*, \mathbf{r}]$ by $\mathbf{A}_S^*$ induces spin flipping terms $\sim \gamma k^3/4$ in the transformed Hamiltonian $\tilde{\mathcal{H}}^*$. The corresponding $H_{so}^* = \frac{1}{36}\pi^2 m^{*2}\gamma^2 n^2/e\hbar$, using its expression in the diffusive regime.

2.4 Experimental Details

We now turn to a discussion of the experiment. Three similarly fabricated samples made on three separate heterostructure materials were measured, all showing qualitatively similar behavior. The sample for which data is presented consists of a GaAs/AlGaAs heterostructure grown in the [001] direction with double δ-doping layers set back 143 Å and 161 Å from the 2DEG and a total distance of 349 Å from the surface to the 2DEG. A 200 μm wide Hall
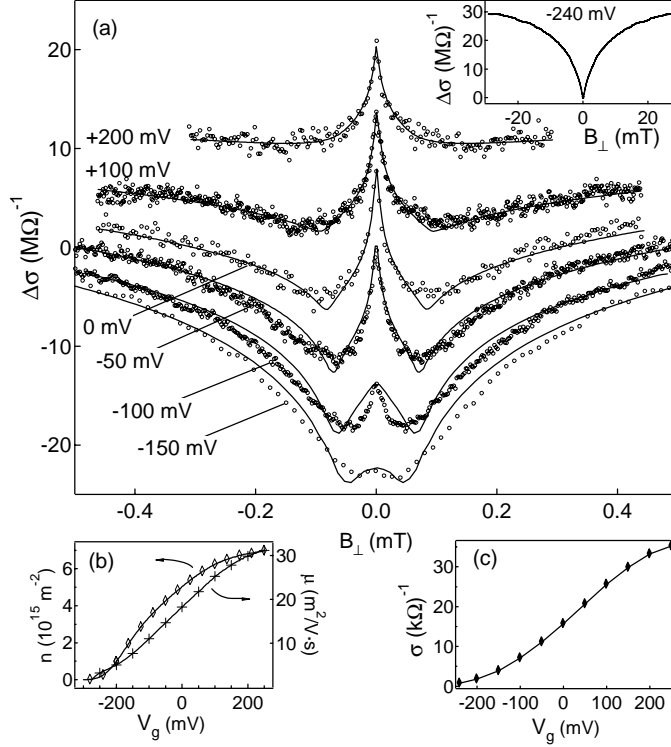
Figure 2.1: (a) Experimental magnetoconductance, $\Delta\sigma = \sigma(B) - \sigma(0)$, (circles) offset for clarity, along with three-parameter fits to Eq. (2.2) (solid curves) for several gate voltages. Inset: Experimental magnetoconductance data for the most negative gate voltage, showing pure WL. (b) Density and mobility as a function of V_g, extracted from longitudinal and Hall voltage measurements. (c) Experimental conductivity, showing strong dependence on V_g. Note that $\Delta\sigma \sim 10^{-3}\sigma$.

bar with 700 μm between voltage probes was patterned by wet etching. A lithographically defined Cr/Au top gate was used to control density and mobility in the Hall bar over the range $n = 1.4\text{-}7.0 \times 10^{15}$ m^{-2} and $\mu = 3.6\text{-}31$ m^2/Vs. Measurements were made in a ^{3}He cryostat at temperature $T = 300$ mK using ac lock-in techniques with bias currents ranging from 50 to 500 nA (depending on the gate voltage). At each gate voltage, the bias current was experimentally determined not to affect the results.

2.5 Crossover from WL to AL and Separation of Spin-Orbit Parameters

Figure 2.1 (a) shows the longitudinal magnetoconductance as a function of V_g. A crossover from pure WL (Figure 2.1(a), inset) at $V_g = -240$ mV to essentially pure AL at $V_g =$
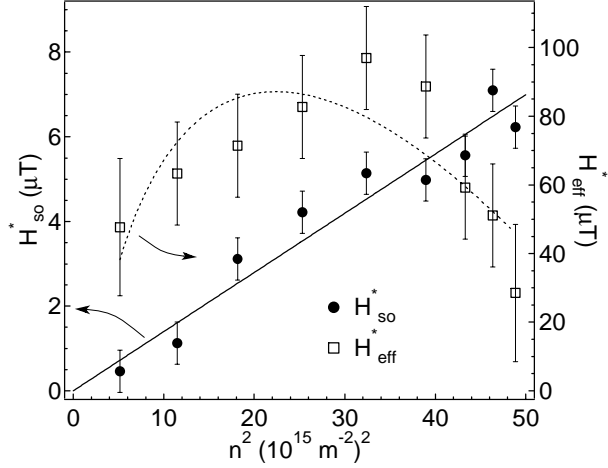
Figure 2.2: Spin-orbit effective fields, H_{so}^* (filled circles) and H_{eff}^* (open squares), as extracted using Eq. (2.2), plotted as a function of sheet density squared. The best fit of Eq. (2.3) to H_{eff}^* (dotted curve) is used to extract γ, α_1 and α_2. Alternatively, the best linear fit to H_{so}^* (solid line) is used to extract γ.

+250 mV is observed. This crossover demonstrates that a gate can be used to control SO over a wide range, as pure WL corresponds to negligible SO rotations within the phase coherence length L_φ, while AL corresponds to spin rotations $\gtrsim 2\pi$. The solid curves in Figure 2.1(a) are fits of Eq. (2.2) with three free parameters, H_ϕ, H_{so}^*, and H_{eff}^*. H_{tr} is fixed at each gate voltage by measured values of density and mobility.

Figure 2.2 shows extracted parameters H_{so}^* and H_{eff}^* as a function of n^2. H_{so}^* is well described by the predicted linear dependence on n^2, with a best fit (Figure 2.2, solid line) giving $\gamma = 31 \pm 3$ eVÅ^3 with zero y-intercept (see Equation (2.1c)). The density dependence of H_{eff}^* is well described by Equation (2.3), (Figure 2.2, dotted curve), giving fit parameters $\gamma = 28 \pm 4$ eVÅ^3, $\alpha_1 = 4 \pm 1$ meVÅ and $\alpha_2 = 5 \pm 1$ meVÅ. In this way, the three SO parameters α_1, α_2, and γ are separately obtained from transport measurements by explicitly making use of the density dependence of H_{eff}^* and H_{so}^*. Extracted values of H_φ correspond to dephasing times in the range $\tau_\varphi \sim 0.1$-1.0 ns at 300 mK, which decrease by more than an order of magnitude as temperature is increased to 2.5 K. Within the error bars, H_{so}^* and H_{eff}^* do not depend on temperature over this temperature range.

Figure 2.3(a) displays the magnitudes of the three spin-orbit terms as functions of V_g, n, and μ, determined using Eq. (2.1) and the extracted values of α_1, α_2, and γ. Plotted are
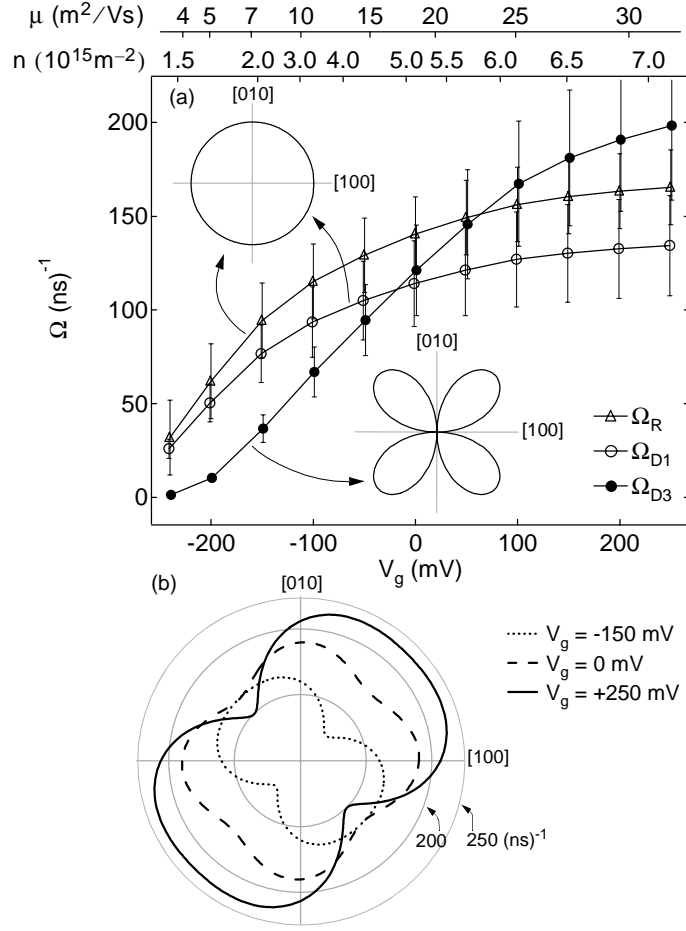
Figure 2.3: (a) Magnitudes of isotropic linear Dresselhaus (Ω_{D1}) and Rashba (Ω_R) terms, and nonisotropic cubic Dresselhaus (Ω_{D3}) term as functions of gate voltage, V_g, density, n, and mobility, μ. Insets show theoretical dependence on momentum direction for the three terms, indicating that the linear terms are isotropic, while the cubic term has a four-fold symmetry and is highly anisotropic. Maximum magnitude (when $\phi = (j + \frac{1}{4})\pi$) is shown for the anisotropic (Ω_{D3}) term. (b) Angular variation of Ω, the magnitude of the total SO precession vector at $V_g = -150$ mV (dotted), 0 mV (dashed), and 250 mV (solid), corresponding to densities of 2.3, 5.0, and 7.0×10^{15} m^{-2} respectively.

values along the [110] direction, $\phi \equiv \tan^{-1}(k_y/k_x) = \frac{\pi}{4}$, where Ω_{D3} is maximum. Error bars indicate uncertainties in the fitting procedure and noise in the data.

2.6 Angular Dependence of Spin Precession Rates

The total spin precession rate, Ω, is plotted as a function of the direction, ϕ, of the electron momentum in Figure 2.3(b). While for most directions Ω is an increasing function of density, it is seen to decrease with increasing density near $\phi = \frac{3\pi}{4}$ and $\frac{7\pi}{4}$. The linear Dresselhaus

and Rashba terms (Ω_{D1} and Ω_R) are of comparable magnitude to each other for all densities and in all directions. Near $\phi = \frac{j\pi}{2}$ (j an integer), $\Omega_{D3} \ll \Omega_{D1}, \Omega_R$ and the SO is controlled by the linear terms. For ϕ near $\frac{(2j+1)\pi}{4}$, the cubic term becomes comparable to or even exceeds (at high densities) the linear terms. Depending on ϕ, the linear and cubic terms either add ($\phi \sim \frac{\pi}{4}, \frac{5\pi}{4}$) or subtract ($\phi \sim \frac{3\pi}{4}, \frac{7\pi}{4}$).

The extracted values for γ (31 ± 3 eVÅ^3 using H_{so}^*, 28 ± 4 eVÅ^3 using H_{eff}^*) are in good agreement with the value 27.5 eVÅ^3 from band structure calculations [113, 166]. Estimates for α_1 give values for $\langle k_z^2 \rangle$ that correspond to a wave function width of ~ 10 nm in the $\hat{z}$ direction, which is also reasonable. The extracted α_2 corresponds to a uniform [102] electric field $E \sim 10$ MV/m, using $\alpha_2 = \alpha_0 eE$ and a value of $\alpha_0 = 5.33$ Å^2 from a $\mathbf{k} \cdot \mathbf{p}$ model [113, 166].

2.7 Comparison with previous Theory

We note that previously existing models for WL/AL [8, 101, 113] provide fits to the data that appear qualitatively reasonable, giving values for H_{so} that are ~ 5 times higher than those found using Eq. (2.2). However, these fits also lead to the unphysical result that $\tau_{so} < \tau$. Such unphysical results are not surprising given that, for $V_g > -50$ mV, the SO length, $v_F/\langle \Omega \rangle$, is less than ℓ, while theory [8, 101, 113] assumes diffusive spin evolution $\ell \ll \lambda_{so}, L_\varphi$. Finally we note that a theory for arbitrarily strong SO coupling [136] may also be used to fit this data by including B via L_φ, yielding values for Ω_{D3} and Ω_{D1} for all V_g's which agree with our estimates using Eq. (2.2) to within a factor of ~ 3. However, the theory in [136] does not separate Ω_{D1} and Ω_R terms.

2.8 Conclusion

In conclusion, we have realized an *in situ* gate-controlled crossover from weak localization to antilocalization in a GaAs/AlGaAs 2DEG, experimentally demonstrating that spin rotation can be strongly modulated in a clean, phase-coherent system. New theory addresses spin-

orbit effects in the quasi-ballistic regime and allows separate measurement of the Rashba, linear Dresselhaus, and cubic Dresselhaus terms.

Spin-Orbit Coupling, Antilocalization, and Parallel Magnetic Fields in Quantum Dots

D. M. Zumbühl, J. B. Miller*, C. M. Marcus

Department of Physics, Harvard University, Cambridge, Massachusetts 02138

*Division of Engineering and Applied Science

Harvard University, Cambridge, Massachusetts 02138

K. Campman, A. C. Gossard

Materials Department, University of California at Santa Barbara

Santa Barbara, California, 93106

We investigate antilocalization due to spin-orbit coupling in ballistic GaAs quantum dots. Antilocalization that is prominent in large dots is suppressed in small dots, as anticipated theoretically. Parallel magnetic fields suppress both antilocalization and also, at larger fields, weak localization, consistent with random matrix theory results once orbital coupling of the parallel field is included. *In situ* control of spin-orbit coupling in dots is demonstrated as a gate-controlled crossover from weak localization to antilocalization.

3.1 Introduction

The combination of quantumcoherence and electron spin rotation in mesoscopic systems produces a number of interesting transport properties. Numerous proposals for potentially revolutionary electronic devices that use spin-orbit (SO) coupling have appeared in recent years, including gate-controlled spin rotators [40] as well as sources and detectors of spin-polarized currents [27, 112, 108]. It has also been predicted that the effects of some types of SO coupling will be strongly suppressed in small 0D systems, i.e., quantum dots [109, 110, 87, 4, 37].

In this Letter, we investigate SO effects in ballistic-chaotic GaAs/AlGaAs quantum dots. We identify the signature of SO coupling in ballistic quantum dots to be *antilocalization* (AL), leading to characteristic magnetoconductance curves, analogous to known cases of disordered 1D and 2D systems [94, 8, 19, 45, 151, 150, 113]. AL is found to be prominent in large dots and suppressed in smaller dots, as anticipated theoretically [109, 110, 87, 4, 37]. Results are generally in excellent agreement with a new random matrix theory (RMT) that includes SO and Zeeman coupling [4, 37]. Moderate magnetic fields applied in the plane of the 2D electron gas (2DEG) in which the dots are formed cause a crossover from AL to weak localization (WL). This can be understood as a result of Zeeman splitting, consistent with RMT [4, 37]. At larger parallel fields WL is also suppressed, which is not expected within RMT. The suppression of WL is explained by orbital coupling of the parallel field, which breaks time-reversal symmetry [56, 148]. Finally, we demonstrate *in situ* electrostatic control of the SO coupling by tuning from AL to WL in a dot with a center gate.

In mesoscopic conductors, coherent backscattering of time-reversed electron trajectories leads to a conductance *minimum* (WL) at $B = 0$ in the spin-invariant case, and a conductance *maximum* (AL) in the case of strong SO coupling [94, 8]. In semiconductor heterostructures, SO coupling results mainly from electric fields [46] (appearing as magnetic fields in the electron frame), leading to momentum dependent spin precessions due to crystal inversion asymmetry (Dresselhaus term [44]) and heterointerface asymmetry (Rashba

term [31]).

3.2 Previous Experiments

SO coupling effects have been previously measured using AL in GaAs 2DEGs [45, 151, 150] and other 2D heterostructures [113]. Other means of measuring SO coupling in heterostructures, such as from Shubnikov-de Haas oscillations [91, 163, 80] and Raman scattering [105] are also quite developed. SO effects have also been reported in mesoscopic systems such as Aharonov-Bohm rings, wires, and carbon nanotubes [124, 11, 154, 157, 185, 53, 24, 152]. Recently, parallel field effects of SO coupling in quantum dots were measured [85, 59]. The observed reduction of conductance fluctuations in a parallel field [59] was explained in terms of SO effects [87, 4, 37], leading to an extension of random matrix theory (RMT) to include new symmetry classes associated with SO and Zeeman coupling [4, 37].

3.3 Random Matrix Theory

This RMT addresses quantum dots coupled to two reservoirs via N total conducting channels, with $N \gg 1$. It assumes $(\gamma, \epsilon_Z) \ll E_T$, where $\gamma = N\Delta/(2\pi)$ is the level broadening due to escape, Δ is the mean level spacing, $\epsilon_Z = g\mu_B B$ is the Zeeman energy and E_T is the Thouless energy (Table 3.3). Decoherence is included as a fictitious voltage probe [29, 15, 25, 4, 37] with dimensionless dephasing rate $N_\varphi = h/(\Delta\tau_\varphi)$, where τ_φ is the phase coherence time. SO lengths $\lambda_{1,2}$ along respective principal axes [110] and [1$\bar{1}$0] are assumed (within the RMT) to be large compared to the dot dimensions $L_{1,2}$ along these axes. We define the mean SO length $\lambda_{so} = \sqrt{|\lambda_1\lambda_2|}$ and SO anisotropy $\nu_{so} = \sqrt{|\lambda_1/\lambda_2|}$. SO coupling introduces two energy scales: $\epsilon_\perp^{so} = \kappa_\perp E_T(L_1 L_2/\lambda_{so}^2)^2$, representing a spin-dependent Aharonov-Bohm-like effect, and $\epsilon_\parallel^{so} \sim ((L_1/\lambda_1)^2 + (L_2/\lambda_2)^2)\epsilon_\perp^{so}$, providing spin flips. AL appears in the regime of strong SO coupling, $(\epsilon_\perp^{so}, \epsilon_\parallel^{so}) \gg \tilde{\gamma}$, where $\tilde{\gamma} = (\gamma + \hbar/\tau_\varphi)$ is the total level broadening. Note that large dots reach the strong SO regime at relatively weaker SO coupling than small dots. Parameters λ_{so}, τ_φ, and $\kappa_\perp$ (a factor related to trajectory

A μm^2	Δ μeV	τ_d ns	E_T/Δ	$\epsilon_\perp^{so}/\Delta$	$\epsilon_\parallel^{so}/\Delta$	a_1, a_2 $(ns)^{-1}T^{-2}$	b_2 $(ns)^{-1}T^{-6}$
1.2	6.0	0.35	33	0.15	0.04	6.6, 6.6	0.24
5.8	1.2	1.7	73	0.32	0.33	3.2, 0	140
8	0.9	2.3	86	3.6	3.1	1.4, 0.9	3.7

Table 3.1: Dot area $A = L_1 L_2$ (130 nm edge depletion); spin-degenerate mean level spacing $\Delta = 2\pi\hbar^2/m^* A$ ($m^* = 0.067 m_e$); dwell time $\tau_d = h/(N\Delta)$; Thouless energy $E_T = \hbar v_F/\sqrt{A}$; $\epsilon_\perp^{so}/\Delta$ and $\epsilon_\parallel^{so}/\Delta$ for the fits in Figure 3.1; B^2 coefficients a_1 and a_2 from one and two parameter fits; B^6 coefficient b_2 from two parameter fit, see text.

areas) are extracted from fits to dot conductance as a function of perpendicular field, $B_\perp$. The asymmetry parameter, ν_{so}, is estimated from the dependence of magnetoconductance on parallel field, $B_\parallel$.

The quantum dots are formed by lateral Cr-Au depletion gates defined by electron-beam lithography on the surface of a GaAs/AlGaAs heterostructure grown in the [001] direction. The 2DEG interface is 349 Å below the wafer surface, comprising a 50 Å GaAs cap layer and a 299 Å AlGaAs layer with two Si δ-doping layers 143 Å and 161 Å from the 2DEG. An electron density of $n \sim 5.8 \times 10^{15}\,\mathrm{m}^{-2}$ [1] and bulk mobility $\mu \sim 24\,\mathrm{m}^2/\mathrm{Vs}$ (cooled in the dark) gives a transport mean free path $\ell_e \sim 3\,\mu\mathrm{m}$. This 2DEG is known to show AL in 2D [150]. Measurements were made in a ^{3}He cryostat at $0.3\,\mathrm{K}$ using current bias of $1\,\mathrm{nA}$ at $338\,\mathrm{Hz}$. Shape-distorting gates were used to obtain ensembles of statistically independent conductance measurements [33] while the point contacts were actively held at one fully transmitting mode each ($N = 2$).

3.4 Antilocalization and Confinement Suppression of Spin-Orbit Effects

Figure 1 shows average conductance $\langle g \rangle$, and variance of conductance fluctuations, $\mathrm{var}(g)$, as a function of $B_\perp$ for the three measured dots: a large dot ($A \sim 8\,\mu\mathrm{m}^2$), a variable size dot with an internal gate ($A \sim 5.8\,\mu\mathrm{m}^2$ or $8\,\mu\mathrm{m}^2$, depending on center gate voltage), and a

[1] All measured densities are below the threshold for second subband occupation $n \sim 6.6 \times 10^{15}\,\mathrm{m}^{-2}$, which is known from Shubnikov-de Haas measurements and a decreasing mobility with increasing density near the threshold.
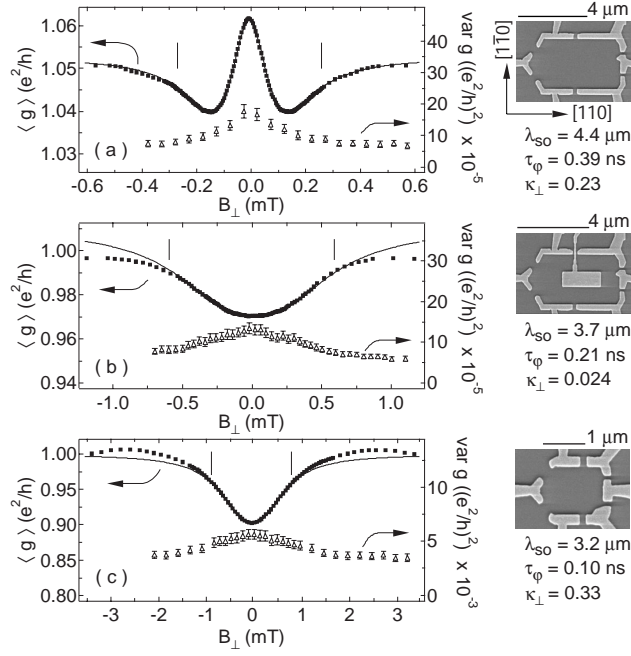
Figure 3.1: Average conductance $\langle g \rangle$ (squares) and variance of conductance var(g) (triangles) calculated from ~ 200 statistically independent samples (see text) as a function of perpendicular magnetic field $B_\perp$ for (a) $8.0\,\mu\mathrm{m}^2$ dot (b) $5.8\,\mu\mathrm{m}^2$ center-gated dot and (c) $1.2\,\mu\mathrm{m}^2$ dot at $T = 0.3\,\mathrm{K}$, along with fits to RMT (solid curves). In (b), the center gate is fully depleted. Vertical lines indicate the fitting range, error bars of $\langle g \rangle$ are about the size of the squares.

smaller dot $(1.2\,\mu\mathrm{m}^2)$. Each data point represents ~ 200 independent device shapes. The large dot shows AL while the small and gated dots show WL. Estimates for λ_{so}, τ_φ and $\kappa_\perp$, from RMT fits are listed for each device below the micrographs in Figure 3.1 (see Table 3.3 for corresponding $\epsilon_\perp$ and $\epsilon_\parallel$). When AL is present (i.e., for the large dot), estimates for λ_{so} have small uncertainties ($\pm 5\%$) and give upper and lower bounds; when AL is absent (i.e., for the small and gated dots) only a lower bound for λ_{so} (-5%) can be extracted from fits. The value $\lambda_{so} \sim 4.4\,\mu\mathrm{m}$ is consistent with all dots and in good agreement with AL measurements made on an unpatterned 2DEG sample from the same wafer [150].

Comparing Figures 3.1(a) and 1(c), and recalling that all dots are fabricated on the same wafer, one sees that AL is suppressed in smaller dots, even though λ_{so} is sufficient to produce AL in the larger dot. We note that these dots do not strongly satisfy the inequalities $L/\lambda_{so} \ll 1, N \gg 1$, having $N = 2$ and $L/\lambda_{so} = 0.64$ (0.34) for the large (small) dot. Nevertheless, Figure3.1 shows the very good agreement between experiment and the new

RMT.

3.5 Suppression of Antilocalization by an In-Plane Magnetic Field

We next consider the influence of $B_\parallel$ on $\langle g \rangle$. In order to apply tesla-scale $B_\parallel$ while maintaining subgauss control of $B_\perp$, we mount the sample with the 2DEG aligned to the axis of the primary solenoid (accurate to $\sim 1°$) and use an independent split-coil magnet attached to the cryostat to provide $B_\perp$ as well as to compensate for sample misalignment [59]. Figure 3.2 shows shape-averaged magnetoconductance (relative to $B_\perp \gg \phi_0/A$, i.e., fully broken time-reversal symmetry), $\delta g(B_\perp, B_\parallel) = \langle g(B_\perp, B_\parallel) \rangle - \langle g(B_\perp \gg \phi_0/A, B_\parallel) \rangle$ as a function of $B_\perp$ at several values of $B_\parallel$, along with fits of RMT [4, 37] with parameters λ_{so}, τ_φ and $\kappa_\perp$ set by a single fit to the $B_\parallel = 0$ data. The low-field dependence of $\delta g(0, B_\parallel)$ on $B_\parallel$ [Figure 3.2(b)] allows the remaining parameter, ν_{so}, to be estimated as described below.

Besides Zeeman energy ϵ_Z (calculated using $g = -0.44$ rather than fit), parallel field combined with SO coupling introduces an additional new energy scale, $\epsilon_\perp^Z = \frac{\kappa_z \epsilon_Z^2 A}{2E_T} \sum_{i,j=1,2} \frac{l_i}{\lambda_i} \frac{l_j}{\lambda_j}$, where κ_Z is a dot-dependent constant and $l_{1,2}$ are the components of a unit vector along $B_\parallel$ [4, 37]. Because orbital effects of $B_\parallel$ on $\delta g(B_\perp, B_\parallel)$ dominate at large $B_\parallel$, $\epsilon_\perp^Z$ must instead be estimated from RMT fits of $\text{var}(g)$ with already-broken time reversal symmetry, which is unaffected by orbital coupling [206].

The RMT formulation [4, 37] is invariant under $\nu_{so} \to r/\nu_{so}$, where $r = L_1/L_2$ [2], and gives an extremal value of $\delta g(0, B_\parallel)$ at $\nu_{so} = \sqrt{r}$. As a consequence, fits to $\delta g(0, B_\parallel)$ cannot distinguish between ν_{so} and r/ν_{so}. As shown in Figure 3.2(b), data for the $8\mu\text{m}^2$ dot ($r \sim 2$) are consistent with $1 \leq \nu_{so} \leq 2$ and appear best fit to the extremal value, $\nu_{so} \sim 1.4$. Values of ν_{so} that differ from one indicate that both Rashba and Dresselhaus terms are significant, which is consistent with 2D data taken on the same material [150].

---

[2]The symmetry is precise if one takes $\epsilon_\perp^Z = \kappa_z \frac{\epsilon_Z^2}{2E_T} \frac{A}{\lambda_{so}^2}$. See Ref. [4, 37].
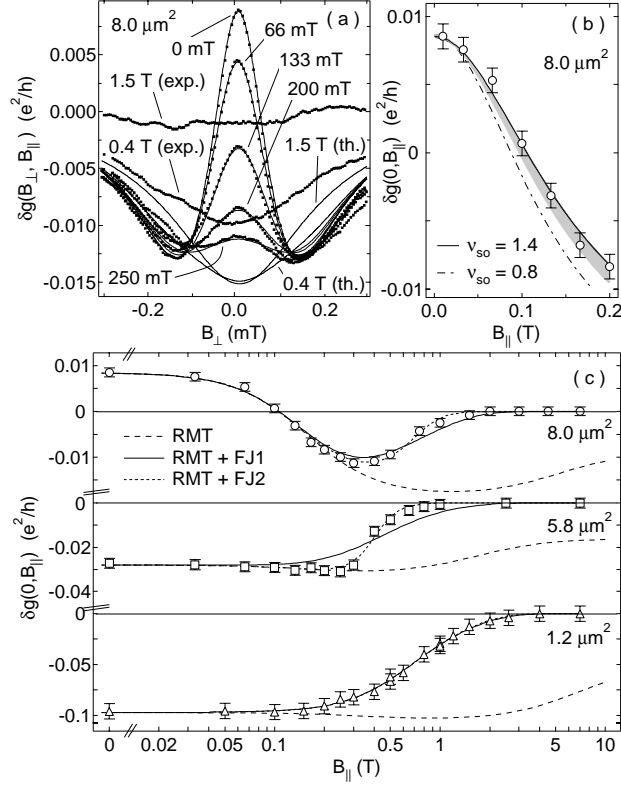
Figure 3.2: (a) Difference of average conductance from its value at large $B_\perp$, $\delta g(B_\perp, B_\parallel)$, as a function of $B_\perp$ for several $B_\parallel$ for the $8.0\,\mu\mathrm{m}^2$ dot at $T = 0.3\,\mathrm{K}$ (squares) with RMT fits (curves). (b) Sensitivity of $\delta g(0, B_\parallel)$ to ν_{so} for the $8.0\,\mu\mathrm{m}^2$ dot, $1 \le \nu_{so} \le 2$ (shaded), $\nu_{so} = 1.4$ (solid line) and $\nu_{so} = 0.8$ (dashed line) (c) $\delta g(0, B_\parallel)$ (markers) with RMT predictions (dashed curves) and one parameter (solid curves) or two parameter fits (dotted curves) using RMT including a suppression factor due to orbital coupling of $B_\parallel$, see text.

43

3.6 Breaking of Time-Reversal Symmetry due to an In-Plane Magnetic Field

Using $\nu_{so} = 1.4$ and values of λ_{so}, τ_φ, and $\kappa_\perp$ from the $B_\parallel = 0$ fit, RMT predictions for $\delta g(B_\perp, B_\parallel)$ agree well with experiment up to about $B_\parallel \sim 0.2\,\mathrm{T}$ [Figure 3.2(a)], showing a crossover from AL to WL. For higher parallel fields, however, experimental δg's are suppressed relative to RMT predictions. By $B_\parallel \sim 2\,\mathrm{T}$, WL has vanished in all dots [Figure 3.2(c)] while RMT predicts significant remaining WL at large $B_\parallel$.

One would expect WL/AL to vanish once orbital effects of $B_\parallel$ break time-reversal symmetry. Following Ref. [56, 148] (FJ), we account for this with a suppression factor $f_{FJ}(B_\parallel) = (1 + \tau_{B\parallel}^{-1}/\tau_{esc}^{-1})^{-1}$, where $\tau_{B\parallel}^{-1} \sim aB_\parallel^2 + bB_\parallel^6$, and assume that the combined effects of SO coupling and flux threading by $B_\parallel$ can be written as a product, $\delta g(0, B_\parallel) = \delta g_{RMT}(0, B_\parallel) \cdot f_{FJ}(B_\parallel)$. The $B_\parallel^2$ term reflects surface roughness or dopant inhomogeneities; the $B_\parallel^6$ term reflects the asymmetry of the quantum well. We either treat a as a single fit parameter (a_1, Table 3.3), using $b = 1.4\,10^8\,\mathrm{s}^{-1}\mathrm{T}^{-6}$ from device simulations [3], or treat both a and b as fit parameters (a_2 and b_2, Table 3.3). Fitting both parameters only improves the fit for the (unusually shaped) center-gated dot.

3.7 Effects of Temperature on Antilocalization

Increased temperature reduces the overall magnitude of δg and also suppresses AL compared to WL, causing AL at $300\,\mathrm{mK}$ to become WL by $1.5\,\mathrm{K}$ in the $8\,\mu\mathrm{m}^2$ dot [Figure 3.3(a)]. Fits of RMT to $\delta g(B_\perp, 0)$ yield λ_{so} values that are roughly independent of temperature [Figure 3.3(b)], consistent with 2D results [151], and τ_φ values that decrease with increasing temperature. Dephasing is well described by the empirical form $(\tau_\varphi[\mathrm{ns}])^{-1} \sim 7.5\,\mathrm{T}[\mathrm{K}] + 2.5\,(\mathrm{T}[\mathrm{K}])^2$, consistent with previous measurements in low-SO dots [98, 96]. As dephasing increases, long trajectories that allow large amounts of spin rotations are cut off, diminishing the AL feature.

---

[3]V. Falko, T. Jungwirth, private communication.
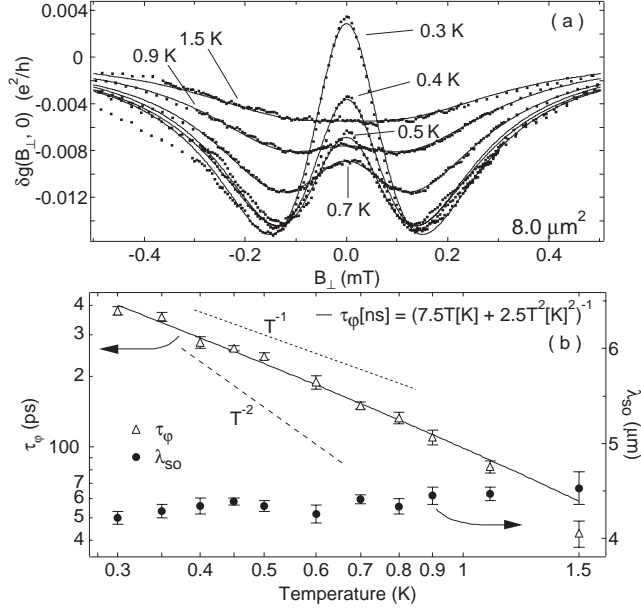
Figure 3.3: (a) Difference of average conductance from its value at large $B_\perp$, $\delta g(B_\perp, 0)$, for various temperatures with $B_\parallel = 0$ for the $8.0\,\mu\text{m}^2$ dot (squares), along with RMT fits (solid curves). (b) Spin-orbit lengths λ_{so} (circles) and phase coherence times τ_φ (triangles) as a function of temperature, from data in (a).

3.8 *In Situ* Control of Spin-Orbit Coupling with a Center Gate

Finally, we demonstrate *in situ* control of the SO coupling using a center-gated dot. Figure 3.4 shows the observed crossover from AL to WL as the gate voltage V_g is tuned from $+0.2\,\text{V}$ to $-1\,\text{V}$. At $V_g = -1\,\text{V}$, the region beneath the center gate is fully depleted, giving a dot with area $5.8\,\mu\text{m}^2$ that shows WL. In the range of $V_g \geq -0.3$ V, the amount of AL is controlled by modifying the density under the gate. For $V_g > 0\,\text{V}$ the AL peak is larger than in the ungated $8\,\mu\text{m}^2$ dot. We interpret this enhancement not as a removal of the SO suppression due to an inhomogeneous SO coupling [26], which would enhance AL in dots with $L/\lambda_{so} \ll 1$ (not the case for the $8\,\mu\text{m}^2$ dot), but rather as the result of increased SO coupling in the higher-density region under the gate when $V_g > 0\,\text{V}$.

One may wish to use the evolution of WL/AL as a function of V_g to extract SO parameters for the region under the gate. To do so, the dependence may be ascribed to either a gate-dependent λ_{so} or to a gate-dependence of a new parameter $\kappa_\parallel = \epsilon_\parallel^{so}/(((L_1/\lambda_1)^2 +$
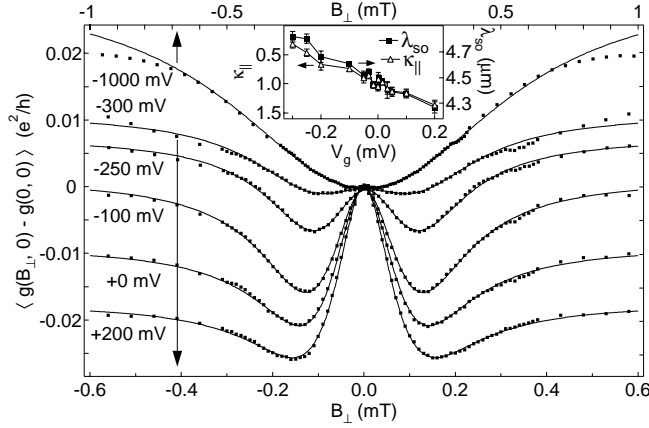
Figure 3.4: Difference of average conductance $\langle g \rangle$ from its value at $B_\perp = 0$ as a function of $B_\perp$ for various center gate voltages V_g in the center-gated dot (squares), along with fits to RMT [4, 37]. Good fits are obtained though the theory assumes homogeneous SO coupling. Error bars are the size of the squares. Inset: λ_{so} and $\kappa_\parallel$ as a function of V_g extracted from RMT fits, see text.

$(L_2/\lambda_2)^2)\epsilon_\perp^{so}$). Both options give equally good agreement with the data (fits in Figure 3.4 assume $\lambda_{so}(V_g)$), including the parallel field dependence (not shown). Resulting values for λ_{so} or $\kappa_\parallel$ (assuming the other fixed) are shown in the inset in Figure3.4. We note that the 2D samples from the same wafer did not show gate-voltage dependent SO parameters [150]. However, in the 2D case a cubic Dresselhaus term that is not included in the RMT of Ref. [4, 37] was significant. For this reason, fits using [4, 37] might show $\lambda_{so}(V_g)$ though the 2D case did not. Further investigation of the gate dependence of SO coupling in dots will be the subject of future work.

3.9   Acknowledgements

Conductance Fluctuations in Open Quantum Dots with Spin-Orbit Coupling and Zeeman Fields

D. M. Zumbühl, J. B. Miller*, C. M. Marcus

Department of Physics, Harvard University, Cambridge, Massachusetts 02138

*Division of Engineering and Applied Science

Harvard University, Cambridge, Massachusetts 02138

D. Goldhaber-Gordon

Department of Physics, Harvard University, Cambridge, Massachusetts 02138

Department of Physics, Stanford University

Stanford, California 94305

J. S. Harris, Jr.

Departement of Electrical Engineering

Stanford University, Stanford, California 94305

K. Campman, A. C. Gossard

Materials Department, University of California at Santa Barbara

Santa Barbara, California, 93106

We present measurements of conductance fluctuations in open quantum dots fabricated in a GaAs 2D electron gas. The variance of the fluctuations in a magnetic field in the 2D plane depends on spin-orbit coupling, reflecting novel spin-rotation symmetries in the system. In a large in-plane field, the variance becomes independent of the perpendicular field due to breaking of time-reversal symmetry by the in-plane field. These results are in quantitative agreement with recent theories.

4.1 Introduction

The combination of quantum confinement, spin-orbit (SO) coupling and Zeeman effects in lateral semiconductor quantum dots gives rise to rich physics, including novel spin-rotation symmetries [4, 37], a suppression of SO effects due to confinement [109, 110, 87, 4, 37, 205, 59] leading to very long spin life times [109, 110, 66, 52, 76] and lifting of the SO suppression by an in-plane field [87, 4, 37, 59] as well as by a spatial dependence of the SO parameters [26]. Further, magnetic fields $B_{\parallel}$ applied in the plane of the 2D electron gas (2DEG) change the electron dispersion and in particular can break time reversal symmetry (TRS) [56, 148, 205, 207], adding additional complexity to this system.

In this communication, we present an experimental study of the variance of conductance fluctuations var g through open quantum dots defined by lateral gates on a GaAs/AlGaAs 2DEG. The $B_{\parallel}$ dependence of the variance var $g(B_{\perp} \neq 0, B_{\parallel})$ with TRS broken by a perpendicular field $B_{\perp} \neq 0$ is seen to depend strongly on the SO strength and can be characterized by novel spin-rotation symmetries found in Ref. [4, 37], which gives good fits to our data. Further, var $g(B_{\perp}, B_{\parallel})$ is seen to become independent of $B_{\perp}$ at large $B_{\parallel}$ due to effects of $B_{\parallel}$ breaking TRS. This is in good agreement with theory [148, 56] as well as experiments on average [205] and correlations [207] of conductance fluctuations.

4.2 Previous Work

Theory of low-dimensional, diffusive systems has long predicted conductance fluctuations [6, 130] to be reduced by both SO coupling [144, 137] as well as Zeeman effects [9, 187, 57]. Random matrix theories [100, 17, 5, 9] offer a universal classification of statistical properties such as the average and variance of conductance in terms of the fundamental symmetry classes. These theories were widely confirmed by experiments in diffusive 2D and 1D systems in both metals and GaAs 2DEG's, including observed reductions in variance due to Zeeman splitting [41, 153], SO coupling [151, 68] and breaking of TRS both in the presence [22] and absence of SO coupling [138].

In open quantum dots, an observed large reduction of conductance fluctuations in $B_\parallel$ [59, 85, 82, 81] has been explained by SO effects that increase upon application of $B_\parallel$ while SO effects at $B_\parallel = 0$ are confinement suppressed [87]. This has led to an extended random matrix theory (RMT) [4, 37], including a classification of transport properties in terms of spin-rotation symmetries. Subsequent experiments found AL [205, 86] in high density dots due to strong SO coupling at $B_\parallel = 0$, allowing the SO length λ_{so} to be extracted. Orbital effects of $B_\parallel$ were observed via a suppression of weak (anti)localization [205] as well as in correlations of conductance fluctuations [207]. In this study, we report on effects of $B_\parallel$ on the variance in dots of various SO strength.

4.3   Spin-Rotation Symmetry Classes

The RMT [4, 37] gives the variance (at zero temperature $T = 0$) in terms of symmetry parameters: $\operatorname{var} g \propto s/(\beta\Sigma)$ [4, 37], where β is the conventional parameter describing time-reversal symmetry, s is the Kramers degeneracy parameter and Σ characterizes mixing of different spins when Kramers degeneracy is already broken. Spin rotation symmetry is classified as either not broken ($s = 2, \Sigma = 1$), partially broken ($s = 1, \Sigma = 1$) or completely broken ($s = 1, \Sigma = 2$). The variance is reduced by a factor of two when a crossover into the class with next-lower symmetry occurs. The Kramers degeneracy can be lifted by a Zeeman field as well as SO coupling if $B_\perp \neq 0$. Once Kramers degeneracy is broken ($s = 1$), mixing of spins ($\Sigma = 2$) is due to SO coupling and can be possible already at $B_\parallel = 0$ due to SO coupling or can be revived by $B_\parallel$ when SO coupling is confinement suppressed [87] at $B_\parallel = 0$. Finite temperatures and decoherence strongly reduce $\operatorname{var}(g)$ [4, 37], but the relative reduction factor $R = \operatorname{var} g(B_\perp \neq 0, B_\parallel = 0)/\operatorname{var} g(B_\perp \neq 0, B_\parallel \gg 0)$ is affected only weakly.

4.4 Experimental Techniques

Four quantum dots of various sizes were measured, made on two different 2DEG's with electron densities $n = 2 \times 10^{11} cm^{-2}$ and $n = 5.8 \times 10^{11} cm^{-2}$, see Ref. [205, 207] for details. Figures 1 and 2 show device micrographs (insets). Measurements were made in a ^{3}He cryostat at $0.3\,\text{K}$ using current bias of $1\,\text{nA}$ at $338\,\text{Hz}$. In order to apply tesla-scale $B_\parallel$ while maintaining sub-gauss control of $B_\perp$, we mount the sample with the 2DEG aligned to the axis of the primary solenoid (accurate to $\sim 1°$) and use an independent split-coil magnet attached to the cryostat to provide $B_\perp$ [59]. The Hall effect measured in a GaAs Hall bar as well as the location of weak (anti)localization extrema in transport through the dot itself (visible $B_\parallel \lesssim 2T$) were used to determine $B_\perp = 0$.

Statistics of conductance fluctuations were gathered using two shape-distorting gates [33] while the point contacts were actively held at one fully transmitting mode each ($N = 2$). Based on about ~ 400 (~ 200) statistically independent samples for the low density (high density) dots, the average and variance of conductance were obtained. Measurements were taken at various fixed $B_\parallel$ as a function of $B_\perp$, with high resolution around $B_\perp = 0$, increasing the number of statistically independent samples for $B_\perp \neq 0$ by about a factor of 5.

4.5 Characterization of Spin-Orbit Strength at Zero In-Plane Field

The average conductance $\langle g(B_\perp) \rangle$ is used to characterize the strength of SO coupling. The large dot on high density material shows AL due to SO coupling [Fig. 4.1(a)], while the smaller dot on the same material displays WL [Fig. 4.1(b)], showing that SO effects in the small dot are suppressed due to the extra confinement, as previously reported [205]. Fits of $\langle g(B_\perp) \rangle$ to the RMT [4, 37] give the average SO length $\lambda_{so} = \sqrt{|\lambda_1 \lambda_2|}$, where $\lambda_{1,2}$ are the SO lengths along the main crystal axes, the phase coherence time τ_φ and $\kappa_\perp$, a parameter related to typical trajectory area. The SO inhomogeneity $\nu_{so} = \sqrt{|\lambda_1/\lambda_2|}$ can be extracted from $\langle g(B_\parallel) \rangle$ in the presence of AL, and is taken as $\nu_{so} = 1.4(1.0)$ for the high(low) density
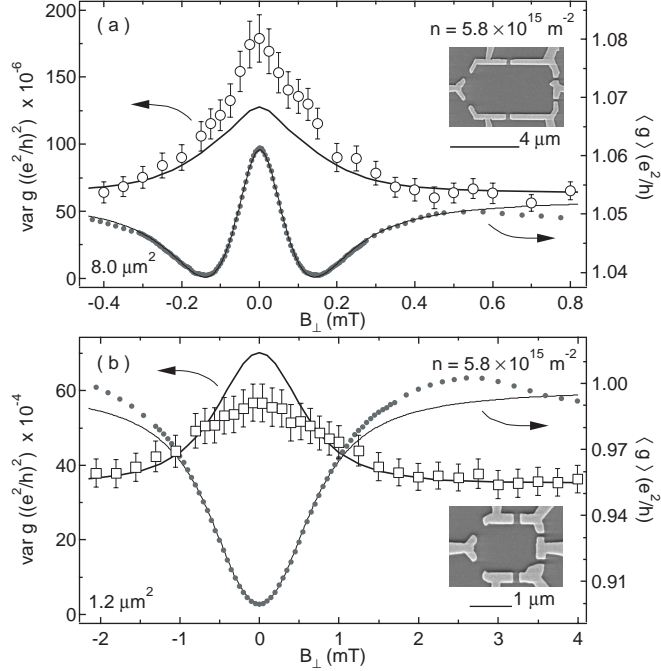
Figure 4.1: Average $\langle g(B_\perp)\rangle$ (solid dots) and variance var $g(B_\perp)$ (open symbols) of conductance as a function of magnetic field $B_\perp$ perpendicular to the 2DEG at a temperature $T = 300\,\mathrm{mK}$ and zero magnetic field $B_\parallel = 0$ in the plane of the 2DEG, measured in the devices on high density 2DEG. Insets show device micrographs. AL due to SO coupling is seen in the big $8\,\mu\mathrm{m}^2$ dot (a). WL is seen in the smaller $1.2\,\mu\mathrm{m}^2$ dot (b) fabricated on the same material, demonstrating confinement suppression of SO effects. Both dots show a larger variance at $B_\perp = 0$ when TRS is not broken. Fits of the RMT [4, 37] to $\langle g(B_\perp)\rangle$ are shown as dashed curves. Solid curves are the RMT for var $g(B_\perp)$ with the same parameters as obtained from fits to $\langle g\rangle$ times an overall correction factor (see text).
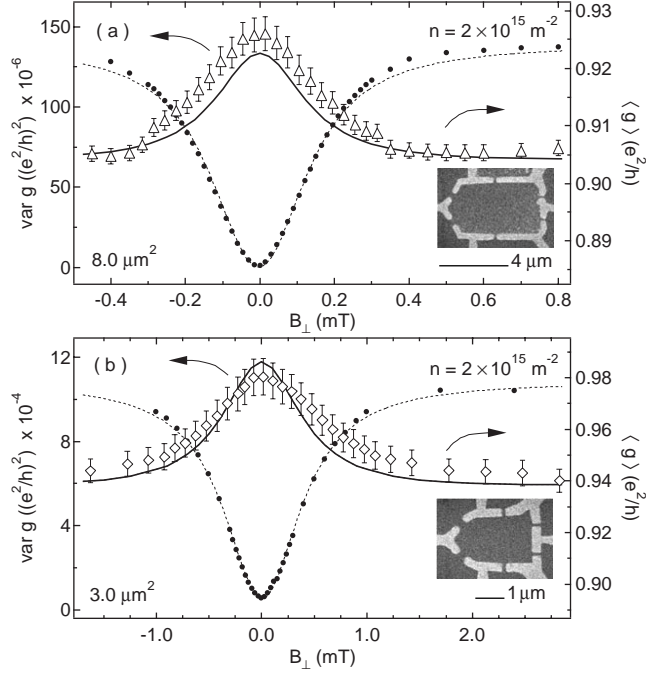
Figure 4.2: Average $\langle g(B_\perp)\rangle$ (solid dots) and variance var $g(B_\perp)$ (open symbols) at a temperature $T = 300\,\text{mK}$ and $B_\parallel = 0$, measured in the devices on low density 2DEG. Both devices display WL, indicating that SO effects are weak. Note that while both $8\,\mu\text{m}^2$ dots have nominally identical geometry, only the high density device shows AL. RMT is shown as dashed and solid curves, as described in the caption of Figure 1.

devices. An additional parameter κ' of order one in the RMT—relevant in the strong SO limit—is taken as $\kappa' = 1$ for all devices. For fit details see Ref. [205], parameters are listed in Table I. In absence of AL, only a lower bound on λ_{so} can be found. The extracted coherence times are comparable for all devices and consistent with previous experiments [96]. Note that the SO length λ_{so} is comparable to the device diameter $L = \sqrt{A}$ of the big dot.

On the low density material, both devices show WL, see Figure 4.2, indicating that for both dots $\lambda_{so} \gg L$, the regime of confinement suppressed SO coupling. Note that while both $8\,\mu\text{m}^2$ dots have nominally identical geometries, only the device on the high density 2DEG shows AL. Constrained by experiments observing WL (rather than AL) in identical devices made on this wafer [96] down to the lowest dilution-refrigerator temperatures, a lower bound $\lambda_{so} \gtrsim 8.5\,\mu\text{m}$ is estimated. It is noted that a $\lambda_{so} = 8.5\,\mu\text{m}$ noticeably reduces the WL correction amplitude at the lowest temperatures $T = 50\,\text{mK}$. The resulting low-temperature saturation of coherence times extracted using theory neglecting SO effects is

n	A	τ_φ	λ_{so}	ν_{so}	$\kappa_\perp$	f_{var}	ξ	a	b
m^{-2}	$\mu\mathrm{m}^2$	ns	μm					$\mathrm{ns}^{-1}\mathrm{T}^{-2}$	$\mathrm{ns}^{-1}\mathrm{T}^{-6}$
2.0	3.0	0.18	8.5	1.0	0.15	1.0	2.8	0.5±0.1	0.028
2.0	8.0	0.21	8.5	1.0	0.25	0.6	3.0	0.37±0.07	0.028
5.8	1.2	0.10	3.2	1.4	0.33	1.9	1.0	6.6±1	0.14
5.8	8.0	0.39	4.4	1.4	0.23	0.7	0.45	1.4±0.4	0.14

Table 4.1: Carrier density n, dot area $A = L^2$, coherence time τ_φ, spin-orbit parameters λ_{so} and ν_{so}, RMT parameters $\kappa_\perp$, f_{var} and ξ and FJ parameters a and b, see text.

consistent with the large dot results of Ref. [96].

4.6   Variance at Zero In-Plane Field

The variance of conductance fluctuations var $g(B_\perp)$ at $B_\parallel = 0$ is seen to be reduced upon application of a small perpendicular field $B_\perp$ [Figures 4.1 and 4.2]. This is due to breaking of TRS by $B_\perp$ and is well known [33, 97]. Using the parameters obtained from fits to $\langle g(B_\perp)\rangle$ and an additional overall factor f_{var} (Table I) to match the RMT variance at $B_\perp \neq 0$ with the experiment, the solid RMT curves in Figures 4.1 and 4.2 are obtained from Eq. (37) of Ref. [4, 37], which includes effects of thermal smearing and decoherence. The RMT—applicable for $N \gg 1$ in chaotic dots—calculates a ratio var $g(B_\perp = 0, B_\parallel)/$var $g(B_\perp \neq 0, B_\parallel)$ of two, independent of $B_\parallel$ (see below). Theories valid for $N = 2$ are not currently including SO effects [10].

4.7   Effects of Spin-Rotation Symmetry on the Variance

The variance in an in-plane field $B_\parallel$ when TRS is broken by $B_\perp \neq 0$ depends strongly on the SO properties. The open symbols in the main panels of Figures 4.3 and 4.4 show that the variance is reduced upon application of $B_\parallel$ and saturates at large $B_\parallel$, giving reduction factors $R =$ var $g(B_\perp \neq 0, B_\parallel = 0)/$var $g(B_\perp \neq 0, B_\parallel \gg 0)$ between $R \sim 1.6$ for the dot showing pronounced SO effects at $B_\parallel = 0$ and $R \sim 4$ for the low density dots showing WL at $B_\parallel = 0$. Reduction factors as small as $R \sim 1.3$ are seen in center gated devices with stronger SO coupling (not shown). Within the RMT these new experimental results are
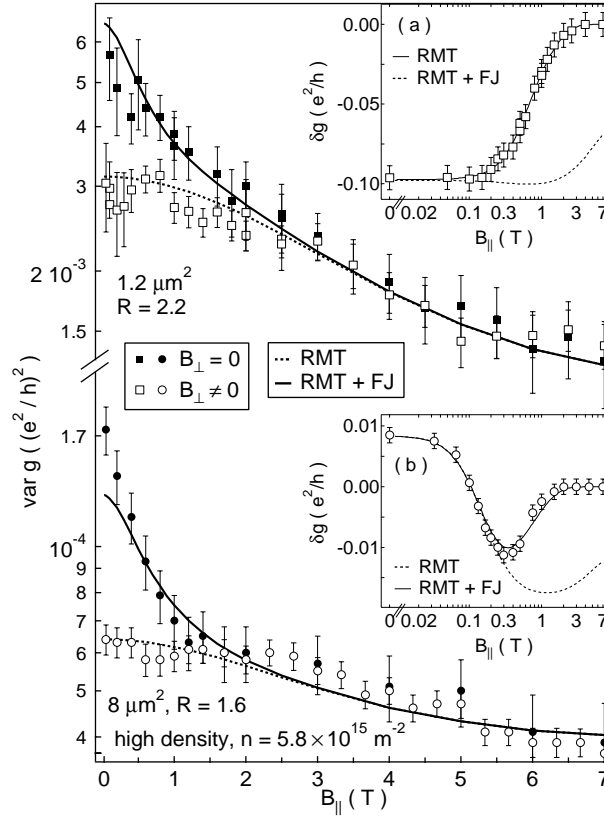
Figure 4.3: Variance of conductance fluctuations through high density devices as a function of in-plane field $B_\parallel$ with $B_\perp = 0$ (solid symbols) and $B_\perp \neq 0$ (open symbols) sufficiently large to break TRS. It is seen that the big dot with strong SO effects at $B_\parallel = 0$ shows a smaller reduction of the variance in $B_\parallel$ than the small dot. Insets show $\delta g(B_\parallel) = \langle g(B_\perp = 0, B_\parallel)\rangle - \langle g(B_\perp \neq 0, B_\parallel)\rangle$ (open symbols). Dashed curves show RMT, the solid curves are RMT+FJ, see text.

54

explained in terms of spin-rotation symmetries: in dots showing AL, SO coupling breaks Kramers degeneracy $s = 1$ and mixes up and down spins to some extent at already $B_\parallel = 0$ if $B_\perp \neq 0$, resulting in small reduction factors $1 \leq R \leq 2$. In dots showing WL, on the other hand, spin-rotation symmetry is intact at $B_\parallel = 0$ ($s = 2, \Sigma = 1$) but can be broken upon application of $B_\parallel$, resulting in reduction factors $R \sim 4$ (low density dots).

Breaking of spin rotation symmetry—besides the Zeeman effect $\epsilon_Z = g\mu_B B$ ($|g| = 0.44$) which breaks Kramers degeneracy—is caused by SO coupling combined with $B_\parallel$, introducing a new energy scale [87, 4, 37] $\epsilon_\perp^Z = \xi^2 \epsilon_Z^2/(2E_T)(A/\lambda_{so}^2)$. A is the device area, ξ is a geometry and $B_\parallel$ direction-dependent coefficient and E_T is the conventional Thouless energy. The associated field scale, given by $\epsilon_\perp^Z \gtrsim \tilde{\gamma}$, where $\tilde{\gamma}$ is the level broadening due to escape and decoherence [205], becomes large in small dots and in the weak SO limit and is inaccessible in the smallest dot, giving $R \sim 2$ due to breaking of Kramers degeneracy only. In the bigger, low density dots, where this field scale is one to two Tesla, the SO strength λ_{so} cannot be independently extracted from a var $g(B_\parallel)$ measurement because of the extra coefficient ξ. Using ξ as the only fit parameter, the dashed RMT curves in Figures 4.3 and 4.4 are obtained, giving good agreement for all devices.

4.8   Orbital effects of $B_\parallel$ on the Variance

Finally, we turn to orbital effects of $B_\parallel$ on the variance measured when TRS is not externally broken ($B_\perp = 0$). As $B_\parallel$ is increased from zero, var $g(B_\perp = 0, B_\parallel)$ is seen to decrease sharply, approaching var $g(B_\perp \neq 0, B_\parallel)$. At large $B_\parallel$, the measured variance becomes independent of $B_\perp$ within the errorbars (solid symbols, Figures 4.3 and 4.4) while the RMT predicts that the variance with $B_\perp = 0$ is twice the value at $B_\perp \neq 0$, independent of $B_\parallel$. On a comparable $B_\parallel$ field scale, quantum corrections to the average conductance, $\delta g(B_\parallel) = \langle g(B_\perp = 0, B_\parallel) \rangle - \langle g(B_\perp \neq 0, B_\parallel) \rangle$, are seen to be vanishing upon application of $B_\parallel$ in all devices (open symbols, insets), whereas the RMT calculates a reduced but finite δg (dashed curves, insets). Suppression of δg in $B_\parallel$ was previously reported [59, 205] and
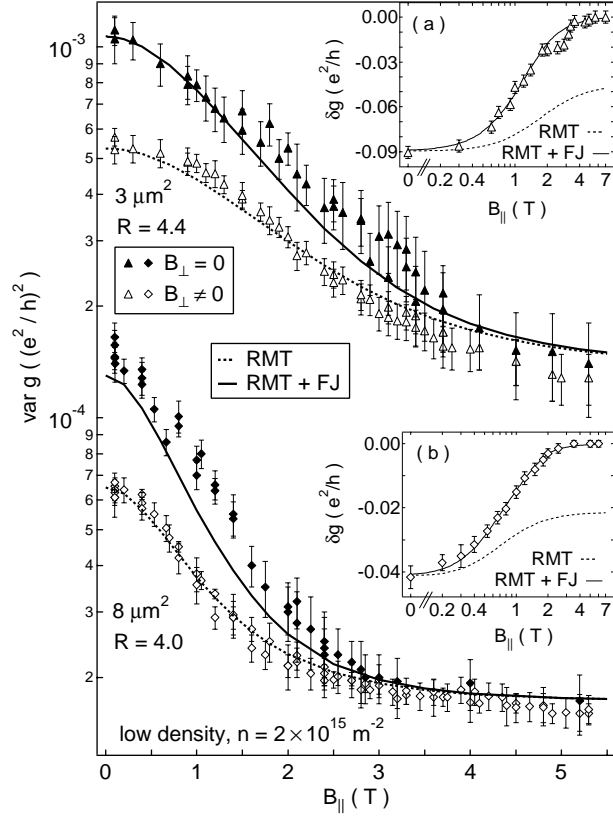
Figure 4.4: As Figure 3 but for low density devices. Due to effects of $B_\parallel$ to break TRS, the variance for $B_\perp = 0$ is seen to be reduced to the variance for $B_\perp \neq 0$ on the same $B_\parallel$ field scale where WL/AL effects are suppressed by $B_\parallel$ (insets).

is due to effects of $B_\parallel$ to break TRS [148, 56].

Following Ref. [56] (FJ), the suppressions of average and variance can be accounted for by a factor $f_{FJ}(B_\parallel) = (1 + \tau_{B\parallel}^{-1}/\tau_{esc}^{-1})^{-1}$, where $\tau_{B\parallel}^{-1} \sim aB_\parallel^2 + bB_\parallel^6$ and $\tau_{esc}^{-1} = N\Delta/h$ is the escape time. The $B_\parallel^2$ term reflects interface roughness and dopant inhomogeneities; the $B_\parallel^6$ term is due to the asymmetry of the well. It is assumed that the combined effects of the RMT and flux threading by $B_\parallel$ can be written as products $\delta g(B_\parallel) = \delta g_{RMT}(B_\parallel)f_{FJ}(B_\parallel)$ and $\text{var}\, g(B_\perp = 0, B_\parallel) = \text{var}\, g_{RMT}(B_\perp \neq 0, B_\parallel)(1 + f_{FJ}(B_\parallel))$ [4]. The coefficient a is obtained from a fit to the experimental $\delta g(B_\parallel)$ while b is estimated from device simulations[5] (Table I). The resulting theory curves for both $\delta g(B_\parallel)$ (solid curves, insets) and $\text{var}\, g(B_\perp = 0, B_\parallel)$ (solid curves, main panels) are in good agreement with the experiment. We emphasize that the theoretical variance curves are not fit. The coefficients a, b estimated from correlation functions [207] are consistent with the values obtained here from $\delta g(B_\parallel)$.

4.9   Conclusion and Acknowledgements

In summary, the variance of conductance fluctuations in open quantum dots in presence of SO coupling and in plane fields $B_\parallel$ is understood in terms of symmetries in the system, including novel spin rotation symmetries as well as time reversal symmetry, which can be broken both by perpendicular fields $B_\perp$ and parallel fields $B_\parallel$.

---

[4]V. Fal'ko and T. Jungwirth, private communication
[5]V. Fal'ko and T. Jungwirth, private communication

Orbital Effects of In-Plane Magnetic Fields Probed by Mesoscopic Conductance Fluctuations

D. M. Zumbühl, J. B. Miller*, C. M. Marcus

Department of Physics, Harvard University, Cambridge, Massachusetts 02138

**Division of Engineering and Applied Science*

Harvard University, Cambridge, Massachusetts 02138

V. I. Fal'ko

Physics Department, Lancaster University, LA1 4YB Lancaster, United Kingdom

T. Jungwirth

Institute of Physics ASCR, Cukrovarnická 10, 162 53 Praha 6, Czech Republic

University of Texas at Austin, Physics Department

1 University Station C1600, Austin TX 78712-0264

J. S. Harris, Jr.

Departement of Electrical Engineering

Stanford University, Stanford, California 94305

We use the high sensitivity to magnetic flux of mesoscopic conductance fluctuations in large quantum dots to investigate changes in the two-dimensional electron dispersion caused by an in-plane magnetic field. In particular, changes in effective mass and the breaking of momentum reversal symmetry in the electron dispersion are extracted quantitatively from correlations of conductance fluctuations. New theory is presented, and good agreement between theory and experiment is found.

5.1 Introduction

A simplified view of transport in a planar two-dimensional conductor, as formed for instance by a semiconductor heterostructure, suggests that when only the lowest quantized subband is occupied, an in-plane magnetic field couples only to the electron spin, allowing the influence of an applied magnetic field to be separated into spin and orbital parts. However, the emerging picture of quantum transport in parallel fields [148, 149, 56, 205, 206] has turned out to be surprisingly rich, indicating that even modest parallel (i.e., in-plane) fields can have significant orbital coupling, break time-reversal symmetry, and generate mesoscopic conductance fluctuations with field-dependent correlations—even without spin-orbit coupling or occupation of higher subbands.

In this Letter, we use the high sensitivity of mesoscopic conductance fluctuations (CF's) to magnetic flux and time-reversal symmetry (TRS) to examine in detail the orbital effects of an in-plane magnetic field, $B_{\parallel}$, in a quasiballistic quantum dot formed in a GaAs/AlGaAs 2D electron gas (2DEG). Quantitative comparison of experiment and theory developed here allows the effects of $B_{\parallel}$ on the electron dispersion in a planar 2DEG, including an anisotropic effective mass and a breaking of TRS (in spatially asymmetric confinement potentials), to be distinguished using various correlation functions of CF's. Effects of nonplanarity of the 2DEG are also included in the theory, and have distinguishable signatures in the CF correlations. The significance of the present work is to demonstrate experimentally that the effects of an in-plane field go far beyond Zeeman coupling, but *cannot* be characterized in terms of simple flux threading through the finite thickness of a 2D electron layer. Also, this study shows that phase coherent CF's can be used as a sensitive quantitative tool, much as one uses a superconducting quantum interference device (SQUID).

5.2 Previous Experiments

Effects of parallel fields on quantum transport have been investigated in 2D systems, including metal films [162, 71], silicon MOSFET's [23, 147, 123], and GaAs/AlGaAs 2DEG's

[132, 92], as well as in ballistic focusing geometries [159, 161]. Those results were mostly interpreted in terms of flux threading due to finite thickness in the confined direction, surface roughness, or deformation of the Fermi circle due to the field. Subband depopulation, decoupling of bilayer systems and diamagnetic shifts caused by $B_\parallel$ have also been observed using cyclotron resonance techniques [179], magnetoresistance measurements [128, 142, 139, 192], and tunneling [34], as well as optical spectroscopy [175, 111, 122]. Related investigations based on quantum-dot weak localization [205, 206] were only sensitive to the breaking of TRS by a parallel field. Here, by using the full CF correlations, the effect of $B_\parallel$ on the full electron dispersion is investigated, and the various contributions are distinguished.

5.3 Experimental Setup

Two quantum dots, with areas $A = 8\,\mu\mathrm{m}^2$ and $3\,\mu\mathrm{m}^2$, made on the same wafer, were measured and showed similar behavior. Data from the $8\,\mu\mathrm{m}^2$ dot (see Figure 5.3, inset) will be presented in detail. The dots are formed by lateral Cr-Au depletion gates defined by electron-beam lithography on the surface of GaAs/AlGaAs heterostructures grown in the [001] direction. The 2DEG interface is $900\,\text{Å}$ below the wafer surface, comprising a $100\,\text{Å}$ GaAs cap layer and a $800\,\text{Å}$ $\mathrm{Al}_{0.34}\mathrm{Ga}_{0.66}\mathrm{As}$ layer with a $400\,\text{Å}$ Si doped layer set back $400\,\text{Å}$ from the 2DEG. An electron density of $n = 2 \times 10^{15}\,\mathrm{m}^{-2}$ and bulk mobility $\mu \sim 14\,\mathrm{m}^2/\mathrm{Vs}$ (cooled in the dark) gives a transport mean free path $\ell_e \sim 1\,\mu\mathrm{m}$. Note that the $8\,\mu\mathrm{m}^2$ dot contains of order 10^4 electrons.

Measurements were made in a ^{3}He cryostat at $0.3\,\mathrm{K}$ using current bias of $1\,\mathrm{nA}$ at $338\,\mathrm{Hz}$. Shape-distorting gates were used to obtain ensembles of statistically independent conductance measurements [141, 33, 98] while the point contacts were actively held at one fully transmitting mode each ($N = 2$). In order to apply tesla-scale $B_\parallel$ while maintaining sub-gauss control of $B_\perp$, we mount the sample with the 2DEG aligned to the axis of the primary solenoid (accurate to $\sim 1°$) and use an independent split-coil magnet attached to the cryostat to provide $B_\perp$ [59]. The Hall effect measured in a separate GaAs Hall bar mounted

next to the quantum dot, as well as the location of weak localization minima in transport through the dot itself (visible $B_\parallel \lesssim 2T$) were used to determine the offset in $B_\perp$ (i.e. the residual sample tilt), which was then corrected by computer control of the two independent magnets.

5.4 Conductance Fluctuations and Symmetries of Conductance in an In-Plane Magnetic Field

The raw data consist of measured dot conductance $g(B_\parallel, B_\perp, V)$ as a function of shape-distorting gate voltage V (inner loop of multiparameter sweeps), $B_\perp$, and $B_\parallel$ (outer loop, swept from $-2.5\,\mathrm{T}$ to $+4\,\mathrm{T}$ over $\sim 20\,\mathrm{h}$), giving 20 independent shape, 15 independent $B_\perp$ and about 10 independent $B_\parallel$ samples. Conductance fluctuations are found by subtracting the gate-voltage averaged conductance over the measured range: $\delta g(B_\parallel, B_\perp, V) = g(B_\parallel, B_\perp, V) - \langle g(B_\parallel, B_\perp, V) \rangle_V$.

Figure 5.1 shows 2D slices of conductance fluctuations in the full 3D space of $B_\parallel$, $B_\perp$, and V. Note that because gate-voltage-averaged conductance is subtracted from the fluctuations, weak localization effects on $\langle g \rangle$ are not evident in Figure 5.1. A principal result is already evident in Figure 5.1: The horizontally elongated features around $|B_\parallel| \sim 0$ in Figure 5.1(c) show qualitatively that CF's are less sensitive to $B_\parallel$ in the vicinity of $|B_\parallel| \sim 0$, giving a larger correlation field near $|B_\parallel| \sim 0$, than at larger parallel fields. This elongation, demonstrating reduced flux sensitivity near $|B_\parallel| \sim 0$, is consistent with the $B_\parallel$ dependent effective mass and momentum reversal symmetry breaking terms of our theory. Effects of nonplanarity alone would result in a $B_\parallel$ independent correlation field. A quantitative analysis is presented in Figure 5.2.

The 2D slices in Figure 5.1 also illustrate the fundamental symmetries of conductance with respect to magnetic fields $B_\parallel$ and $B_\perp$: when $B_\parallel = 0$, conductance is symmetric under inversion of $B_\perp$, $g(B_\perp) = g(-B_\perp)$ [see Figure 5.1(b)]; when $B_\perp = 0$, conductance is symmetric under inversion of $B_\parallel$, $g(B_\parallel) = g(-B_\parallel)$ [see Figure 5.1(c)]. When both $B_\parallel$
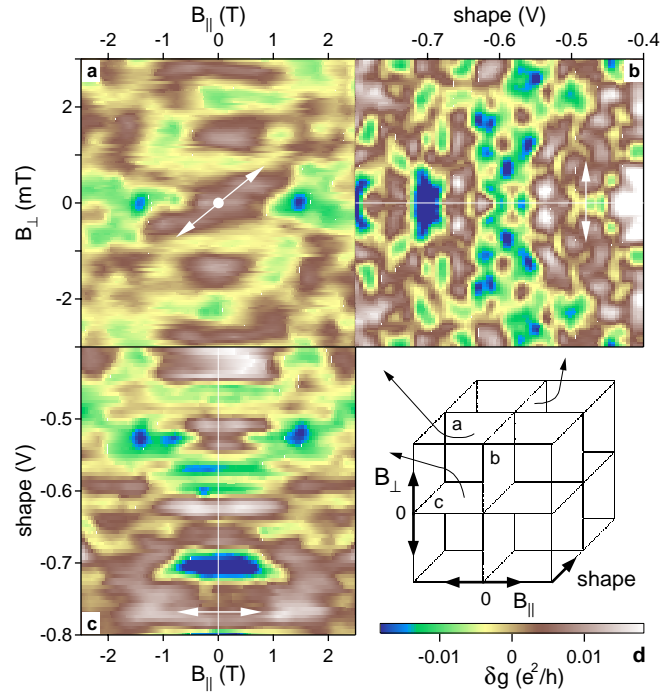
Figure 5.1: Conductance fluctuations $\delta g(B_\parallel, B_\perp, V) = g(B_\parallel, B_\perp, V) - \langle g(B_\parallel, B_\perp, V)\rangle_V$ (color scale) through an $8\,\mu m^2$ dot with one fully transmitting channel in each lead measured at 0.3K with a) shape-gate voltage $V = -515\,mV$, b) $B_\parallel = 0$ and c) $B_\perp = 0$, obtained from 2D slices of the three dimensional CF pattern, as indicated in d).

and $B_\perp$ are nonzero, the symmetry of conductance requires the reversal of both fields, $g(B_\parallel, B_\perp) = g(-B_\parallel, -B_\perp)$ [see Figure 5.1(a)] [30]. The fact that a nonzero $B_\parallel$ breaks the symmetry $g(B_\perp) = g(-B_\perp)$ is a simple qualitative demonstration that $B_\parallel$ breaks TRS [205, 206]. A quantitative analysis of this effect is presented in Figure 5.3.

5.5 Theory of Correlations of Conductance Fluctuations in an In-Plane Field

To quantify the correlations of the various parameters used to generate CF's — including in particular $B_\parallel$ — we define the normalized correlation functions,

$$C_v(B_\parallel) = \frac{\langle \delta g(B_\parallel, V) \delta g(B_\parallel, V + v) \rangle}{\langle \delta g^2(B_\parallel) \rangle} \tag{5.1}$$

$$C_{b_\perp}(B_\parallel) = \frac{\langle \delta g(B_\parallel, B_\perp) \delta g(B_\parallel, B_\perp + b_\perp) \rangle}{\langle \delta g^2(B_\parallel) \rangle} \tag{5.2}$$

$$C_{b_\parallel}(B_\parallel) = \frac{\langle \delta g(B_\parallel) \delta g(B_\parallel + b_\parallel) \rangle}{\sqrt{\langle \delta g^2(B_\parallel) \rangle \langle \delta g^2(B_\parallel + b_\parallel) \rangle}}, \tag{5.3}$$

where $\langle \ldots \rangle$ is shorthand for $\langle \ldots \rangle_{V,B_\perp}$, i.e., averaging over both gate voltage and $B_\perp$, with $B_\perp$ sufficiently large to fully break TRS throughout the measured range.

Theoretical expressions for the correlation functions in Equations (3.1-3.3) can be found using the effective 2D Hamiltonian

$$\hat{H}_{2D} = \frac{\mathbf{p}^2}{2m} - p_\perp^2 \gamma(B_\parallel) + p_\perp^3 \beta(B_\parallel) + u(\mathbf{r}), \tag{5.4}$$

for electrons confined to a plane perpendicular to $\hat{z}$ [56]. Here, $\mathbf{p} = -i\hbar\nabla - \frac{e}{c}\mathbf{A}_{2D}$, with $\mathrm{rot}\mathbf{A}_{2D} = B_\perp$, is the 2D momentum operator in the plane, with component $p_\perp = \vec{p} \cdot [\vec{B}_\parallel \times \vec{l}_z]/B_\parallel$ perpendicular to $B_\parallel$, and $u(\mathbf{r})$ is the impurity and dot confining potential. The middle terms in $\hat{H}_{2D}$ arise from $p_\perp$-dependent subband mixing: the $\gamma(B_\parallel)$ term lifts rotational symmetry with an anisotropic mass enhancement [92] but does not break TRS;

63

the $\beta(B_\parallel)$ arises from the broken spatial inversion symmetry of the heterointerface and breaks TRS in presence of $B_\parallel$.

Extending the analysis of Ref. [56] to higher temperature yields a correlation between conductance fluctuations at $B_\parallel$ and at $B_\parallel + b_\parallel$ of the form

$$C_{b_\parallel}(B_\parallel) = \left[1 + \frac{\tau_d^{-1}(B_\parallel, b_\parallel)}{\tau_{esc}^{-1}}\right]^\alpha, \tag{5.5}$$

in the unitary ensemble, where $\tau_{esc}^{-1} = N\Delta/h$ is the escape rate from the dot, with $\Delta = 2\pi\hbar^2/m^*A$ the mean level spacing of the corresponding closed dot (effective electron mass $m^* = 0.067m_e$), τ_d^{-1} is an additional escape rate due to orbital effects of $B_\parallel$, as discussed below. The exponent α equals -1 in the high temperature limit $kT \gg (\hbar\tau_{esc}^{-1}, \hbar\tau_d^{-1}, \epsilon_Z)$, applicable in the present experiment, and -2 in the low temperature limit, where $\epsilon_Z = g\mu_B B$ is the Zeeman energy, with $g = -0.44$ for GaAs. The difference between the high and low temperature regimes is caused by the necessity to average the interference contributions coming from electrons at different energies. For parallel fields with $\epsilon_Z \lesssim 3kT$, appropriate for the present measurements, the deviation of Equation (5.5) from the full expression is negligible [6].

The additional escape rate τ_d^{-1} due to $B_\parallel$ is given by

$$\begin{aligned}
\tau_d^{-1}(B_\parallel, b_\parallel) &= \frac{\tau p_F^4}{8\hbar^2}\left[\gamma(B_\parallel) - \gamma(B_\parallel + b_\parallel)\right]^2 \\
&+ \frac{\tau p_F^6}{8\hbar^2}\left[\frac{\beta(B_\parallel) - \beta(B_\parallel + b_\parallel)}{2}\right]^2 + \frac{\zeta^2 p_F^2}{2\tau}b_\parallel^2,
\end{aligned} \tag{5.6}$$

where $\tau = \mu m^*/e$ is the elastic scattering time in a diffusive dot or the crossing time $\tau = m^*L/p_F$ in a ballistic device, where L is the diameter of the device and $p_F = \hbar(2\pi n)^{1/2}$ is the Fermi momentum. The ζ term describes effects of nonplanarity, including interface roughness and dopant inhomogeneities, and also breaks TRS.

---

[6] V. I. Fal'ko and T. Jungwirth, unpublished.
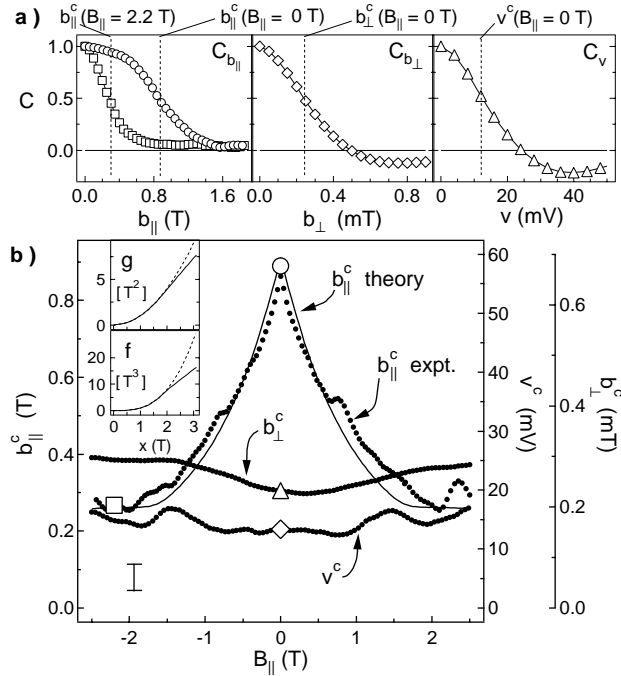
Figure 5.2: a) Correlation functions $C_{b_\parallel}$ at $B_\parallel = 0, 2.2\,\mathrm{T}$ (open circles, squares) as well as $C_{b_\perp}$ (open diamonds) and C_v (open triangles) at $B_\parallel = 0$. Half width at half maximum values give the characteristic voltage v^c and fields $b_\perp^c$ and $b_\parallel^c$, shown in b) (solid circles) as a function of $B_\parallel$. Markers in b) refer to corresponding curves in a). The solid curve shows the three-parameter theory. A typical error bar is indicated. Insets: $g(x)$ and $f(x)$ used for fits (see text) as obtained from numerical simulations (solid curves) as well as quadratic and cubic low field approx. (dashed curves).

Writing the functions $\gamma(x)$ and $\beta(x)$ in Equation (5.6) in terms of scale factors $\tilde\gamma$ and $\tilde\beta$ and normalized functions $g(x)$ and $f(x)$ as $\gamma(x) = \tilde\gamma g(x)$ and $\beta(x) = \tilde\beta f(x)$, we find $g(x)$ and $f(x)$ from self-consistent simulations of the heterostructure [7] and treat $\tilde\gamma$ and $\tilde\beta$ as fit parameters. Below ~ 2 T , the normalized functions are well approximated by $g(x) \approx x^2$ and $f(x) \approx x^3$ [see Figure 5.2(b), insets]; however, the full functions are used for all comparison of theory and experiment. We note that $\tilde\gamma$ and $\tilde\beta$ can also be obtained from the heterostructure simulations, giving values in reasonable agreement with those obtained from the fits.

---

[7]The simulations take into account band offsets, Hartree and exchange-correlation potentials as well as the potential due to residual acceptor impurities, as obtained from the onset of second subband population.

5.6 Correlation Lengths

Figure 5.2(a) shows experimental correlation functions, $C_{b_{\parallel}}$, $C_{b_{\perp}}$, and C_v, for representative parallel fields, as indicated. The corresponding characteristic voltage v^c and fields $b_{\parallel}^c$ and $b_{\perp}^c$ are shown in Figure 5.2(b) as a function of $B_{\parallel}$, as obtained from the half width at half maximum (HWHM) values of the correlation functions, indicated by dashed lines in Figure 5.2(a). It is evident from Figure 5.2(b) that both $b_{\perp}^c$ and v^c *are independent of* $B_{\parallel}$ within the error bars, in agreement with theory and previous experiments [59]. (An alternative procedure, not shown, for extracting these same quantities from the slopes of log-power spectra of CF's yields similar values for v^c and $b_{\parallel}^c$ that are again independent of $B_{\parallel}$, within error bars.)

In contrast, the parallel field correlation length, $b_{\parallel}^c$, shown in Figure 5.2(b) decreases substantially from its zero-field value on a field scale of $\sim 1\,\mathrm{T}$. Good agreement with theory is found: the solid curve in Figure 5.2(b) is the best-fit (described below) theoretical HWHM correlation field for $C_{b_{\parallel}}(B_{\parallel})$ obtained from Equation (5.5). This decrease is due to the γ and β terms in Equation (5.6) and cannot be accounted for with the ζ term alone.

5.7 Symmetries of Conductance Fluctuations

Symmetries of conductance in parallel and perpendicular fields are investigated in Figure 5.3. We define the cross-correlation functions

$$C_{\pm\pm}(B_{\parallel}) = \frac{\langle \delta g(B_{\parallel}, B_{\perp}) \delta g(\pm B_{\parallel}, \pm B_{\perp}) \rangle}{\sqrt{\langle \delta g^2(B_{\parallel}, B_{\perp}) \rangle \langle \delta g^2(\pm B_{\parallel}, \pm B_{\perp}) \rangle}}. \tag{5.7}$$

With this definition, the first (second) subscript index of C refers to whether $B_{\parallel}(B_{\perp})$ is reversed when computing the correlation function. Correlations for total field reversal, C_{--} (i.e., both $B_{\parallel}$ and $B_{\perp}$ inverted) remain near unity for all parallel fields, as expected from the full Landauer-Büttiker (Onsager) symmetry [see Figure 5.3(a)]. Deviations from a perfect
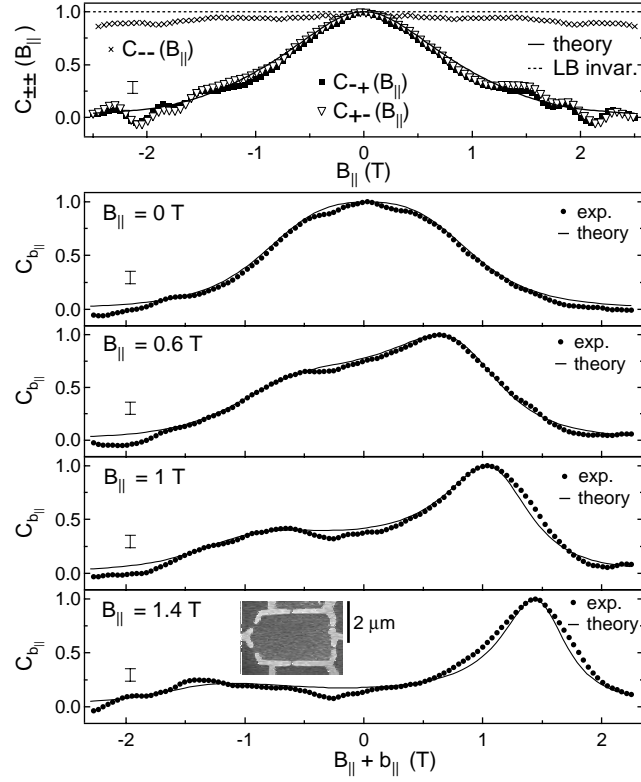
Figure 5.3: Top: Cross-correlations of CF's at $(B_\parallel, B_\perp)$ with CF's at $(-B_\parallel, -B_\perp)$ (C_{--}, crosses), $(-B_\parallel, B_\perp)$ (C_{-+}, squares) and $(B_\parallel, -B_\perp)$ (C_{+-}, triangles) as a function of $B_\parallel$. Landauer-Büttiker (LB) symmetry for full field reversal gives $C_{--} = 1$ (Dashed line). Below: Correlation functions $C_{b_\parallel}(B_\parallel)$ at $B_\parallel = 0, 0.6, 1, 1.4$ T. Solid curves show theory based on Equation (5.5). Typical error bars as indicated.

correlation $C_{--} = 1$ are small, indicating that the confining potential of the dot did not drift significantly over periods of a day. Figure 5.3(a) also shows conductance fluctuations at $(B_\parallel, B_\perp)$ and $(B_\parallel, -B_\perp)$ (C_{+-}) become uncorrelated $(C_{+-} \sim 0)$ at parallel fields of a few tesla, indicating the field scale at which $B_\parallel$ breaks TRS. Within error bars, C_{-+} is indistinguishable from C_{+-}, as expected from Landauer-Büttiker symmetry, $\delta g(-B_\parallel, B_\perp) = \delta g(B_\parallel, -B_\perp)$. The theoretical cross-correlation using Equation 5.5), shown as a solid curve in Figure 5.3(a), is in very good agreement with experiment data.

5.8   Full Conductance Correlations and Echo

Finally, we discuss the full correlation, $C_{b_\parallel}(B_\parallel)$, of CF's at $B_\parallel$ with CF's at $B_\parallel + b_\parallel$. Representative curves for $B_\parallel = 0$, 0.6, 1, 1.4 T are shown in the lower part of Figure 5.3 as a function of $B_\parallel + b_\parallel$, along with best-fit theory curves based on Equation (5.5). Besides the perfect correlation at $b_\parallel = 0$ $(C_{b_\parallel=0} = 1)$, there is an "echo" of correlations, both in experiment and theory, that occurs at $b_\parallel \sim -2B_\parallel$. Within the present theory, this field-reversed correlation "echo", $C_{-2B_\parallel}$, is suppressed from unity only to the extent that parallel field breaks TRS. The agreement between theory and experiment, including the unusual asymmetric curves in Figure 5.3, is quite good. A single, consistent set of three parameters $(\tilde{\gamma}, \tilde{\beta}, \zeta)$ have been obtained from fits of Equation (5.5) to 131 curves like those in Figure 5.3, ranging over $-2.5\,\mathrm{T} \leq B_\parallel \leq 4\,\mathrm{T}$. We emphasize that *all* theory curves shown in Figure 5.2 and Figure 5.3 used this single set of three fit parameters and were not individually fit. The values obtained in this way were $\tilde{\gamma} = 11 \pm 2 \times 10^{-4}\,[m^*]^{-1}T^{-2}$, $\tilde{\beta} = 4 \pm 4 \times 10^{-4}[m^*p_F]^{-1}T^{-3}$, and $\zeta = 44 \pm 8 \times 10^{-3}[p_F]^{-1}T^{-1}$, consistent within the error bars with values extracted for the $3\,\mu\mathrm{m}^2$ dot. We note that parameters $\tilde{\beta}$ and ζ obtained from the parallel-field-induced crossover from the orthogonal to the unitary ensemble [205, 206] are in good agreement. The self-consistent simulations give theoretical values of $\tilde{\gamma} = 35 \times 10^{-4}\,[m^*]^{-1}T^{-2}$, $\tilde{\beta} = 3 \times 10^{-4}[m^*p_F]^{-1}T^{-3}$.

5.9 Conclusion

In summary, orbital effects of an in-plane magnetic field $B_\parallel$ were experimentally investigated using the high sensitivity of CF's to magnetic flux in a large quasiballistic quantum dot. Detailed quantitative comparison of correlations of CF's induced by $B_\parallel$ with theory developed here reveal the mechanisms of coupling, including an induced anisotropic effective mass, the breaking of time-reversal symmetry due to the heterostructure asymmetry and effects of nonplanarity. In the present experiment, spin-orbit coupling is weak. On the other hand, the combined influence of stronger spin-orbit coupling [205, 206] and parallel fields is expected to yield interesting additional features in the correlations and symmetries of CF's [37, 4]. These remain to be investigated experimentally.

Cotunneling Spectroscopy in Few-Electron Quantum Dots

D. M. Zumbühl, C. M. Marcus

Department of Physics, Harvard University, Cambridge, Massachusetts 02138

M. P. Hanson, A. C. Gossard

Materials Department, University of California at Santa Barbara

Santa Barbara, California, 93106

Few-electron quantum dots are investigated in the regime of strong tunneling to the leads. Inelastic cotunneling is used to measure the two-electron singlet-triplet splitting above and below a magnetic field driven singlet-triplet transition. Evidence for a non-equilibrium two-electron singlet-triplet Kondo effect is presented. Cotunneling allows orbital correlations and parameters characterizing entanglement of the two-electron singlet ground state to be extracted from dc transport.

6.1 Introduction

Transport studies of few-electron quantum dots have proven to be a rich laboratory for investigating the energetics of electrons in artificial atoms [193, 121, 89, 168, 51] as well as related spin effects, including ground-state spin transitions [191, 13, 182, 126, 66, 67, 76], spin lifetimes [76, 66, 67, 52] and Kondo effects [74, 39, 177, 181, 197, 64]. The interplay of electron-electron interactions, electron spin, and coupling to a Fermi sea makes transport in the few-electron regime a subtle problem in many-body physics [77, 78, 199, 165, 90, 54, 169, 72, 55, 170, 95, 171, 174]. Of particular importance is the two-electron case ("quantum dot helium") [174] since this is a paradigm for the preparation of entangled electronic states [28], and in double quantum dots is the basis of a quantum gate proposal [133].

In this Letter, we present a detailed experimental investigation of cotunneling through quantum dots containing one, two, and three electrons. Measurements of inelastic cotunneling are used to extract the singlet-triplet (ST) splitting across the two-electron ST transition. Evidence of a non-equilibrium ST Kondo effect for two electrons is presented. Cotunneling and Kondo effects are used to determine the g-factor for magnetic fields along different directions in the plane of the 2D electron gas (2DEG), giving isotropic g-factors close to the bulk GaAs value. Using both cotunneling and sequential tunneling data, we extract quantum correlations of the two-electron singlet ground state, allowing the degree of spatially separated entanglement to be measured.

6.2 Previous Experiments and Theories

Previous transport studies of few-electron quantum dots have identified the ST ground state transition for two electrons [193, 121, 66, 67, 126, 191, 13, 182] as well as for larger electron numbers [117, 65, 194]. Inelastic cotunneling was recently investigated in few-electron vertical structures in Ref. [42, 200]. These authors demonstrated that inelastic cotunneling provides a direct and sensitive measure of excited state energies. Here, we use this fact to measure the ST splitting, J, across the ST transition (for both negative
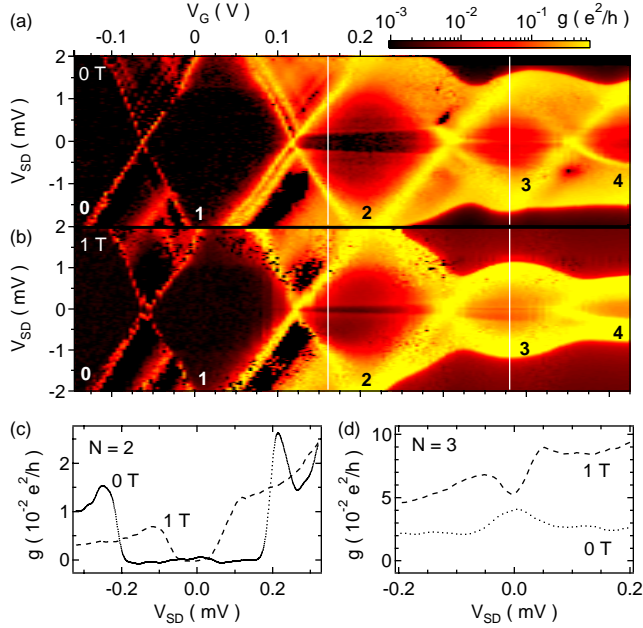
Figure 6.1: (a) Differential conductance g (log color scale) as a function of source-drain bias V_{SD} and gate voltage V_G at $B_\perp = 0$, at base electron temperature $T_{el} = 45$ mK. Numbers 0 through 4 are number of electrons in the dot. White vertical lines identify the locations for data shown in (c) and (d). (b) Same as (a), at $B_\perp = 1$ T. (c) Differential conductance through the $N = 2$ diamond showing step with overshoot at $V_{SD} = J(B_\perp)/e$ at $B_\perp = 0$ and 1 T. (d) Differential conductance through the $N = 3$ diamond showing Kondo peak at $V_{SD} = 0$ for $B = 0$, split by $B_\perp = 1$ T.

and positive J), and for the first time extract two-electron ground state wave function correlations from cotunneling.

Transport through the ST transition has been studied theoretically [199, 165, 90], with a prediction of enhanced Kondo correlations at the ST crossing [54, 169]. Effects of lifting spin degeneracy of the triplet have also been theoretically investigated [72, 55, 170]. For the degenerate triplet case, a characteristic asymmetric peak in conductance at the ST crossing has been predicted [95, 171, 77, 78]. This predicted asymmetric peak is observed in the present experiment. Previous measurements of ST Kondo effects [177, 181, 197, 64, 158, 131] in dots have not treated the two-electron case.

Measurements were carried out on two similar lateral quantum dots formed by Ti/Au depletion gates on the surface of a $GaAs/Al_{0.3}Ga_{0.7}As$ heterostructure 105 nm above the 2DEG layer (Figure 6.5, inset). The two devices showed similar results; most data are from one of

the dots, except those in Figure 6.5. The dilution refrigerator base electron temperature was $T_{el} = 45 \pm 5$ mK, measured from Coulomb blockade peak widths. Differential conductance $g = dI/dV_{SD}$ was measured with typical ac excitations of $5\,\mu$V.

6.3   Few Electron Coulomb Blockade Spectroscopy

Figures 6.1(a,b) provide an overview of transport spectroscopy data. Diamond patterns of high conductance correspond to gate voltages V_G where the ground state of the dot aligns with the chemical potential of either the source or drain, allowing sequential tunneling through the dot [8] [3]. Transport is absent at more negative gate voltages, indicating the absolute occupancy of the dot ($N = 0$ to 4). Conductance features that vanish below a finite source-drain voltage $|V_{SD}| = \Delta/e$ involve transport through an excited state at energy Δ above the ground state. An example of the latter is the nearly horizontal band running through the center of the $N = 2$ diamond. Beyond this band transport through the excited triplet channel of the $N = 2$ dot becomes allowed, as discussed below.

Inside the diamonds, sequential tunneling is Coulomb blockaded and transport requires higher order (cotunneling) processes [42, 200, 3]. Elastic cotunneling leaves the energy of the dot unchanged; inelastic cotunneling, which leaves the dot in an excited state, requires energy supplied by the source-drain bias. The inelastic mechanism becomes active above a threshold V_{SD} and is independent of V_G.

6.4   One Electron Inelastic Cotunneling

We first discuss the one-electron regime. A conduction threshold within the $N = 1$ diamond [Figures 6.1(a,b)] emerges from the crossing of ground-state and excited-state sequential tunneling lines [42, 200]. These features correspond to the onset of inelastic cotunneling through the first orbital excited state lying $\Delta_1 \sim 1.2(1.0)$ meV above the ground state

---

[8]Density of states modulations in the leads, here due to nanostructures adjacent to the dot, can give additional weak diagonal lines (see for example $V_{SD} > 0$, $V_G \sim -0.05$ V
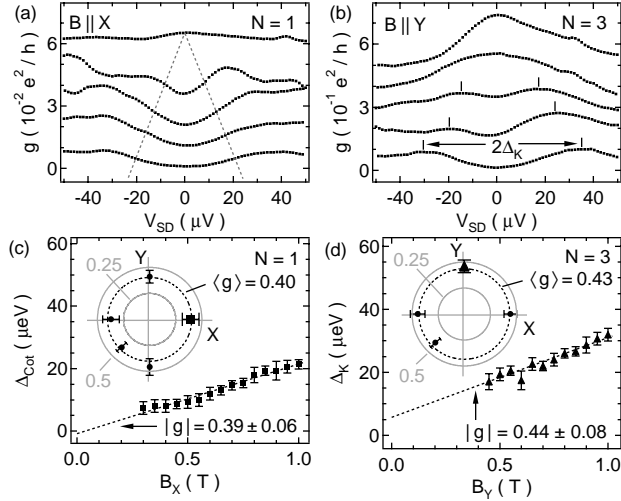
Figure 6.2: (a) Differential conductance g as a function of V_{SD} in the $N = 1$ diamond ($V_G = 0.1$ V) for in-plane fields $B_X = 0, 0.4, 0.6, 0.8, 1$ T, (top to bottom, curves offset). Dashed grey lines are guides to the eye showing the cotunneling gap. (b) $g(V_{SD})$ shows a zero-bias peak in the $N = 3$ valley ($V_G = 0.42$ V) that splits in an in-plane field $B_Y = 0, 0.25, 0.45, 0.7, 0.95$ T (top to bottom, curves offset). (c,d) splitting energies (see text) versus magnetic field as in (a,b) with linear fits. Insets: angular dependence of the g-factor in the plane of the 2DEG indicating isotropic behavior. Dashed circles show direction-averaged g-factors. Directions X and Y in the plane are arbitrary.

for a field $B_\perp = 0(1)$ T perpendicular to the 2DEG. Measurements with magnetic fields up to 1 T along different directions in the plane of the 2DEG show inelastic cotunneling through Zeeman split one-electron states [Figure 6.2(a)]. Measurement of Zeeman energies via cotunneling was established in Ref. [116]. The cotunneling gap Δ_{Cot}—extracted by taking half the peak splitting of dg/dV_{SD}—is shown in Figure 6.2(c) for one of the field directions. The g-factors are extracted from a linear fit to $\Delta_{\text{Cot}}(B)$ and are found to be isotropic within experimental error, giving a value of $\langle g \rangle = 0.40 \pm 0.03$ averaged over the measured field directions. This is close to the bulk GaAs value and consistent with previous (few-electron) experiments [89, 168, 51].

6.5   Three Electron Kondo Effect

For $N = 3$, a zero-bias conductance peak, presumably due to the Kondo effect [74, 39], splits in both perpendicular [Figure 6.1(d)] and in-plane [Figure 6.2(b)] magnetic fields. The splitting Δ_K due to in-plane field—taken as half the distance between maxima of
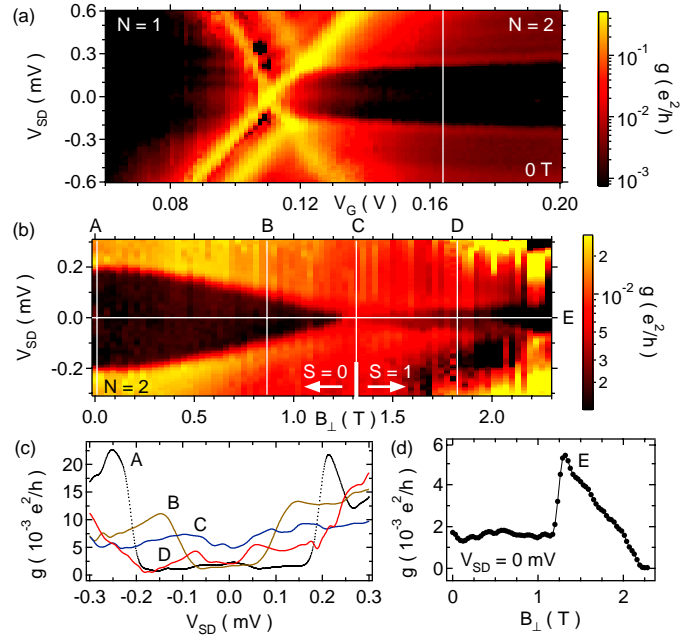
Figure 6.3: (a) Differential conductance g (log color scale) as a function of V_{SD} and V_G for $B = 0$ T in the vicinity of the $N = 1 \rightarrow 2$ transition. (b) $g(V_{SD}, B_\perp)$ at $V_G = 0.164$ V (vertical white line in (a)) shows the perpendicular field dependence of the singlet-triplet gap. (c) Cuts showing $g(V_{SD})$ at the positions of the vertical lines in (b), marked A, B, C, D. (d) Horizontal cut (E in (b)) showing $g(B_\perp)$ at zero bias. Note the asymmetric peak in g at the singlet-triplet transition.

the split peaks [indicated in Figure 6.2(b)]—is shown in Figure 6.2(d) along with a best fitting line. Slopes from the fits do not depend on direction in the plane, and give $\langle g \rangle = 0.43 \pm 0.03$, consistent with the one-electron cotunneling data [Figure 6.2(c)]. Note that unlike the cotunneling data, the Kondo data does not extrapolate to $\Delta_{\mathrm{K}}(0) = 0$, as also reported in previous experiments [116]. The threshold in-plane field B_K for the appearance of Kondo peak splitting gives an estimate of the Kondo temperature $(g\mu_B B_K \gtrsim k_B T_K)$ of $T_K \sim 150$ mK [116].

6.6 Two-Electron Singlet-Triplet Crossover in a Magnetic Field

A detailed view of two-electron transport is shown in Figure 6.3(a). The nearly horizontal band running through the $N = 2$ diamond [see also Figure 6.1(a,b)] corresponds to the onset of inelastic cotunneling through the triplet excited state, which becomes active for $|V_{SD}| > J/e$. The inelastic cotunneling edges align with the triplet excited state lines seen in sequential tunneling outside the diamond, as expected [42, 200]. We use this cotunneling feature to measure the ST splitting J. The zero-field value measured here, $J(B = 0) \sim 0.2$ meV, is much less than the $N = 1$ orbital level spacing due to strong interactions, consistent with theoretical estimates [28] and previous measurements [126]. A surprising zero-bias conductance peak in the middle of the cotunneling gap, visible in Figure 6.3(a) in the range 0.12 V$\lesssim V_G \lesssim 0.15$ V is not understood.

Perpendicular field dependence of the ST splitting $J(B_\perp)$ is investigated by plotting g along a cut through the $N = 2$ valley as a function of $B_\perp$ [Figure 6.3(b)]. Near $B_\perp = B^* \sim 1.3$ T the ST gap closes and then re-opens at larger fields. We interpret this as a ST crossing where the triplet state becomes the ground state for $B_\perp > B^*$ [Figure 6.4(b)]. We note that in-plane fields up to 1 T cause no observable change in the two electron spectrum. We also find that J depends on the gate voltage V_G [Figure 6.4(c)], as observed previously [117, 126], though at larger fields this dependence becomes significantly weaker [Figure 6.4(d)]. The zero-bias conductance within the $N = 2$ diamond as a function of field

76
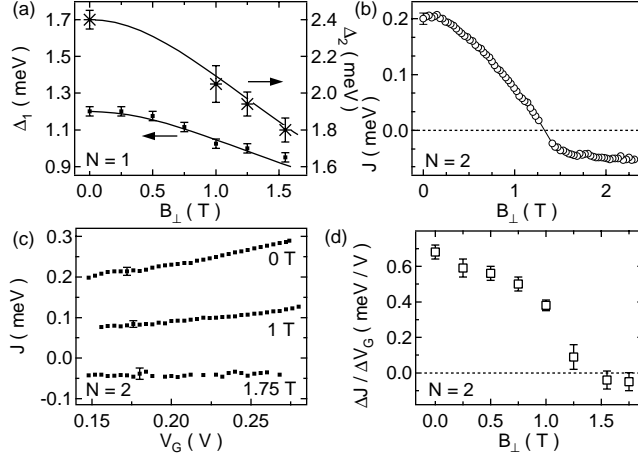
Figure 6.4: (a) First and second one-electron excited state energies Δ_1 and Δ_2, measured from sequential tunneling along with fits to a 2D anisotropic harmonic oscillator model with $\hbar\omega_a = 1.2$ meV and $\hbar\omega_b = 3.3$ meV (see text). (b) Singlet-triplet splitting J as a function of magnetic field $B_\perp$. (c) Dependence of J on gate voltage V_G for various $B_\perp$ as indicated. (d) Average slopes $\Delta J(V_G)/\Delta V_G$ from (c) as a function of magnetic field $B_\perp$, showing strong reduction of gate voltage dependence of J at large $B_\perp$.

shows a large, asymmetric peak at $B_\perp = B^*$ [Figure 6.3(d)], consistent with predictions for elastic cotunneling at the ST crossing [77, 78] (see also [95, 171]).

6.7   Anisotropic Confinement Potential of the Quantum Dot

Before turning to wave function correlations, we first extract some useful information about the dot shape from the $N = 1$ excitation spectrum. Transport spectra for the $N = 0 \rightarrow 1$ transition, extracted from plots like Figure 6.1(a) in the region between the $N = 0$ and $N = 1$ diamonds, give first (second) excited state energies lying $\Delta_{1(2)}$ above the ground state. We find $\Delta_2 \sim 2\Delta_1$, indicating roughly harmonic confinement. Dependencies of $\Delta_{1(2)}$ on perpendicular field are well described by a 2D anisotropic harmonic oscillator model [183]. From zero-field data, we extract $\hbar\omega_a = 1.2$ meV where $a(b)$ is along the larger (smaller) dimension of the dot; the energy scale for the smaller direction is found by fitting the field dependence of $\Delta_1(B_\perp)$, which gives $\hbar\omega_b = 3.3$ meV [183]. As a check of these values, good agreement between experimental and predicted values for $\Delta_2(B_\perp)$ is found [Figure 6.4(a)]. We conclude that the dot potential is spatially elongated by a factor of $\sim 1.6 = \sqrt{\omega_b/\omega_a}$.
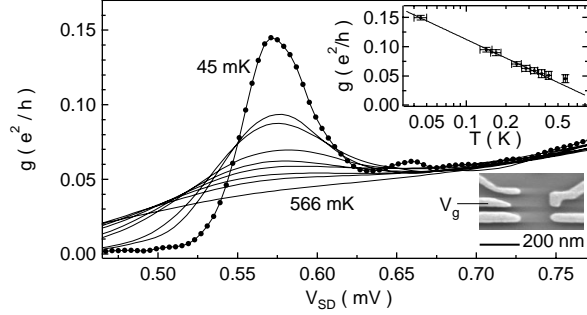
Figure 6.5: Differential conductance g as a function of V_{SD} for temperatures $T_{el} = 45, 140, 170, 240, 280, 330, 380, 420, 570$ mK (top to bottom) showing overshoot at $V_{SD} \sim J/e$. Inset: peak conductance as a function of temperature with best-fit $log(T)$ dependence (line).

6.8 Two-Electron Singlet-Triplet Kondo Effect at Finite Bias

We note that for strong coupling of the dot to the leads, the onset of inelastic cotunneling at $V_{SD} = J/e$ shows considerable overshoot, as seen in Figure 6.5 (measured in a device similar to the one discussed above, with larger ST splitting, $J(0) \sim 0.57$ meV). The temperature dependence of the maximum overshoot is shown in the inset of Figure 6.5 along with a line indicating a Kondo-inspired $log(T)$ dependence [177, 181, 197, 64, 158, 131]. The FWHM of the corresponding positive peak in dg/dV_{SD} is proportional to T at high temperatures and saturates at $T \sim 80$ mK, giving an estimate of T_K for this device. However, a quantitative theory of nonequilibrium ST Kondo effect would be needed to further analyze these data.

6.9 Measurement of Quantum Correlations in the Two-Electron Singlet Ground State

Finally, we investigate correlations in the two-electron wave function following the analysis of Ref. [77, 78]. We note that Ref. [77, 78] specifically considers a two-electron *double* quantum dot; we anticipate that the elongated shape of our single dot will lead to a spatially separated charge arrangement for $N = 2$, not unlike a double dot in the limit of strong interdot coupling. Selecting basis states appropriate for a double dot but applicable here as well—i.e., symmetric ($|+\rangle$) and antisymmetric ($|-\rangle$) states along the long axis of the dot—we

identify $|+\rangle$ and $|-\rangle$ with the orbital ground and first excited states of the one-electron dot. Because of electron-electron interactions, the $N = 2$ ground-state singlet generally comprises an admixture of the one-electron ground and excited orbital states. The amount of admixed excited state $|-\rangle$ is parameterized by ϕ ($0 \leq \phi \leq 1$), the so-called interaction parameter. Knowing ϕ allows two other important quantities to be extracted: the double occupancy, $D = (1 - \phi)^2/2(1 + \phi^2)$, and the concurrence [180], $c = 2\phi/(1 + \phi^2)$, which respectively parameterize correlations and entanglement of the two-electron singlet ground state [77, 78].

To extract ϕ from elastic cotunneling data, one also needs to know the charging energy for adding the second electron, the operating position within the $N = 2$ diamond, and the couplings to each lead for both the singlet and the triplet, $\Gamma_{1,2}^{S,T}$. At fields well below the ST transition, these Γ's can be estimated from excitation spectra at the $N = 1 \rightarrow 2$ transition by fitting a thermally broadened Lorentzian to the tunneling lines [63]. Upon inserting these quantities into Eqs. 8 and 10 of Ref. [77, 78], we find $\phi \sim 0.5\pm0.1$, indicating that the $N = 2$ ground-state singlet contains a significant admixture of the excited one-electron orbital state due to electron-electron interactions. We emphasize that this method does not rely explicitly on a double dot interpretation [9]. From this value of ϕ we extract a concurrence of $c \sim 0.8$ for the two-electron singlet. This is close to the maximum concurrence value $c = 1$, which characterizes a pair of singlet-correlated electrons in fully non-overlapping orbital states.

Two alternative methods for estimating ϕ give consistent results with the cotunneling method. First, one may adapt the formula $\phi = \sqrt{1 + (4t/U)^2} - 4t/U$ from [77, 78] by associating the measured Δ_1 with the tunnel splitting $2t$ of the two lowest noninteracting single-particle states, and the charging energy to add the second electron with U. The second alternative method uses the size of the elastic cotunneling step at the ST transition [see Figure 6.3(d)] which is shown to be related to ϕ in [77, 78]. It is notable that all three methods allow the concurrence, a measure of "useful" (i.e., spatially separated) two-particle entanglement, to be extracted from a dc transport measurement.

---

[9]V. Golovach and D. Loss, private communication.

References

[1] E. Abrahams, P. W. Anderson, D. C. Licciardello, and T. V. Ramakrishnan, *Scaling Theory of Localization: Absence of Quantum Diffusion in Two Dimensions*, Phys. Rev. Lett. **42**, 673 (1979).

[2] Y. Aharonov and D. Bohm, *Significance of Electromagnetic Potentials in the Quantum Theory*, Phys. Rev. **115**, 485 (1959).

[3] I. L. Aleiner, P. W. Brouwer, and L. I. Glazman, *Quantum Effects in Coulomb Blockade*, Phys. Rep. **358**, 309 (2002).

[4] I. L. Aleiner and V. I. Fal'ko, *Spin-Orbit Coupling Effects on Quantum Transport in Lateral Semiconductor Dots*, Phys. Rev. Lett. **87**, 256801 (2001).

[5] Y. Alhassid, *The Statistical Theory of Quantum Dots*, Rev. Mod. Phys. **72**, 895 (2000).

[6] B. L. Al'tshuler, *Fluctuations in the Extrinsic Conductivity of Disordered Conductors*, JETP Lett. **41**, 648 (1985).

[7] B. L. Altshuler and A. G. Aronov, *Electron-Electron Interactions in Disordered Systems, edited by A. L. Efros and M. Pollak*, page 11, North Holland, Amsterdam, 1985.

[8] B. L. Al'tshuler, A. G. Aronov, A. I. Larkin, and D. E. Khmel'nitskii, *Anomalous Magnetoresistance in Semiconductors*, Sov. Phys. JETP **54**, 411 (1981).

[9] B. L. Al'tshuler and B. I. Shklovskii, *Repulsion of Energy Levels and Conductivity of Small Metal Samples*, Sov. Phys. JETP **64**, 127 (1986).

[10] E. R. P. Alves and C. H. Lewenkopf, *Conductance Fluctuations and Weak Localization in Chaotic Quantum Dots*, Phys. Rev. Lett. **88**, 256805 (2002).

[11] A. G. Aronov and Y. B. Lyanda-Geller, *Spin-Orbit Berry-Phase in Conducting Rings*, Phys. Rev. Lett. **70**, 343 (1993).

[12] R. C. Ashoori, *Electrons in Artificial Atoms*, Nature **379**, 413 (1996).

[13] R. C. Ashoori, H. L. Stormer, J. S. Weiner, L. N. Pfeiffer, K. W. Baldwin, and K. W. West, *N-Electron Ground State Energies of a Quantum Dot in Magnetic Field*, Phys. Rev. Lett. **71**, 613 (1993).

[14] D. Awschalom, D. Loss, and N. Samarth, *Semiconductor Spintronics and Quantum Computation*, Springer-Verlag, 2002.

[15] H. U. Baranger and P. A. Mello, *Effect of Phase Breaking on Quantum Transport through Chaotic Cavities*, Phys. Rev. B **51**, 4703 (1995).

[16] C. W. J. Beenakker, *Theory of Coulomb Blockade Oscillations in the Conductance of a Quantum Dot*, Phys. Rev. B **44**, 1646 (1991).

[17] C. W. J. Beenakker, *Random Matrix Theory of Quantum Transport*, Rev. Mod. Phys. **69**, 731 (1997).

[18] G. Bergmann, *Weak-Antilocalization – An Experimental Proof for the Destructive Interference of Rotated Spin 1/2*, Solid State Comm. **42**, 815 (1982).

[19] G. Bergmann, *Weak Localization in Thin Films*, Phys. Rep. **107**, 1 (1984).

[20] M. V. Berry, *The Bakerian Lecture, 1987: Quantum Chaology*, Proceedings of the Royal Society of London, Series A, Mathematical and Physical Sciences **413**, 183 (1987).

[21] M. V. Berry and J. P. Keating, *A New Asymptotic Representation for $\zeta(1/2+it)$ and Quantum Spectral Determinants*, Proceedings: Mathematical and Physical Sciences **437**, 151 (1992).

[22] N. O. Birge, B. Golding, and W. H. Haemmerle, *Electron Quantum Interference and 1/f Noise in Bismuth*, Phys. Rev. Lett. **62**, 195 (1989).

[23] D. J. Bishop, R. C. Dynes, and D. C. Tsui, *Magnetoresistance in Si Metal-Oxide-Semiconductor Field Effect Transistors: Effect of Weak Localization and Correlations*, Phys. Rev. B **26**, 773 (1982).

[24] A. Braggio, M. Sassetti, and B. Kramer, *Control of Spin in Quantum Dots with Non-Fermi-Liquid Correlations*, Phys. Rev. Lett. **87**, 146802 (2001).

[25] P. W. Brouwer and C. W. J. Beenakker, *Voltage Probe and Imaginary-Potential Models for Dephasing in a Chaotic Quantum Dot*, Phys. Rev. B **55**, 4695 (1997).

[26] P. W. Brouwer, J. N. H. J. Cremers, and B. I. Halperin, *Weak Localization and Conductance Fluctuations of a Chaotic Quantum Dot with Tunable Spin-Orbit Coupling*, Phys. Rev. B **65**, R81302 (2002).

[27] E. N. Bulgakov, K. N. Pichugin, A. F. Sadreev, P. Streda, and P. Seba, *Hall-like Effect Induced by Spin-Orbit Interaction*, Phys. Rev. Lett. **83**, 376 (1999).

[28] G. Burkard, D. Loss, and D. P. DiVincenzo, *Coupled Quantum Dots as Quantum Gates*, Phys. Rev. B **59**, 2070 (1999).

[29] M. Buttiker, *Role of Quantum Coherence in Series Resistors*, Phys. Rev. B **33**, 3020 (1986).

[30] M. Büttiker and Y. Imry, *Magnetic Field Asymmetry in the Multichannel Landauer Formula*, J. Phys. C **17**, L467 (1985).

[31] Y. L. Bychkov and E. I. Rashba, *Oscillatory Effects and the Magnetic Susceptibility of Carriers in Inversion-Layers*, J. Phys C **17**, 6093 (1983).

[32] A. Cassam-Chenai and B. Shapiro, *Two-Dimensional Weak Localization beyond the Diffusion Approximation*, J. Phys. I France **4**, 1527 (1994).

[33] I. H. Chan, R. M. Clarke, C. M. Marcus, K. Campman, and A. C. Gossard, *Ballistic Conductance Fluctuations in Shape Space*, Phys. Rev. Lett. **74**, 3876 (1995).

[34] K. K. Choi, B. F. Levine, N. Jarosik, J. Walker, and R. Malik, *Anisotropic Magneto-transport in Weakly Coupled GaAs-AlGaAs Multiple Quantum Wells*, Phys. Rev. B **38**, 12362 (1988).

[35] K. K. Choi, D. C. Tsui, and K. Alavi, *Dephasing time and One-Dimensional Localization of Two-Dimensional Electrons in GaAs/AlGaAs Heterostructures*, Phys. Rev. B **36**, 7751 (1987).

[36] M. Ciorga, A. S. Sachrajda, P. Hawrylak, C. Gould, P. Zawadzki, S. Jullian, Y. Feng, and Z. Wasilewski, *Addition Spectrom of a Lateral Dot from Coulomb Blockade and Spin-Blockade Spectroscopy*, Phys. Rev. B **61**, R16315 (2000).

[37] J. N. H. J. Cremers, P. W. Brouwer, I. L. Aleiner, and V. I. Fal'ko, *Weak Localization and Conductance Fluctuations in a Quantum Dot with Parallel Magnetic Field and Spin-Orbit Scattering*, Phys. Rev. B **68**, 125329 (2003).

[38] M. F. Crommie, C. P. Lutz, and D. M. Eigler, *Confinement of Electrons to Quantum Corrals on a Metal Surface*, Science **262**, 218 (1993).

[39] S. M. Cronenwett, T. H. Oosterkamp, and L. P. Kouwenhoven, *A Tunable Kondo Effect in Quantum Dots*, Science **281**, 540 (1998).

[40] S. Datta and B. Das, *Eletric Analog of the Electro-Optic Modulator*, Appl. Phys. Lett. **56**, 665 (1990).

[41] P. Debray, J.-L. Pichard, J. Vincente, and P. N. Tung, *Reduction of Conductance Fluctuations Due to Zeeman Splitting in a Disordered Conductor without Spin-Orbit Scattering*, Phys. Rev. Lett. **63**, 2264 (1989).

[42] S. DeFranceschi, S. Sasaki, J. M. Elzerman, W. G. van der Wiel, S. Tarucha, and L. P. Kouwenhoven, *Electron Cotunneling in a Semiconductor Quantum Dot*, Phys. Rev. Lett. **86**, 878 (2001).

[43] G. J. Dolan and D. D. Osheroff, *Nonmetallic Conduction in Thin Metal Films at Low Temperatures*, Phys. Rev. Lett. **43**, 721 (1979).

[44] G. Dresselhaus, *Spin-Orbit Coupling Effects in Zinc-Blende Structures*, Phys. Rev. **100**, 580 (1955).

[45] P. D. Dresselhaus, C. M. A. Papavassiliou, R. G. Wheeler, and R. N. Sacks, *Observation of Spin Precession in GaAs Inversion Layers Using Antilocalization*, Phys. Rev. Lett. **68**, 106 (1992).

[46] M. I. D'yakonov and V. I. Perel', *Spin Orientation of Electrons Associated with Interband Absorption of Light in Semiconductors*, Sov. Phys. JETP **33**, 1053 (1971).

[47] D. M. Eigler and E. K. Schweizer, *Positioning Single Atoms with a Scanning Tunneling Microscope*, Nature **344**, 524 (1990).

[48] A. Einstein, Verh. Dtsch. Phys. Ges. **19**, 82 (1917).

[49] R. J. Elliott, *Theory of the Effect of Spin-Orbit Coupling on Magnetic Resonance in Some Semiconductors*, Phys. Rev. **96**, 266 (1954).

[50] J. M. Elzerman, R. Hanson, J. S. Greidanus, L. H. Willems van Beveren, S. De Franceschi, L. M. K. Vandersypen, S. Tarucha, and L. P. Kouwenhoven, *Few-Electron Quantum Dot Circuit with Integrated Charge Read Out*, Phys. Rev. B **67**, R161308 (2003).

[51] J. M. Elzerman, R. Hanson, L. H. Willems van Beveren, L. M. K. Vandersypen, and L. P. Kouwenhoven, *Excited State Spectroscopy on a Nearly Closed Quantum Dot Via Charge Detection*, App. Phys. Lett. **84**, 4617 (2004).

[52] J. M. Elzerman, R. Hanson, L. H. Willems van Beveren, B. Witkamp, L. M. K. Vandersypen, and L. P. Kouwenhoven, *Single-Shot Read-Out of an Individual Electron Spin in a Quantum Dot*, Nature **430**, 431 (2004).

[53] H. A. Engel and D. Loss, *Conductance FLuctuations in Diffusive Rings: Berry Phase Effects and Criteria for Adiabadicity*, Phys. Rev. B **62**, 10238 (2000).

[54] M. Eto and Y. V. Nazarov, *Enhancement of Kondo Effect in Quantum Dots with an Even Number of Electrons*, Phys. Rev. Lett. **85**, 1306 (2000).

[55] M. Eto and Y. V. Nazarov, *Mean-Field Theory of the Kondo-Effect in Quantum Dots with an Even Number of Electrons*, Phys. Rev. B **64**, 85322 (2001).

[56] V. I. Fal'ko and T. Jungwirth, *Orbital Effect of an In-Plane Magnetic Field on Quantum Transport in Chaotic Lateral Dots*, Phys. Rev. B **65**, 81306 (2002).

[57] S. Feng, *Mesoscopic Conductance Fluctuations in the Presence of Spin-Orbit Coupling*, Phys. Rev. B **39**, 8722 (1989).

[58] R. P. Feynman, R. B. Leighton, and M. Sands, *Feynman Lectures III*, Addison-Wesley, London-Reading, 1971.

[59] J. A. Folk, S. R. Patel, K. M. Birnbaum, C. M. Marcus, C. I. Duruöz, J. S. Harris, and Jr., *Spin Degeneracy and Conductance Fluctuations in Open Quantum Dots*, Phys. Rev. Lett. **86**, 2102 (2001).

[60] J. A. Folk, R. M. Potok, C. M. Marcus, and V. Umansky, *A Gate-Controlled Bidirectional Spin Filter Using Quantum Coherence*, Science **299**, 679 (2003).

[61] A. B. Fowler, A. Harstein, and R. A. Webb, *Conductance in Restricted Dimensionality Accumumation Layers*, Phys. Rev. Lett. **48**, 196 (1982).

[62] E. B. Foxman, P. L. McEuen, U. Meirav, N. S. Wingreen, Y. Meir, P. A. Belk, N. R. Belk, M. A. Kastner, and S. J. Wind, *Effects of Quantum Levels on transport through a Coulomb Island*, Phys. Rev. B **47**, 10020 (1993).

[63] E. B. Foxman, P. L. McEuen, U. Meirav, N. S. Wingreen, Y. Meir, P. A. Belk, N. R. Belk, M. A. Kastner, and S. J. Wind, *Effects of Quantum Levels on Transport Through a Coulomb Island*, Phys. Rev. B **50**, 14193 (1994).

[64] C. Fühner, U. F. Keyser, R. J. Haug, D. Reuter, and A. D. Wieck, *Flux-Quantum-Modulated Kondo Conductance in a Multielectron Dot*, Phys. Rev. B **66**, 161305 (2002).

[65] A. Fuhrer, T. Ihn, K. Ensslin, W. Wegscheider, and M. Bichler, *Singlet-Triplet Transitions Tuned by Asymmetric Gate Voltages in a Quantum Ring*, Phys. Rev. Lett. **91**, 206802 (2003).

[66] T. Fujisawa, D. G. Austing, Y. Tokura, Y. Hirayama, and S. Tarucha, *Allowed and Forbidden Transitions in Artificial Hydrogen and Helium Atoms*, Nature **419**, 278 (2002).

[67] T. Fujisawa, D. G. Austing, Y. Tokura, Y. Hirayama, and S. Tarucha, *Electrical Pluse Measurement, Inelastic Relaxation and Non-Equilibrium Transport in a Quantum Dot*, J. Phys.: Cond. Mat. **15**, R1395 (2002).

[68] Y. K. Fukai, H. Nakano, S. Nakata, S. Tarucha, and K. Arai, *Transition from Weak to Strong Spin-Orbit Scattering Regime in Diffusive InGaAs/InAlAs Quantum Wires*, Solid State Comm. **94**, 757 (1995).

[69] T. A. Fulton and G. J. Dolan, *Observation of Single-Electron Charging Effects in Small Tunnel Junctions*, Phys. Rev. Lett. **59**, 109 (1987).

[70] V. M. Gasparyan and A. Yu. Zyuzin, *Field Dependence of the Anomalous Magnetoresistance*, Sov. Phys. Solid State **27**(6), 999 (1985).

[71] N. Giordano and M. A. Pennington, *Two Dimensional Weak Localization in Combined Perpendicular and Parallel Magnetic Fields*, Phys. Rev. B **47**, 9693 (1993).

[72] D. Giuliano and A. Tagliacozzo, *Spin Fractionalization of an Even Number of Electrons in a Quantum Dot*, Phys. Rev. Lett. **84**, 4677 (2000).

[73] L. I. Glazman and M.E. Raikh, *Resonant Kondo Transparency of a Barrier with Quasilocal Impurity States*, JETP **47**, 452 (1988).

[74] D. Goldhaber-Gordon, H. Shtrikman, D. Mahalu, D. Abusch-Magder, U. Meirav, and M. A. Kastner, *Kondo-Effect in a Single-Electron Transistor*, Nature **391**, 156 (1998).

[75] H. Goldstein, *Classical Mechanics*, Addison-Wesley, London-Reading, 1980.

[76] V. Golovach, A. Khaetskii, and D. Loss, *Phonon-Induced Decay of the Electron Spin in Quantum Dots*, Phys. Rev. Lett. **93**, 16601 (2004).

[77] V. Golovach and D. Loss, *Kondo Effect and Singlet-Triplet Splitting in Coupled Quantum Dots in a Magnetic Field*, Europhys. Lett. **62**, 83 (2003).

[78] V. Golovach and D. Loss, *Transport Through a Double Quantum Dot in the Sequential Tunneling and Cotunneling Regimes*, Phys. Rev. B **69**, 245327 (2004).

[79] L. P. Gor'kov, A. I. Larkin, and D. E. Khmel'nitskii, *Particle Conductivity in a Two-Dimensional Random Potential*, JETP Lett. **30**, 228 (1979).

[80] D. Grundler, *Large Rashba Splitting in InAs Quantum Wells due to Electon Wave Function Penetration into the Barrier Layers*, Phys. Rev. Lett. **84**, 6074 (2000).

[81] C. Gustin, S. Faniel, B. Hackens, S. Melinte, M. Shayegan, and V. Bayot, *Parallel Magnetic-Field-Induced Conductance Fluctuations in One- and Two-Subband Ballistic Quantum Dots*, Phys. Rev. B **68**, 241305R (2003).

[82] C. Gustin, S. Faniel, B. Hackens, E. P. De Poortere, M. Shayegan, and V. Bayot, *Evidence for Universal Conductance Fluctuations in an Open Quantum Dot under a Strictly Parallel Magnetic Field*, Physica E **17**, 154 (2003).

[83] M. C. Gutzwiller, J. Math. Phys. **12**, 343 (1971).

[84] J. h. F. Scott-Thomas, S. B. Field, M. A. Kastner, H. I. Smith, and D. A. Antoniadis, *Conductance Oscillations Periodic in the Density of a One-Dimensional Electron Gas*, Phys. Rev. Lett. **62**, 583 (1989).

[85] B. Hackens, C. Gustin, V. Bayot, and M. Shayegan, *Evidence for Spin-Orbit Effects in an Open Ballistic Quantum Dot*, Physica E **12**, 833 (2002).

[86] B. Hackens, J. P. Minet, G. Farhi, G. Faniel, C. Gustin, and V. Bayot, *Weak Antilocalization and UCFs in an Open Bismuth Quantum Dot*, Physica E **17**, 156 (2003).

[87] B. I. Halperin, A. Stern, Y. Oreg, J. N. H. J. Cremers, J. A. Folk, and C. M. Marcus, *Spin-Orbit Effects in a GaAs Quantum Dot in a Parallel Field*, Phys. Rev. Lett. **86**, 2106 (2001).

[88] J. E. Hansen, R. Taboryski, and P. E. Lindelof, *Weak-Localization in a GaAs Heterostructure Close to Population of the Second Subband*, Phys. Rev. B **47**, 16040 (1993).

[89] R. Hanson, B. Witkamp, L. M. K. Vandersypen, L. H. Willems van Beveren, J. M. Elzerman, and L. P. Kouwenhoven, *Zeeman Energy and Spin Relaxation in a One-Electron Quantum Dot*, Phys. Rev. Lett. **91**, 196802 (2003).

[90] P. Hawrylak, *Single-Electron Capacitance Spectroscopy of Few-Electron Artificial Atoms in a Magnetic Field: Theory and Experiment*, Phys. Rev. Lett. **71**, 3347 (1993).

[91] J. P. Heida, B. J. van Wees, J. J. Kuipers, T. M. Klapwijk, and G. Borghs, *Spin-Orbit Interaction in a Two-Dimensional Electron Gas in a InAs/AlSb Quantum Well with Gate-Controlled Electron Density*, Phys. Rev. B **57**, 11911 (1998).

[92] J. M. Heisz and E. Zaremba, *Transverse Magnetoresistance of Transverse GaAs/AlGaAs Heterojunctions in the Presence of Parallel Magnetic Fields*, Phys. Rev. B **53**, 13594 (1996).

[93] E. J. Heller, *Bound-State Eigenfunctions of Classically Chaotic Hamiltonian Systems: Scars of Periodic Orbits*, Phys. Rev. Lett. **53**, 1515 (1984).

[94] S. Hikami, A. I. Larkin, and Y. Nagaoka, *Spin-Orbit Interaction and Magnetoresistance in the Two Dimensional Random System*, Prog. Theor. Phys. **63**, 707 (1980).

[95] W. Hofstetter and H. Schoeller, *Quantum Phase Transition in a Multilevel Dot*, Phys. Rev. Lett. **88**, 16803 (2002).

[96] A. G. Huibers, J. A. Folk, S. R. Patel, C. M. Marcus, C. I. Duruöz, J. S. Harris, and Jr., *Low Temperature Saturation of the Dephasing TIme and Effects of Microwave Radiation on Open Quantum Dots*, Phys. Rev. Lett. **83**, 5090 (1999).

[97] A. G. Huibers, S. Patel, C. M. Marcus, P. W. Brouwer, C. I. Duruöz, and Jr. J. S. Harris, *Distributions of the Conductance and its Parametric Derivatives in Quantum Dots*, Phys. Rev. Lett. **81**, 1917 (1998).

[98] A. G. Huibers, M. Switkes, C. M. Marcus, K. Campman, and A. C. Gossard, *Dephasing in Open Quantum Dots*, Phys. Rev. Lett. **81**, 200 (1998).

[99] W. Hunziker, *Quantenmechanik I + II*, Vorlesungsnotizen, ETH Zürich, 1995/96.

[100] Y. Imry, *Active Transmission Channels and Universal Conductance Fluctuations*, Europhys. Lett. **1**, 249 (1986).

[101] S. V. Iordanskii, Y. B. Lyanda-Geller, and G. E. Pikus, *Weak Localization in Quantum Wells with Spin-Orbit Interaction*, JETP Lett. **60**, 206 (1994).

[102] E. L. Ivchenko and G. E. Pikus, *Superlattices and Other Heterostructures: Symmetry and Optical Phenomena*, volume 110 of *Springer Series in Solid-State Sciences*, Springer-Verlag, 1995.

[103] J. D. Jackson, *Classical Electrodynamics*, Wiley, 1975.

[104] A. T. Johnson, L. P. Kouwenhoven, W. de Jong, N. C. van der Vaart, C. J. P. M. Harmans, and C. T. Foxon, *Zero-Dimensional States and Single-Electron Charging in Quantum Dots*, Phys. Rev. Lett. **69**, 1592 (1992).

[105] B. Jusserand, D. Richards, G. Allan, C. Priester, and B. Etienne, *Spin Orientation at Semiconductor Heterointerfaces*, Phys. Rev. B **51**, 4707 (1995).

[106] M. A. Kastner, *The Single-Electron Transistor*, Rev. Mod. Phys. **64**, 849 (1992).

[107] A. Kawabata, *On the Field Dependence of Magnetoresistance in Two-Dimensional Systems*, J. Phys. Soc. Jpn. **53**, 3540 (1984).

[108] S. Keppeler and R. Winkler, *Anomalous Magneto-Oscillations and Spin Precession*, Phys. Rev. Lett. **88**, 46401 (2002).

[109] A. V. Khaetskii and Y. V. Nazarov, *Spin Relaxation in Semiconductor Quantum Dots*, Phys. Rev. B **61**, 12639 (2000).

[110] A. V. Khaetskii and Y. V. Nazarov, *Spin-Flip Transitions between Zeeman Sublevels in Semiconductor Quantum Dots*, Phys. Rev. B **64**, 2001 (2001).

[111] V. E. Kirpichev, I. V. Kukushkin, V. B. Timofeev, and V. I. Fal'ko, *Energy-Spectrum of 2D Electrons in Inclined Magnetic Fields*, JETP Lett. **51**, 436 (1990).

[112] A. A. Kiselev and K. W. Kim, *T-shaped Ballistic Spin Filter*, Appl. Phys. Lett. **78**, 775 (2001).

[113] W. Knap, C. Skierbiszewski, A. Zduniak, E. Litwin-Staszewska, D. Bertho, F. Kobbi, J. L. Robert, G. E. Pikus, F. G. Pikus, S. V. Iordanskii, V. Mosser, K. Zekentes, and Y. B. Lyanda-Geller, *Weak Antilocalization and Spin Precession in Quantum Wells*, Phys. Rev. B **53**, 3912 (1996).

[114] T. Koga, J. Nitta, T. Akazaki, and H. Takayanagi, *Rashba Spin-Orbit Coupling Probed by the Weak Antilocalization Analysis in InAlAs/InGaAs/InAlAs Quantum Wells as a Function of Quantum Well Asymmetry*, Phys. Rev. Lett. **89**, 046801 (2002).

[115] T. Koga, J. Nitta, H. Takayanagi, and S. Datta, *Spin-Filter Device Based on the Rashba Effect Using a Nonmagnetic Resonant Tunneling Diode*, Phys. Rev. Lett. **88**, 126601 (2002).

[116] A. Kogan, S. Amasha, D. Goldhaber-Gordon, G. Granger, M. A. Kastner, and H. Shtrikman, *Measurements of Kondo and Spin-Splitting in Single-Electron Transistors*, Cond-Mat/ **0312186** (2003).

[117] A. Kogan, G. Granger, M. A. Kastner, D. Goldhaber-Gordon, and H. Shtrikman, *Singlet-Triplet Transition in a Single-Electron Transistor at Zero Magnetic Field*, Phys. Rev. B **67**, 113309 (2003).

[118] L. Kouwenhoven and C. M. Marcus, *Quantum Dots*, Physics World **11**, 35 (1998).

[119] L. P. Kouwenhoven, D. G. Austing, and S. Tarucha, *Few-Electron Quantum Dots*, Rep. Prog. Phys. **2001**, 701 (64).

[120] L. P. Kouwenhoven, C. M. Marcus, P. L. McEuen, S. Tarucha, R. M. Westervelt, and N. S. Wingreen, *Electron Transport in Quantum Dots*, NATO ASI conference proceedings, edited by L. L. Sohn, L. P. Kouwenhoven and G. Schön, (Kluwer, Dordrecht 1997).

[121] L. P. Kouwenhoven, T. H. Oosterkamp, M. W. S. Danoesastro, M. Eto, D. G. Austing, T. Honda, and S. Tarucha, *Excitation Spectra of Circular Few-Electron Quantum Dots*, Science **278**, 1788 (1997).

[122] I. V. Kukushkin, V. I. Fal'ko, K. von Klitzing, K. Ploog, and D. Heitmann, *Quasi One-Dimensional Electrons in a Quantizing Oblique Magnetic Field*, JETP Lett. **53**, 335 (1991).

[123] U. Kunze, *Effective Mass Change of Electrons in Si Inversion Layers under Parallel Magnetic Fields*, Phys. Rev. B **35**, 9168 (1987).

[124] C. Kurdak, A. M. Chang, A. Chin, and T. Y. Chang, *Quantum Interferecen Effects and Spin-Orbit Interaction in Quasi One-Dimensional Wires and Rings*, Phys. Rev. B **46**, 6846 (1992).

[125] R. F. Kwasnick, M. A. Kastner, J. Melngailis, and P. A. Lee, *Nonmonotonic Variation of the Conductance with Electron Density in $\tilde{7}0nm$-Wide Inversion Layers*, Phys. Rev. Lett. **52**, 224 (1984).

[126] J. Kyriakidis, M. Pioro-Lardiere, M. Ciorga, A. S. Sachrajda, and P. Hawrylak, *Voltage-Tunable Singlet-Triplet Transition in Lateral Quantum Dots*, Phys. Rev. B **66**, 35320 (2002).

[127] R. B. Laughlin, *Nobel Lecture: Fractional Quantization*, Rev. Mod. Phys. **71**, 863 (1998).

[128] D. R. Leadley, R. J. Nicholas, J. J. Harris, and C. T. Foxon, *Inter-Subband Scattering Rates in GaAs-GaAlAs Heterojunctions*, Semicond. Sci. Technol. **5**, 1081 (1990).

[129] P. A. Lee and T. V. Ramakrishnan, *Disordered Electronic Systems*, Rev. Mod. Phys. **57**, 287 (1975).

[130] P. A. Lee and A. D. Stone, *Universal Conductance Fluctuations in Metals*, Phys. Rev. Lett. **55**, 1622 (1985).

[131] W. Liang, M. Bockrath, and H. Park, *Shell Filling and Exchange Coupling in Metallic Single-Wall Carbon Nanotubes*, Phys. Rev. Lett. **88**, 126801 (2002).

[132] B. J. F. Lin, M. A. Paalanen, A. C. Gossard, and D. C. Tsui, *Weak Localization of Two-Dimensional Electrons in GaAs-AlGaAs Heterostructures*, Phys. Rev. B **29**, 927 (1984).

[133] D. Loss and D. P. DiVincenzo, *Quantum Computation with Quantum Dots*, Phys. Rev. A **57**, 120 (1998).

[134] J. P. Lu, J. B. Yau, S. P. Shukla, M. Shayegan, L. Wissinger, U. Rössler, and R. Winkler, *Tunable Spin-Splitting and Spin-Resolved Ballistic Transport in GaAs/AlGaAs Two-Dimensional Holes*, Phys. Rev. Lett. **81**, 1282 (1998).

[135] Y. Lyanda-Geller, 2002, unpublished.

[136] Y. B. Lyanda-Geller, *Quantum Interference and Electron-Electron Interactions at Strong Spin-Orbit Coupling in Disordered Systems*, Phys. Rev. Lett. **80**, 4273 (1998).

[137] Y. B. Lyanda-Geller and A. D. Mirlin, *Novel Symmetry of a Random Matrix Ensemble: Partially Broken Spin Rotation Invariance*, Phys. Rev. Lett. **72**, 1894 (1994).

[138] D. Mailly, M. Sanquer, J.-L. Pichard, and P. Pari, *Reduction of Quantum Noise in a GaAlAs/GaAs Heterojunction by a Magnetic Field: an Orthogonal-to-Unitary Wigner Statistics Transition*, Europhys. Lett. **8**, 471 (1989).

[139] O. N. Makarovskii, L. Smrcka, P. Vasek, T. Jungwirth, M. Cukr, and L. Jansen, *Magnetoresistance and Electronic Structure of Asymmetric GaAs/AlGaAs Double Quantum Wells in an In-Plane or Tilted Magnetic Field*, Phys. Rev. B **62**, 10908 (2000).

[140] H. C. Manoharan, C. P. Lutz, and D. M. Eigler, *Quantum Mirages formed by Coherent Projection of Electronic Structure*, Nature **403**, 512 (2000).

[141] C. M. Marcus, A. J. Rimberg, R. M. Westervelt, P. F. Hopkins, and A. C. Gossard, *Conductance Fluctuations and Chaotic Scattering in Ballistic Microstructures*, Phys. Rev. Lett. **69**, 506 (1992).

[142] J. J. Mares, J. Kristofik, P. Hubik, E. Hulicius, K. Melchiar, J. Pangrac, J. Novak, and S. Hasenöhrl, *Out-of-Plane Weak Localization in Two-Dimensional Electron Structures*, Phys. Rev. Lett. **80**, 4020 (1998).

[143] H. Mathur and A. D. Stone, *Quantum Transport and the Electronic Aharonov-Casher Effect*, Phys. Rev. Lett. **68**, 2964 (1992).

[144] Y. Meir, Y. Gefen, and O. Entin-Wohlman, *Universal Effects of Spin-Orbit Scattering in Mesoscopic Systems*, Phys. Rev. Lett. **63**, 798 (1989).

[145] Y. Meir and N. S. Wingreen, *Spin-Orbit Scattering and the Kondo Effect*, Phys. Rev. B **50**, 4947 (1994).

[146] U. Meirav, M. A. Kastner, and S. J. Wind, *Single-Electron Charging and Periodic Conductance Resonances in GaAs Nanostructures*, Phys. Rev. Lett. **65**, 771 (1990).

[147] P. M. Mensz and R. G. Wheeler, *Magnetoconductance due to Parallel Magnetic Fields in Silicon Inversion Layers*, Phys. Rev. B **35**, 2844 (1987).

[148] J. S. Meyer, A. Altland, and B. L. Al'tshuler, *Quantum Transport in Parallel Magnetic Fields: A Realization of the Berry-Robnik Symmetry Phenomenon*, Phys. Rev. Lett. **89**, 206601 (2002).

[149] J. S. Meyer, V. I. Fal'ko, and B. L. Al'tshuler, *Field Theory of Strongly Correlated Fermions and Bosons in Low-Dimensional Disordered Systems*, in NATO Science Series II, edited by I.V. Lerner, B.L. Altshuler, V.I. Fal'ko and T. Giamarchi (Kluwer Academic Publishers, Dordrecht) **Vol. 72**, 117–164 (2002).

[150] J. B. Miller, D. M. Zumbühl, C. M. Marcus, Y. B. Lyanda-Geller, K. Campman, and A. C. Gossard, *Gate-Controlled Spin-Orbit Quantum Interference Effects in Lateral Transport*, Phys. Rev. Lett. **90**, 76807 (2003).

[151] O. Millo, S. J. Klepper, M. W. Keller, D. E. Prober, S. Xiong, A. D. Stone, and R. N. Sacks, *Reduction of the Mesoscopic Conductance Fluctuation Amplitude in GaAs/AlGaAs Heterojunctions due to Spin-Orbit Scattering*, Phys. Rev. Lett. **65**, 1494 (1990).

[152] F. Mireles and G. Kirczenow, *Ballistic Spin-Polarized Transport and Rashba Spin-Precession in Semiconductor Nanowires*, Phys. Rev. B **64**, 24426 (2001).

[153] J. S. Moon, N. O. Birge, and B. Golding, *Observation of Universal Conductance-Fluctuation Crossovers in Mesoscopic Li Wires*, Phys. Rev. B **56**, 15124 (1997).

[154] A. F. Morpurgo, J. P. Heida, T. M. Klapwijk, B. J. van Wees, and G. Broghs, *Ensemble-Average Spectrom of Aharonov-Bohm Conductance Oscillations: Evidence for Spin-Orbit-Induced Berry's Phase*, Phys. Rev. Lett. **80**, 1050 (1998).

[155] T. K. Ng and P. A. Lee, *On-Site Coulomb Repulsion and Resonant Tunneling*, Phys. Rev. Lett. **61**, 1768 (1988).

[156] J. Nitta, T. Akazaki, and H. Takayanagi, *Gate Control of Spin-Orbit Interaction in an Inverted InGaAs/InAlAs Heterostructure*, Phys. Rev. Lett. **78**, 1335 (1997).

[157] J. Nitta, F. E. Meijer, and H. Takayanagi, *Spin-Interference Device*, App. Phys. Lett. **75**, 695 (1999).

[158] J. Nygard, D. H. Cobden, and P. E. Lindelof, *Kondo Physics in Carbon Nanotubes*, Nature **408**, 342 (2000).

[159] K. Ohtsuka, S. Takaoka, K. Oto, K. Murase, and K. Gamo, *Distortion of Fermi Surface Induced by Parallel Magnetic Field in a Two-Dimensional Electron Gas*, Physica B **249-251**, 780 (1998).

[160] K. Ono, D. G. Austing, Y. Tokura, and S. Tarucha, *Current Rectification by Pauli Exclusion in a Weakly Coupled Double Quantum Dot System*, Science **297**, 1313 (2002).

[161] K. Oto, S. Takaoka, K. Murase, and K. Gamo, *Effect of Parallel High Magnetic Field on Two-Dimensional Electron Gas Investigated by Ballistic Electron Transport*, Physica E **11**, 177 (2001).

[162] Z. Ovadyahu, Y. Gefen, and Y. Imry, *Dimensionality Crossover Induced by a Magnetic Field in thin Metallic Films*, Phys. Rev. B **32**, 781 (1985).

[163] S. J. Papadakis, E. P. DePoortere, H. C. Manoharan, M. Shayegan, and R. Winkler, *The Effect of Spin-Splitting on the Metallic Behaviour of a Two-Dimensional System*, Science **283**, 2056 (1999).

[164] S. J. Papadakis, E.P. De Poortere, M. Shayegan, and R. Winkler, *Spin-Splitting in GaAs Two-Dimensional Holes*, Physica E **9**, 31 (2001).

[165] D. Pfannkuche, V. Gudmundsson, and P. A. Maksym, *Comparison of a Hartree, a Hartree-Fock and an Exact Treatment of Quantum-Dot Helium*, Phys. Rev. B **47**, 2244 (1993).

[166] P. Pfeffer, *Effect of Inversion Asymmetry on the Conduction Subbands in GaAs/GaAlAs Heterostructures*, Phys. Rev. B **59**, 15902 (1999).

[167] M. Pioro-Lardière, M. Ciorga, J. Lapointe, P. Zawadzki, M. Korkusiński, P. Hawrylak, and A. S. Sachrajda, *Spin-Blockade Spectroscopy of a Two-Level Artificial Molecule*, Phys. Rev. Lett. **91**, 26803 (2003).

[168] R. M. Potok, J. A. Folk, C. M. Marcus, V. Umansky, M. P. Hanson, and A. C. Gossard, *Spin Polarized Current from Coulomb Blockaded Quantum Dots*, Phys. Rev. Lett. **91**, 16802 (2003).

[169] M. Pustilnik and L. I. Glazman, *Conduction Through a Quantum Dot Near a Singlet-Triplet Transition*, Phys. Rev. Lett. **85**, 2993 (2000).

[170] M. Pustilnik and L. I. Glazman, *Kondo Effect Induced by a Magnetic Field*, Phys. Rev. B **64**, 45328 (2001).

[171] M. Pustilnik, L. I. Glazman, and W. Hofstetter, *Singlet-Triplet Transition in a Lateral Quantum Dot*, Phys. Rev. B **68**, R161303 (2003).

[172] P. Ramvall, B. Kowalski, and P. Omling, *Zero-Magnetic-Field Splittings in Al-GaAs/GaAs Heterojunctions*, Phys. Rev. B **55**, 7160 (1997).

[173] M. A. Reed, J. N. Randall, R. J. Aggarwal, R. J. Matyi, T. M. Moore, and A. E. Wetsel, *Observation of Discrete Electronic States in a Zero-Dimensional Semiconductor Nanostructure*, Phys. Rev. Lett. **60**, 535 (1988).

[174] S. M. Reimann and M. Manninen, *Electronic Structure of Quantum Dots*, Rev. Mod. Phys. **74**, 1283 (2002).

[175] D. C. Reynolds, K. K. Bajaj, C. W. Litton, R. L. Greene, P. W. Yu, C. K. Peng, and H. Morkoc, *Magneto-Optical Studies of GaAs/AlGaAs Multi-Quantum-Well Structures Grown by Molecular Beam Epitaxy*, Phys. Rev. B **35**, 4515 (1987).

[176] A.S. Sachrajda, C. Gould, P. Hawrylak, Y. Feng, and Z. Wasilewski, *A Lateral Few Electron Dot*, Physica Scripta **T79**, 16 (1999).

[177] S. Sasaki, S. De Franceschi, J. M. Elzerman, W. G. van der Wiel, M. Eto, S. Tarucha, and L. P. Kouwenhoven, *Kondo-Effect in an Integer-Spin Quantum Dot*, Nature **405**, 764 (2002).

[178] T. Schäpers, G. Engels, J. Lange, Th. Klocke, M. Hollfelder, and H. Lüth, *Effect of the Heterointerface on the Spin Splitting in Modulation Doped InGaAs/InP Quantum Wells for B→0*, J. Appl. Phys. **83**, 4324 (1998).

[179] Z. Schlesinger, J. C. M. Hwang, and Jr. S. J. Allen, *Subband-Landau-Level Coupling in a Two-Dimensional Electron Gas*, Phys. Rev. Lett. **50**, 2098 (1983).

[180] J. Schliemann, D. Loss, and A. H. MacDonald, *Double-Occupancy Errors, Adiabadicity and Entanglement of Spin-Qubits in Quantum Dots*, Phys. Rev. B **63**, 85311 (2001).

[181] J. Schmid, J. Weis, K. Eberl, and K. von Klitzing, *Absence of Odd-Even Parity Behavior for Kondo Resonances in Quantum Dots*, Phys. Rev. Lett. **84**, 5824 (2000).

[182] T. Schmidt, M. Tewordt, R. H. Blick, R. J. Haug, D. Pfannkuche, K. von Klitzing, A. Förster, and H. Lüth, *Quantum Dot Ground States in a Magnetic Field Studied Single Electron Tunneling Spectroscopy on Double-Barrier Heterostructures*, Phys. Rev. B **51**, 5570 (1995).

[183] B. Schuh, *Algebraic Solution of a Non-Trivial Oscillator Problem*, J. Phys. A: Math. Gen. **18**, 803 (1985).

[184] M. Schultz, F. Heinrichs, U. Merkt, T. Colin, T. Skauli, and S. Lovold, *Rashba Spin Splitting in a Gated HgTe Quantum Well*, Semicond. Sci. Technol. **11**, 1168 (1996).

[185] H. R. Shea, R. Martel, and Ph. Avouris, *Electrical Transport in Rings of Single-Wall Nanotubes: One-Dimensional Localization*, Phys. Rev. Lett. **84**, 4441 (2000).

[186] D. R. Stewart, D. Sprinzak, C. M. Marcus, C. I. Duruöz, and Jr. J. S. Harris, *Correlations between Ground and Excited State Spectra of a Quantum Dot*, Science **278**, 1784 (1997).

[187] A. D. Stone, *Reduction of Low-Frequency Noise in Metals by Magnetic Field: Observability of the Transition between Random-Matrix Ensembles*, Phys. Rev. B **39**, 10736 (1989).

[188] H. L. Stormer, *Nobel Lecture: The Fractional Quantum Hall Effect*, Rev. Mod. Phys. **71**, 875 (1998).

[189] H. L. Stormer, D. C. Tsui, and A. C. Gossard, *The Fractional Quantum Hall Effect*, Rev. Mod. Phys. **71**, S298 (1999).

[190] B. Su, V. J. Goldman, and J. E. Cunningham, *Observation of Single Electron Charging in Double-Barrier Heterostructures*, Science **255**, 313 (1992).

[191] Bo Su, V. Goldman, and J. E. Cunningham, *Single-Electron Tunneling in Nanometer-Scale Double-Barrier Heterostructure Devices*, Phys. Rev. B **46**, 7644 (1992).

[192] P. Svoboda, Y. Krupko, L. Smrcka, M. Cukr, T. Jungwirth, and L. Jansen, *Novel Critical Field in Magnetoresistance Oscillation in Asymmetric GaAs/AlGaAs Double Wells Measured as a Function of the In-Plane Magnetic Field*, Physica E **12**, 315 (2002).

[193] S. Tarucha, D. G. Austing, T. Honda, R. J. van der Hage, and L. P. Kouwenhoven, *Shell Filling and Spin Effects in a Few Electron Quantum Dot*, Phys. Rev. Lett. **77**, 3613 (1996).

[194] S. Tarucha, D. G. Austing, Y. Tokura, W. G. van der Wiel, and L. P. Kouwenhoven, *Direct Coulomb and Exchange Interaction in Artificial Atoms*, Phys. Rev. Lett. **84**, 2485 (2000).

[195] D. C. Tsui, *Nobel Lecture: Interplay of Disorder and Interaction in Two-Dimensional Electron Gases in Intense Magnetic Fields*, Rev. Mod. Phys. **71**, 891 (1998).

[196] C. P. Umbach, S. Washburn, R. B. Laibowitz, and R. A. Webb, *Magnetoresistance of Small, Quasi-One-Dimensional, Normal-Metal Rings and Lines*, Phys. Rev. B **30**, 4048 (1984).

[197] W. G. van der Wiel, S. De Franceschi, J. M. Elzerman, S. Tarucha, and L. P. Kouwenhoven, *Two-Stage Kondo Effect in a Quantum Dot at High Magnetic Field*, Phys. Rev. Lett. **88**, 126803 (2002).

[198] K. von Klitzing, *The Quantized Hall Effect*, Rev. Mod. Phys. **58**, 519 (1986).

[199] M. Wagner, U. Merkt, and A. V. Chapilk, *Spin-Singlet-Spin-Triplet Oscillations in Quantum Dots*, Phys. Rev. B **45**, 1951 (1992).

[200] M. R. Wegewijs and Y. V. Nazarov, *Inelastic Cotunneling Through an Excited State of a Quantum Dot*, Cond-Mat/ **0103579** (2001).

[201] R. Winkler, H. Noh, E. Tutuc, and M. Shayegan, *Anomalous Rashba Spin Splitting in Two-Dimensional Hole Systems*, Phys. Rev. B **65**, 155303 (2002).

[202] S. A. Wolf, D. D. Awschalom, R. A. Buhrman, J. M. Daughton, S. von Molnár, M. L. Roukes, A. Y. Chtchelkanova, and D. M. Treger, *Spintronics: A Spin-Based Electronics Vision for the Future*, Science **294**, 1488 (2001).

[203] A. Zduniak, M. I. Dyakonov, and W. Knap, *Universal Behavior of Magnetoconductance due to Weak Localization in Two Dimensions*, Phys. Rev. B **56**, 1996 (1997).

[204] I. V. Zozoulenko, A. S. Sachrajda, C. Gould, K. F. Berggren, P. Zawadzki, Y. Feng, and Z. Wasilewski, *Few-Electron Open Dots: Single Level Transport*, Phys. Rev. Lett. **83**, 1838 (1999).

[205] D. M. Zumbühl, J. B. Miller, C. M. Marcus, K. Campman, and A. C. Gossard, *Spin-Orbit Coupling, Antilocalization and Parallel Magnetic Fields in Quantum Dots*, Phys. Rev. Lett. **89**, 276803 (2002).

[206] D. M. Zumbühl, J. B. Miller, C. M. Marcus, C. Duruöz, J. S. Harris, Jr., K. Campman, and A. C. Gossard, *Conductance Fluctuations with Spin-Orbit Coupling in an In-Plane field in Open Quantum Dots*, to be published (2004).

[207] D. M. Zumbühl, J. B. Miller, C. M. Marcus, V. I. Fal'ko, T. Jungwirth, and Jr. J. S. Harris, *Orbital Effects of In-Plane Magnetic Fields Probed by Mesoscopic Conductance Fluctuations*, Phys. Rev. B **69**, 121305R (2004).